A Wearable Platform for Monitoring the Tissue Viability of Lower Limb Amputees

by

Neha Mathur

Department of Electronic and Electrical Engineering

University of Strathclyde

A thesis submitted for the degree of

Doctor of Philosophy

2017

Copyright

This thesis is the result of the author's original research. It has been composed by the author and has not been previously submitted for examination which has led to the award of a degree.

The copyright of this thesis belongs to the author under the terms of the United Kingdom Copyright Acts as qualified by University of Strathclyde Regulation 3.50. Due acknowledgement must always be made of the use of any material contained in, or derived from, this thesis.

Signed:

Date:

Dedicated to my beloved grandfather
Dr.Om Prakash Mathur.

Acknowlegements

This thesis is not only a representation of my academic pursuit in the Electronic and Electrical Engineering Department at University of Strathclyde, but is also a major milestone in my life. As I approach the end of my doctoral studies, I realise that this has been one of the most memorable journeys of my life. I have been extremely fortunate to have the support and guidance of family, friends and mentors all along the way - which has made this journey successful and more importantly, worthwhile.

I would like to start by thanking my supervisor Prof. Ivan Glesk for giving me the opportunity to conduct this research. I am grateful for his guidance, inspiration and patience which go way beyond what one can expect from a supervisor. I have learnt a lot from you but without doubt, have a lot more to learn. Hopefully, this is just the beginning of many more academic journeys together.

I would also like to express my gratitude to my joint supervisor Dr. Arjan Buis for all his contributions in arranging for clinical trials with volunteers, for having many meaningful discussions and also for painstakingly going through this document.

I would also like to thank Dr. Anthony McGarry for his continued support throughout.

I gratefully acknowledge the funding source that made my Ph.D. work possible. This research was supported by the Engineering and Physical Sciences Research Council.

I am thankful to Greig Paul for his contributions in programming the server and the android application. This has been extremely useful in providing an overall design solution for the remote monitoring of people with a limb amputation.

Special mention goes to my friends and colleagues Alan Davidson and Stuart Hannah, for their encouragement, camaraderie and most of all humour.

On a more personal note, I would like to thank my parents particularly my mother for ... well everything. She raised me with a love of science and has supported me in all my pursuits.

And in the end, a big thank you to my dear husband for his unbelievable support and patience. I appreciate all the little things that you have done to ease my workload – I would not have been able to accomplish this feat without you by my side. The last word goes out for my daughter, who has been the light of my life and has given me the extra strength and motivation to get things done. Thank you!

Abstract

Around the world the incidence of lower limb amputation is on the rise. These rising numbers puts a huge constraint on the healthcare resources, thereby making the rehabilitative process challenging for both the healthcare services as well as the amputee. People with a lower limb amputation need regular rehabilitative care as their residual limb skin is prone to infections, volume fluctuations, skin breakdown etc. e-Health wearable communication systems show promise in delivering improvements in patient care while at the same time reducing both the demand for resources and the financial burden on healthcare systems. These systems have the capability of monitoring, logging and transmitting patient data to a central health authority.

This thesis investigates the design of a wearable sensor communication platform which is capable of harvesting the data from multiple sensors for in-situ monitoring of residual limb health in amputees. The monitoring of residual limb temperature and gait is done in a contactless way by utilising mathematical algorithms. The platform works with an Android mobile device, in order to allow for the capture of data from a wireless sensor unit, and to give the clinician access to results from the sensors. The results from the analysis, carried out within the secure server, are demonstrated to be of use for remote monitoring. This knowledge will be useful in establishing biomarkers related to a possible deterioration in a patient's health or for assessing the impact of clinical interventions.

Contents

List of Figures

List of Tables

Glossary

ANFIS Adaptive Neuro Fuzzy Inference System

API Application Programming Interface

ATP Adenosine Triphosphate

BP Blood Pressure

CMOS Complimentary Metal-Oxide Semiconductor

DHCP Dynamic Host Configuration Protocol

DOF Degree of Freedom

DTI Deep Tissue Injury

FIR Finite Impulse Response

FIS Fuzzy Inference System

GP Gaussian Process

GPML Gaussian Processes for Machine Learning

GPS Global Positioning System

GUI Graphical User Interface

HTTP Hypertext Transfer Protocol

ICT Information and Communications Technology

IMU Inertial Measurement Unit

MAE Mean Absolute Error

MCU Micro-Controller Unit

MEMS Microelectromechanical Systems

MF Membership Function

NLML Negative Log Marginal Likelihood

P(VDF-TrFE) Poly(vinylidene fluoride trifluoroethylene)

PID Proportional-Integral-Derivative

PVDF Polyvinylidene fluoride

RMSE Root Mean Squared Error

SD Secure Digital

SE Squared Exponential

SPP Serial Port Profile

SSR Solid State Relay

USB Universal Serial Bus

WHO World Health Organization

Chapter 1

Introduction

1.1 e-Health

Recent advances in internet and mobile communications along with a public demand for health monitoring gadgets, have rendered the development of wearable user self-monitoring devices for measuring and logging a wide range of parameters such as the calories burnt, the steps taken, the body mass index, SpO2 and heart rate extremely popular. Additionally, the popularity of smartphone apps for health monitoring purposes is now commonplace. "In fact, it is estimated that at least 70% of Americans monitor at least one health indicator with 60% tracking weight, exercise and diet; while 33% track quantities such as Blood Pressure (BP), glucose and sleep patterns" [1]. Although these devices and apps are designed for the consumer market, this technology has opened up the possibility of the application of e-Health for the purpose of routine remote patient monitoring by the health authorities [2]. As developing technology allows e-Health devices to become increasingly smaller, lighter and smarter, the latter become more attractive for use in the permanent and continuous monitoring of patients.

Such systems, if implemented for lower limb prosthetic users, will enable the re-

mote monitoring of the amputee's residual limb tissue health by measuring the temperature and gait patterns. This would be useful in studying and perhaps predicting the volume fluctuation, pistioning, skin health and poor gait of the user in advance. The architecture of such medical monitoring systems may consist of on-body (non-invasive) or in-body sensors along with a Micro-Controller Unit (MCU) for control and pre-processing. The communication module may consist of a smartphone for the user interface and a transmitter in order to facilitate the data transfer via the internet to a central server.

The data collected can be used in order to provide an early warning of serious health threats along with the geographical location and movement patterns. If there is a deviation in the normal behavioural pattern, it might be an indicator that medical intervention is required which might then be used to trigger an emergency response. This early warning can have multiple benefits such as the reduction in hospital admission in already overstretched health authorities as well as potentially saving lives. Furthermore, the need for scheduled appointments at the outpatient clinics and doctors surgeries can also be reduced. Moreover, this continuous monitoring can be useful in providing a more accurate evidence of the patient health status that would otherwise remain unrecorded [**3**].

In the case of lower limb prosthetic users that need to be monitored continuously for longer periods of time, it is imperative that contactless sensing techniques are employed. Placing the sensors in direct contact with the skin would provide the most accurate reading, but this would lead to practicality issues in the prosthesis, such as, protruding wiring and consistent positioning of the sensors. Furthermore, it could induce possible skin irritation and discomfort. On the other hand, embedding sensors and wires into the hard-prosthetic socket during the manufacturing process for prosthetic sockets would eliminate any of the issues described earlier. In addition, the longevity of the device would not be impaired by the donning

and doffing of the prosthesis.

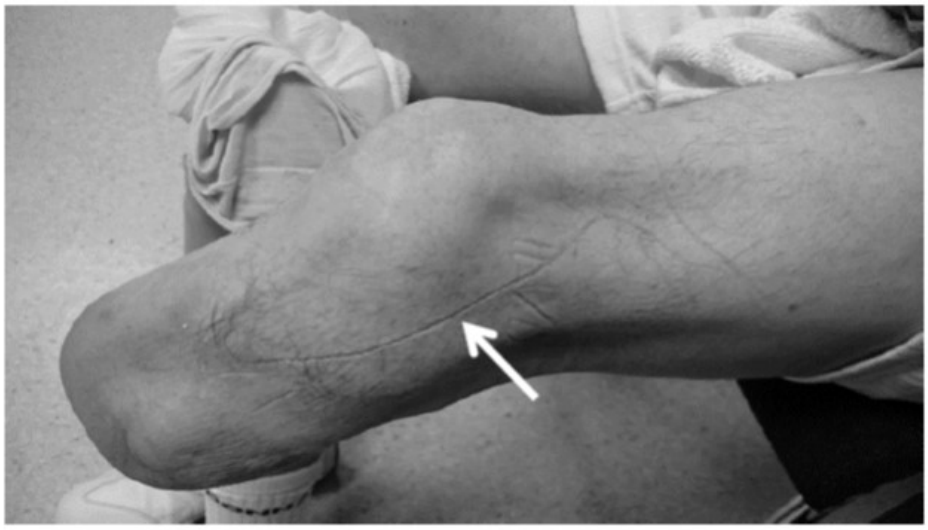

Figure 1.1: The placement of temperature sensors directly on the residual limb even for a short period of time leads to imprints on the skin surface which could lead to skin irritation and chaffing.

Figure 1.1 illustrates the undesirable impact of the temperature sensors when placed directly on the residual limb for a short period of time. This confirms that for the long term monitoring of the in-socket temperature, a contactless approach should be adopted in order to eliminate any increased skin irritation.

1.2 Aims of this Thesis

Lower-limb prosthetic users, particularly those suffering from diabetes, are at an increased risk of losing the remaining 'good' leg because of the compromised blood flow to the limbs and the predisposition to skin breakdown. This coupled with the volume fluctuation of the limb within the socket can result in pistioning, skin breakdown as well as a poor gait. A reliable continuous monitoring and early warning system that can alert both the user and health authority would have many benefits. Additionally, the information provided by a monitoring sys-

tem with reference to the areas that are at risk i.e. bony prominences, could contribute toward improving the prosthesis design. While such technologies and principles may already exist, to date, no such early warning system has been implemented, and thus a continuous monitoring system to provide an early warning of tissue damage presents a novel approach to injury prevention. While designing such a system, a major criteria would be reducing the financial costs associated with it, as approximately 75% of those affected by diabetes live in middle or low income countries [4].

Many healthcare technologies and products presume that internet access and reliable electricity supplies are given, which in turn renders them unsuitable for the developing world. Hence, it is imperative to design a wearable system which is reliable, low-priced, does not rely on a mains power supply and can operate in the absence of internet connectivity for a considerable period of time. Furthermore, if the sensors are placed in direct contact with the skin, then a continuous monitoring could lead to issues such as skin irritation and chaffing. Therefore, the aim of this research is designing a wearable sensor platform for the developing world which is capable of monitoring, logging and transmitting the patient data to a central health authority. This research aims to incorporate the techniques for contactless sensing that may be suitable for use within the prosthetic socket environment in order to predict the residual limb skin temperature and gait pattern. In order to process the recorded data sets such as to extract clinically relevant information, machine learning algorithms are used at the server interface. This approach can be particularly useful for rural and impoverished countries, in which doctors work with limited resources and under challenging conditions and may often not be available at short notice. The continuous monitoring of the residual limb tissue health of prosthetic users would not only be useful as part of the diagnostic procedure, routine maintenance or during the supervised recovery from a surgical procedure, but would also make it possible to reduce the burden on

the overworked doctors.

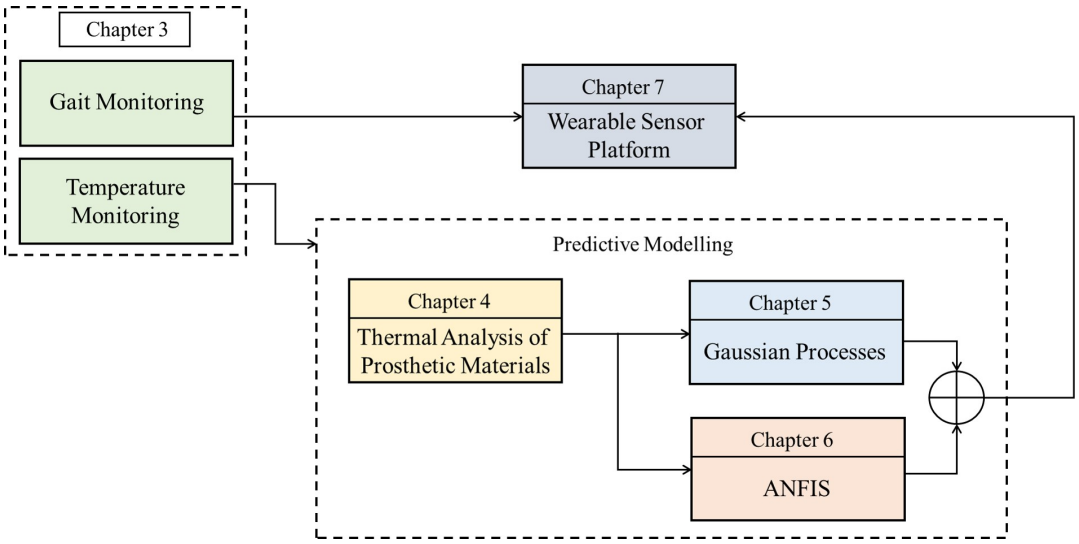

Figure 1.2: Block diagram showing the interconnections between the components of the thesis.

The structure of the thesis is shown in the block diagram of Figure 1.2. The dependence of the residual limb temperature and of the gait pattern on the ambient temperature and the activity level on amputee subjects is investigated in Chapter 3. The gait pattern at different ambient temperatures is analysed using the complementary filter, the design of which is also discussed. The analysis of the walking pattern of the amputee subject conducted by determining the joint angles (in our case, the shank angle) of the residual limb will be useful in differentiating between the normal and abnormal gait profile of an individual, thereby helping to predict the occurrence of pressure ulcers.

In Chapter 4, the prosthetic materials are characterised thermally. This is especially important to investigate as the prosthesis layout also affects the in-socket temperature to a great extent. In order to do so, the thermal time constant of the prosthetic materials (when used individually or in combination) is calculated.

The investigation of the residual limb temperature at different ambient temper-

atures along with the gained knowledge of the thermal behaviour of the socket-liner materials is utilised to formulate a supervised learning algorithm, namely the Gaussian Processes for Machine Learning (GPML), to predict the residual limb temperature from the liner - socket interface temperature. Chapter 5 discusses the design and the results obtained from this mathematical algorithm. By utilising this technique, the residual limb skin temperature can be monitored in a contactless way.

Another mathematical algorithm referred to as Adaptive Neuro Fuzzy Inference System (ANFIS) for the non - invasive temperature measurement of the residual limb is developed. The predictive residual skin temperature results are compared with the Gaussian Process model in Chapter 6.

In Chapter 7, the design and implementation of the wearable sensor platform is discussed. Temperature and gait data is reliably collected, transmitted and stored in a secure local server for post processing (utilising the mathematical modelling and the complementary filter), which subsequently allows medical authorities to access and review the user data in order to identify any possible deterioration in the tissue health. Additional features for the wearable platform like battery monitoring and introduction of estimation techniques are also discussed. The capability of the wearable sensor platform is successfully tested on a volunteer and the results are also summarised.

Chapter 8 contains the conclusion and the scope for future work.

1.3 Contributions to Knowledge

This research represents a seminal contribution to the prediction of the residual limb skin temperature via a contactless approach - by utilising mathematical algorithms such as GPML and ANFIS for this purpose. The comparison metrics

were studied for both algorithms and it was determined that although any one of them can be used for predicting the residual limb skin temperature by monitoring the temperature between the socket and the liner, the predictions by the GPML model are more accurate and consistent.

The results show that the hyperparameters in the GPML model are optimised more efficiently by including the thermal time constant of the prosthetic materials used in the prosthesis of the amputee subject. Since there was limited literature available for the thermal behaviour of the various combinations of prosthetic materials, the thermal time constant of various socket-liner layer combinations were experimentally evaluated.

The encouraging results of the contactless residual limb temperature monitoring, subsequently led to the design and development of a low-power, low-cost wearable sensor platform. This wearable sensor platform is particularly designed for lower limb amputees, based on standard consumer-purchasable components, which are suitable for a self-contained use when there is no reliable electricity supply or internet connectivity available. The platform can monitor both residual limb temperature and gait of the amputee. The platform's design and capability has been tested on an amputee volunteer and is verified by analysing its power consumption, communication methodology and its remote accessibility of medical data feature.

1.4 Publications arising from this Thesis

Journals

[1] N. Mathur, I. Glesk, and A. Buis, "Skin Temperature Prediction in Lower Limb Prosthesis," *IEEE Journal of Biomedical and Health Informatics*, volume 20, issue 1, year 2016, pp. 158 - 165.

[2] N. Mathur, I. Glesk, and A. Buis, "Thermal Time Constant: Optimizing the Skin Temperature Predictive Modelling in Lower Limb Prostheses Using Gaussian Processes, *IET Healthcare Technology Letters*, volume 3, issue 2, year 2016, pp. 98 - 104.

[3] N. Mathur, I. Glesk, and A. Buis, "Comparison of Adaptive Neuro -Fuzzy Inference System (ANFIS) and Gaussian Processes for Machine Learning (GPML) Algorithms for the Prediction of Skin Temperature in Lower Limb Prostheses, *Elsevier: Medical Engineering and Physics*, volume 38, issue 10, year 2016, pp. 1083 - 1089.

[4] N. Mathur, G. Paul, J. Irvine, M. Abuhelala, A. Buis, and I. Glesk, "Towards a Low Cost Platform for Remote Monitoring of Lower Limb Health of Amputees in the Developing World, *IEEE Access*, volume 4, year 2016, pp. 7440 - 7451.

Conferences

[5] A. Davidson, N. Mathur, I. Glesk, and A. Buis, "Power Supply Issues in e-Health Monitoring Applications, *International Conference on Renewable Energies and Power Quality ICREPQ*, Cordoba, Spain, 25 - 27 March 2015.

[6] N. Mathur, I. Glesk, and A. Buis, "Thermal Time Constant: Improving the Accuracy of Skin Temperature Predictive Modelling in Lower Limb Prostheses, 2015 Prosthetics and Orthotic International, vol. 39, no. 1, pp. 72-73, Lyon, France, June 2015.

[7] N. Mathur, I. Glesk, and A. Buis, "Issues in Wearable Mobile Sensor Platform for Lower Limb Prosthetic users, *17th International Conference on Transparent Optical Networks ICTON*, Budapest, Hungary, 5-9 July 2015.

[8] N. Mathur, I. Glesk, A. Davidson, G. Paul, J. Banford, J. Irvine, and A. Buis, "Wearable Mobile Sensor and Communication Platform for the In-situ Monitoring of Lower Limb Health in Amputees, *IEEE International Symposium on Circuits and Systems*, Montreal, Canada, 22-25 May 2016.

[9] N. Mathur, A. Davidson, A. Buis, and I. Glesk, "Tissue Viability Monitoring - A Multi-Sensor Wearable Platform Approach, *20th Slovak-Czech-Polish Optical Conference SCPOC*, vol. 1014205, Slovakia, September 2016.

Posters

[10] N. Mathur, I. Glesk, and A. Buis, "Real Time In-Situ Monitoring of Temperature in Prosthetic Sockets, *5th SU2P Symposium*, Glasgow, UK, April 2014.

[11] N. Mathur, I. Glesk, and A. Buis, "Comparing Non-linear Regression Algorithms for Prediction of Residual Limb Temperature in Prostheses, *25th Congress of the International society of Biomechanics ISB*, Glasgow, UK, 12-16 July 2015.

Please note that the references to my publications in the thesis are highlighted in bold.

Chapter 2

Overview of e-Health

2.1 Introduction

The growing use of wearable technologies has increasingly facilitated the continuous remote monitoring of the patient's physiological data. The roll-out of such schemes shows promise in delivering improvements in patient care while at the same time reducing both the demand for resources and the financial burden on the healthcare systems. These wearable monitoring systems are used in order to monitor, log and transmit patient data to a central health authority. Depending on the patient, it is often critical that the monitoring system reliability is high enough in order to deliver appropriate patient care and ensure patient safety. This would be beneficial in changing the healthcare delivery models and the interaction between the patient and the healthcare providers [5]. This chapter provides an overview of the concept of e-Health and the application thereof in the field of wearable technologies. The concept is then discussed in the context of monitoring the residual limb health of the amputees. Additionally, the challenges associated with the development and integration of such a solution in the healthcare services provided to amputees are also discussed.

2.2 The e-Health Concept

According to the World Health Organization (WHO), e-Health is an all encompassing term for the use of Information and Communications Technology (ICT) in the field of healthcare. The area of e-Health is very broad and includes applications such as telemedicine, electronic records, recruitment, going paperless, procurement, healthcare score cards, audits, information systems etc [6]. Relevant examples include using this technology for treating patients, conducting research, educating the healthcare workforce, tracking diseases and monitoring public health across both local sites and wide geographic locations [7]. The e-Health ecosystem is complex and includes medical devices/sensors in order to provide the data output, a communications network for data transfer, platforms that can process, collate and interpret the data to provide the diagnosis, and finally the medical personnel being able to perform relevant actions such as medical interventions or an emergency response as appropriate. In this context, the successful delivery of the e-Health service is reliant on the interoperability of the following stakeholders, also represented in Figure 2.1:

1. Communication Service Providers (fixed, mobile, satellite)
2. Patient and Family
3. Clinicians
4. Healthcare Providers
5. Health Insurance Companies
6. Diagnostic Centre

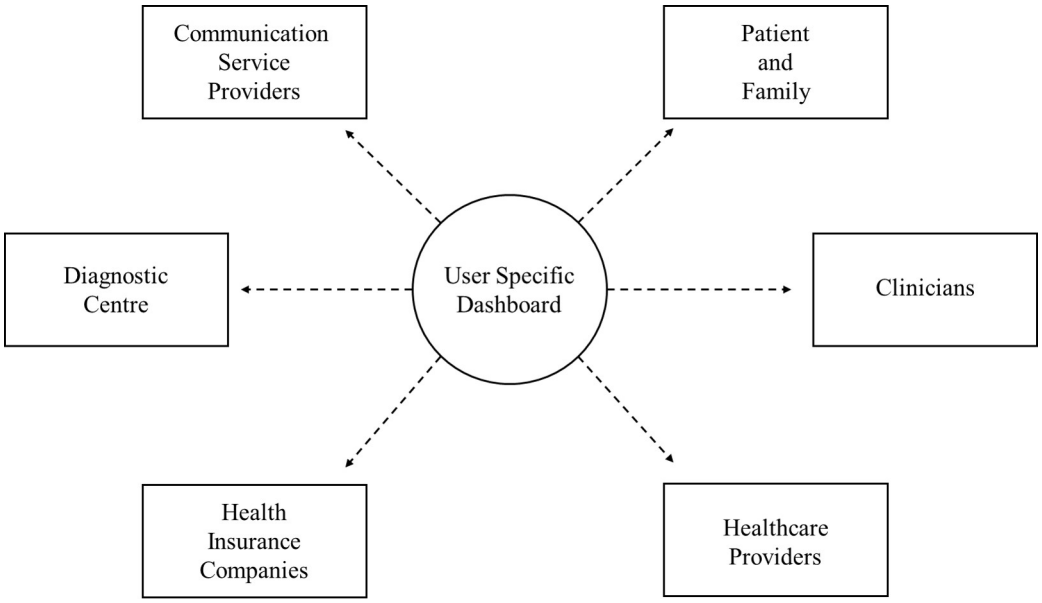

Figure 2.1: e-Health stakeholder ecosystem.

Each of the stakeholders plays an important role in achieving end to end connectivity in e-Health. An example might be that the patient is connected to a medical module or sensor (at home or in a clinical environment) and is monitored at a pre-defined time interval. The data is transferred via a wired or wireless communication application to a central database. In the diagnostic centre, the data is analysed, monitored and managed by the clinicians. The data can be presented to the doctors and patients in a user specific dashboard. This monitoring is useful for patients, healthcare providers and insurance companies alike. For patients this would provide information about their own health as well as an opportunity to change their relationship with the healthcare providers and the insurance companies. The improved communication would not only facilitate remote patient/doctor consultation in the case of patients undergoing rehabilitation and for whom interventions need to be assessed in the home and outdoor environment. It would also enable them to support the early detection of abnormal conditions and the prevention of serious consequences. From the point of view of healthcare providers, this would help in the reduction of unnecessary hospital admissions,

which are both disruptive for the patients and costly for the health authorities. Thus, a reliable continuous monitoring and early warning system that can alert both the user and the health authority would not only be beneficial to the patients but its impact is also directly experienced by the health insurance companies, as it reduces their business operation costs.

These system have the capability to improve the access to all levels of healthcare (primary, secondary and tertiary) for a range of conditions including chronic, psychiatric and rehabilitative care. This has led to an increase in the application of tele-homecare by remote monitoring of the clinical parameters in a home based environment. Such systems will, facilitate the remote monitoring of physiological data and patient vital signs. These medical monitoring systems may utilise on-body (non-invasive) or in-body sensors and will generally incorporate the basic components of a MCU for control and pre-processing; and a transmitter and smartphone for data processing and data transfer via the internet to an e-Health server and database.

2.3 Wearable Technologies

Advances in sensor technologies have led to the latter constituting an integral part of modern medicine. Medical sensors combined with transducers are used for detecting electrical, thermal, optical, chemical, genetic, and other signals using signal processing algorithms in order to estimate the features indicative of a person's health status [8]. These sensors, when interfaced with embedded computing platforms make it possible to design a platform which can be wearable by individuals for the purpose of health monitoring in daily use. By monitoring different types of data (via different sensors) under different parameters and activities and by subsequently correlating them, additional information about the clinical, behavioural and mental health of a patient can be inferred.

1. *Clinical data*: This can be obtained from a number of readily available monitors that can measure the temperature, photoplethysmogram, heart rate, BP, oxygenation (SpO2), respiration and glucose levels. The primary target for this is the older population wherein the monitored data are focused on the parameters related to the patient's clinical condition (diabetes, cognitive heart failure, pulmonary disease etc.). This type of data is integrated in the clinical workflow of the clinicians [9]. If an abnormal condition is developed, an alert is generated at the healthcare provider as well as the patient's level. Furthermore, the monitored data can be utilised for the purpose of risk assessment, such that prospective abnormal conditions may be predicted and prevented [10]. However, there are some off-the-shelf wearables that are not connected with the healthcare providers and are purely commercial in nature. The data monitored by the latter is not treated as clinical data by the physicians. Thus, this type of data is not used for analysis purposes by the healthcare system and is effectively 'lost'. It is hence a challenge for the healthcare systems to securely validate and integrate this data from patients using their own devices.

2. *Behavioural data*: This data collected from the wearable devices includes information about the activity, the type of activity (running, walking, climbing stairs) and daily activity patterns. This can be utilised for the purpose of early detection as well as to gain a better understanding of patient conditions such as motor conditions associated with the Parkinson's disease, along with posture and gait issues using related indicators [5, 11, 12]. Apart from focusing on the elderly population for determining the risk of falls and daily living assessment, the behavioural data can be used to monitor the degree of wellness in healthy people. Many commercially available wearables as well as the sensors embedded in the smartphones, when linked to the Global Positioning System (GPS) and self-help tools on the smartphone,

can help in the early detection of some risks. However, this data is solely provided to the user and it is not shared with the healthcare providers. For the elderly population, such wearable devices are equipped with an emergency button for fall detection and location identification in the case of dementia. These services are linked to emergency centres and are not available to the health carers. If this information is shared with the care providers, the actual condition of the patient can be accessed by the physician.

3. *Mental health data*: The assessment of the mental health and cognitive conditions can be conducted by using wearable technology [9, 13, 14]. For instance if a patient tends to fall, then the monitored data can be used to analyse whether there is a cognitive decline or what stage of dementia the person is at. Studies have shown that 39% of patients of all ages suffer from depression and/or anxiety [15]. Physiological stress and disturbed sleeping patterns, if monitored can serve as indicators for the mental health problems. At present, monitoring health data is in the pilot phase and it is not yet implemented in the healthcare programme. By implementing them in the care process, the quality of care can be improved and the cost of treatment can be reduced.

Wearable technologies have the ability to open up new avenues for patients, healthcare providers and insurance companies by providing new information and knowledge. The use of this knowledge can help develop new analytical tools for the early detection and treatment of chronic pathologies. The implementation of wearables in healthcare is still in its infancy and will develop in the coming years. However, for its successful implementation, certain challenges which are subsequently discussed in the next section need to be addressed.

2.4 Challenges for Wearable Technologies

In order to become ubiquitous, such a monitoring system must be portable, wearable, comfortable, secure, robust and, most critically reliable in terms of the measurement, logging and communication of data. Lost patient data due to unreliable mobile communications could compromise patient safety, whereas false alarms could become costly and potentially deplete the limited healthcare resources. While it is clear that false alarms should be avoided as much as possible, this must not be done at the cost of the patient's safety. Many of the patients who would most benefit from such a monitoring system will be the elderly, the disabled and the infirm, it is desirable that the monitoring system should not only require a minimum amount of user intervention, but should in turn also be well tolerated by the patient. In particular, it is important to make the system as small and light as possible. For example, the incorporation of devices into a ring or a watch has been suggested [16].

However, some of the issues of concern pertaining to the realisation of the aforementioned requirements are the power consumption of the device and the longevity of the battery between charges. Ideally, the device battery should be able to supply enough charge to power the device for extended periods of time. However, the current battery technology is not delivering the improvements in capacity currently demanded by the development of smaller, more resource-hungry devices. Reducing the battery size results in poor battery life between charges and the current technology has therefore proved to be detrimental to prospective device miniaturisation. In fact, the annual improvement thereof is relatively slow compared to the increase in the power demand, with the battery capacity being estimated to improve by only 8% per year [17]. The ubiquitous lithium battery, widely adopted due to its relatively high safety/capacity characteristics, is reaching its peak. New battery technologies are under investigation in order to

improve energy density, however most of these contain toxic or highly flammable materials - for example hydrogen fuel cells - and are therefore not suitable for human monitoring applications. In short, while devices are decreasing in size, the battery size cannot be reduced without incurring a severe penalty in relation to the level of charge it can hold. In fact, many wrist-worn smart devices must be charged on a daily basis, with the most efficient thereof having to be charged at least once every 2 days.

In the absence of adequate battery technologies, it is clearly necessary to minimise the device power consumption and to consider possible solutions, such as incorporating alternative power sources (kinetic, heat or solar), in order to supplement the battery charge. Moreover, the design of the devices operating using the CMOS technology in the sub-threshold region may provide an answer for some applications by extending the battery life up to 10 fold [18]. However problems exist with the process, voltage and temperature range limitations which could adversely affect the key device requirement in terms of reliability. It is however crucial for the monitoring devices that are placed in direct human contact, to be able to operate under varying environmental conditions.

The monitored data can be transmitted to a central health database using three different modes of communication, namely Bluetooth, Wi-Fi and cellular technology. In many e-Health sensing applications, Bluetooth is used for transmitting the data collected from the sensor(s) to the smartphone [19]. Bluetooth is a suitable wireless technology for remote health monitoring due to its inherent simplicity, adaptability and security. Additionally, its incorporation is ubiquitous in modern mobile phones and PCs. Bluetooth technology is designed to have very low power consumption and, as such, uses less than 3% of the power required by a Wi-Fi connection for the same tasks. For example, sending data at the rate of 75 bytes per second over Wi-Fi requires approximately 80 milliwatts of electrical power.

Sending data at the same rate over Bluetooth consumes only 2 milliwatts [20].

Another challenge for healthcare providers is represented by the amount of data. Wearable monitoring systems generate a significant amount of data. Healthcare providers be responsible for treating the data despite the existing constraints in terms of privacy and security.

The standardisation of data in the healthcare domain is not well defined and as such one of the barriers to the adoption thereof is the implementation of the e-Health development standards. There has been a global incentive encouraging projects to develop and define the data flow standards for the purpose of monitoring and integration within the e-Health domain.

2.5 State of the Art

Lower limb amputees are subjected to functional limitations and continued health problems including gait asymmetries [21–23], skin breakdown [24–26], reduced activity level [27, 28] and decreased walking speed [21, 29]. These issues collectively contribute to a decline in the quality of life of the amputees. From healthcare perspective, this rehabilitation process is both time consuming and expensive [30]. Therefore, in order to address the health of the residual limb in amputees, remote monitoring strategies and/or tools are needed.

Periodic clinical check ups are the standard procedure for the rehabilitation process of amputees. Although, continuous assessment in other environments (home or community) provides a variety of benefits (such as a reduced number of hospital visits, reduced medical costs and improved quality of life), the implementation of remote monitoring for the same purpose is largely unseen.

For lower limb amputees the prosthesis provides an ideal housing vehicle for wearable sensors. By attaching the sensors or by integrating them within the

prosthesis it would be possible to alleviate the risk of discontinuous data. Furthermore, the addition of the modest weight of the wearable device on the prosthesis, would not appear to affect movement or the metabolic energy expenditure while walking [31–33]. In order to obtain the residual limb health parameters, several monitoring devices have been mentioned in the literature. But in order to obtain information about the prosthetic patient's activity and the impact thereof on the residual limb the following sensors are widely used - accelerometers, strain gauge based devices (in order to measure pressure), temperature sensors and humidity sensors in the sockets.

Accelerometer based devices are used to measure the motion of the amputee along the reference axes. Resultantly, they can be utilised in order to monitor the intensity and frequency of human movements which can be subsequently interpreted so as to classify the body postures (orientations). They require low power for operation purposes and are very sensitive. Because of their sensitivity, they need to be properly oriented to the patient in order to obtain accurate data [34]. The capability of the accelerometer based wearable devices for posture and movement classification has been studied extensively. Various statistical schemes which are based on a supervised learning approach have been utilised for the same purpose. For example, the k-nearest neighbour classification [35, 36], support vector machines [37,38],the Gaussian mixture model [39] and the hidden Markov model [40, 41] are used in order to describe the probability of activities and transition between possible activities. Accelerometers can also estimate the energy expenditure due to motion by measuring the physical activities [42, 43]. However, the accelerometer based devices are probably best known for the analysis of the gait pattern. Studies on young, elderly and disabled people have been conducted in order to analyse their gait symmetry w.r.t velocity, step length and walking surfaces [44–46].

Mapping the pressure in the prosthesis would provide valuable information about the health of the tissue in the residual lower limb as well as facilitate the detection of the formation of the skin surface and pressure ulcers. Studies on the measurement of the socket pressure have been documented since 1954 [47] and are still being continued to this day [48, 49]. For monitoring the interface pressure, strain-gauge (resistive sensors) are typically used. These sensors are small, light weight and have small power requirements. However, a drawback of these sensors is that they have a tendency to drift over a period of time, thus rendering the data unreliable. With the recent advances in technology, the principles of piezoelectricity are being widely applied as the basis for pressure and force measurement transducers [**50**]. Piezoelectric materials represent a class of dielectrics that have asymmetric crystalline structures and that can be polarised by means of an electric external electric field or upon the application of a mechanical pressure. Thus, the charge produced is proportional to the pressure applied. In some materials such as Polyvinylidene fluoride (PVDF) and Poly(vinylidene fluoride trifluoroethylene) (P(VDF-TrFE)), the piezoelectric effect can be enhanced in the material by poling. Both PVDF and P(VDF-TrFE), have been successfully used as pressure sensors for several years [51], and more recently for the purpose of energy harnessing [52]. Piezoelectric devices require no power supply, since a charge is developed across the piezoelectric material proportional to the applied force, thus producing an output voltage which may be measured directly. However, a drawback in their application for use within prosthetic sockets is that the sensors used in the measurement of such useful quantities such as pressure are generally fabricated on rigid substrates. These rigid substrates cannot be allowed to have prolonged contact with the skin as it may cause the skin to break when stressed. It is therefore desirable to have a flexible and wearable system in order to overcome these difficulties. Thin film polymer pressure sensors show potential in the production of cheap and very flexible sensor arrays which are bio-compatible

i.e. flexible, non-chemically reactive and resistant to corrosion [53]. The sensors, if placed strategically in the array, can help in extracting a maximum amount of information [54].

Studies on the temperature within the prosthetic sockets of transtibial prosthetic users have been described by Peery et al. [55,56]. They investigated the in-socket temperature of five transtibial amputees at 14 different locations on the residual limb and at four different stages, i.e., donning, steady-state resting, initial walking, and steady state walking. Their results indicated that the thermal dissipation characteristics of the socket and liner restrict heat loss from the residual limb and that the temperature increase is larger in areas where there is more muscle bulk. It was also observed that different socket and liner materials affect the temperature increase in the residual limb in a different manner. Additionally, these temperature rises were different between patients. The impact of the environmental factors has also been investigated by Klute et al. [57,58] by observing the in-socket residual limb temperature at four locations throughout a whole day. Simultaneously, they recorded environmental temperature, humidity, and also the activity of the patient. It was found that the in-socket residual limb temperature increased gradually throughout the day, and that an increase in activity caused a further increase in temperature. Moreover, the environmental humidity and temperature influence the perception of the whole body and the residual limb thermal comfort [59]. The limitations to this study were the small sample size and the variation of the prosthetic liners and socket materials between patients. The population on which these studies were conducted was small. Hence, a generalised statement about the temperature of the residual limb skin cannot be made.

However, most of these studies have been based in clinical environments and there is a need to develop them for the home monitoring systems. Additionally, for the

development of a wearable sensor platform, all these sensors should be included such that the limb parameters can be known. This would be an important step in understanding the overall health status of the residual limb of an amputee.

2.6 Need for Non-Invasive Measurement in Prosthesis

Driven by the changing demographics of the UK population and the increasing global burden of disability, the key objective of many government agencies, including health departments, is to extend the independent living and well-being of ageing and disabled populations. In Scotland, one of the key areas of the national programme for health is to focus on the development of innovative, scalable technological solutions compatible with the e-Health concept which will be capable to support the changing health and social care landscape in Scotland.

Worldwide, one individual loses a limb every 30 seconds as a consequence of the complications of diabetes alone. The social and economic consequences of such traumatic amputations are devastating, and even with determined focus on the prevention of amputation, millions of individuals will need and expect prosthetic care for generations to come. Research and development within this field is still in its infancy, and much work is required in order to improve prosthetic designs that deliver optimum patient comfort and functionality. One of the greatest challenges is the interaction between the prosthetic socket and the limb which must support the human weight. When this interface is unsuitable or compromised, it can entail severe consequences for the individual and high costs in order to correct the problem which could have been largely prevented by means of adequate monitoring.

For monitoring the residual limb health in prosthesis, the most obvious way is

to place sensors at the skin level in order to measure the relevant parameters of the limb soft tissue including blood flow, oxygenation, pressure, temperature etc. However placing sensors and wires directly against the skin could cause irritation and chaffing over a short period of time. Another option is to embed wires and sensors in an elastomer for the purpose of monitoring. But this is not practical as it eventually results in elastomer failures because of the high strain induced when donning a liner (amputees roll the liners onto their limbs). This can be overcome by placing the relevant sensors at the liner-socket interface and utilising mathematical algorithms in order to predict the relevant limb tissue parameter from the monitored sensor data. The idea underlying is the development of a battery powered wearable sensor platform for lower limb amputees which would facilitate the in-situ monitoring of the residual limb within a below the knee type of prosthesis in a non-invasive manner. The obtained data is transferred to a central health database where it is processed and if the threshold is achieved a warning signal will be sent wirelessly. A copy of the data can also be saved locally on the platform. In Figure 2.2 the idea of the wearable platform with reference to the placement and schematic thereof is depicted.

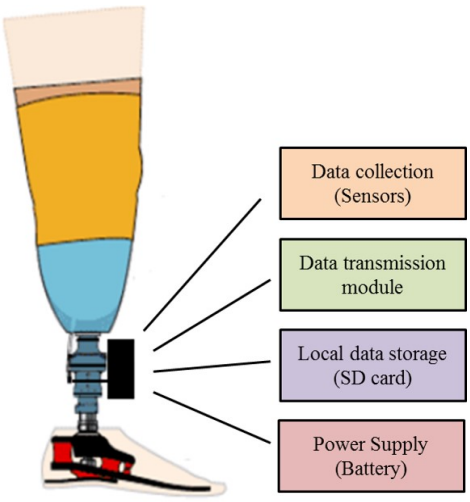

Figure 2.2: Wearable sensor platform for non-invasive monitoring in prosthesis.

2.7 Summary

e-Health has opened up many opportunities for healthcare providers in terms of improving the quality of life of the growing disabled population through remote monitoring. All of the stakeholders in the e-Health ecosystem can benefit from the new information and knowledge generated by the use of the wearable technologies. With the advancement of technology, many wearables are available commercially and can be customised for specific pathologies of the user. However, integrating the monitored data in the healthcare providers' record is a challenge considering that the aspects pertaining to security, privacy and standardisation of the same are still in their nascent stage. The focus of this thesis is the development and implementation of an integrated wearable sensor platform that can encompass temperature and gait sensors for remote monitoring of the residual limb parameters by utilising the principles of e-Health. This knowledge will be useful in establishing the biomarkers related to a possible deterioration in a patient's residual limb health or for assessing the impact of clinical interventions.

Chapter 3

Towards Monitoring the Residual Limb Skin Health

3.1 Introduction

The use of a well-fitting prosthesis by a health impaired or even an otherwise healthy person with a lower limb amputation can cause the development of serious tissue injuries such as pressure ulcers (decubitus ulcers, also called pressure sores) if not regularly monitored by the amputee and relevant health authority. Injuries can start deep inside the residual limb near the bone (deep tissue injury) and/or at the surface of the skin and can affect all types of tissue including the bone [60]. Of particular concern is Deep Tissue Injury (DTI) where the ulcer becomes apparent only when it reaches the surface of the skin and severe injury has therefore already occurred. DTI is caused when the volume of tissue in the residual limb reduces resulting in downward bone movement i.e. pistoning. The downward movement of the residual limb bone may lead to boundary shear at the bone/tissue interface which may result DTI and the formation of ulcers that progress from the bone to the skin. Specifically, this type of injury may be caused by restricted perfusion

(pressure induced ischaemia) and physical trauma caused by mechanical overload of the deep tissues [61]. In addition, shear and normal forces on the skin can result in surface pressure ulcers caused by constriction of blood flow resulting in reduced perfusion and ultimately tissue necrosis. Pressure ulcers at the skin surface can progress from the skin surface down to the bone and are apparent by the breakdown of the skin. This is further exacerbated by elevated temperatures and humid micro environment within the prosthesis which encourages the growth of bacteria and skin breakdown. Thus, monitoring of residual limb temperature, interface pressure and gait can be a useful indicator of tissue viability to predict the occurrence of pressure ulcers. Analysing the gait and interface pressure can be useful for determining the fit of the prosthetic socket as well as the strategies prescribed to accommodate these changes can be commented on. Monitoring the gait of a prosthetic limb can thus be useful for the rehabilitation progress of patients over time.

This chapter investigates how differing activity levels and ambient temperatures influence the in-socket temperature and the gait of the amputee subject. This would hence be useful in establishing mathematical models and techniques for addressing the challenge of non-invasively monitoring the residual limb skin health for a wider amputee population.

3.2 Experimental Design and Process

To investigate the gait and the residual limb temperature, two transtibial traumatic amputees with the details listed in Table 3.1 were recruited to perform in a 35 minute laboratory protocol. The investigation was implemented following ethical approval granted by the University of Strathclyde Ethics Committee (Ref UEC13/04).

Table 3.1: Details of the amputee subjects

Amputee	Age (years)	Weight (kg)	Details of the prosthesis
Subject 1	68	70	OttoBock Technogel (polyurethane liner - 6 mm) with thermosetting lay-up (socket material - 4 mm)
Subject 2	63	69.8	Pelite (closed cell foam - 5 mm) with thermoplastic (socket material - 4.7 mm)

For the experiment, the subjects were dressed in shorts and t-shirt. Hence, it should be noted that there was no extra clothing layer on the prosthesis. To monitor and record the skin and in-socket temperatures, four K-type thermocouples via a data logger (type HH1384; Omega Engineering) were used. Two thermocouples were taped onto the residual limb in lateral and medial position. The other two thermocouples were put on the corresponding positions on the liner (in-socket). This is indicated in Figure 3.1. Data from the four channels were simultaneously collected at 0.5 Hz at a predetermined ambient temperature. To monitor the gait, an inertial sensor is placed on the shank of the subject with the data being recorded at 25 Hz.

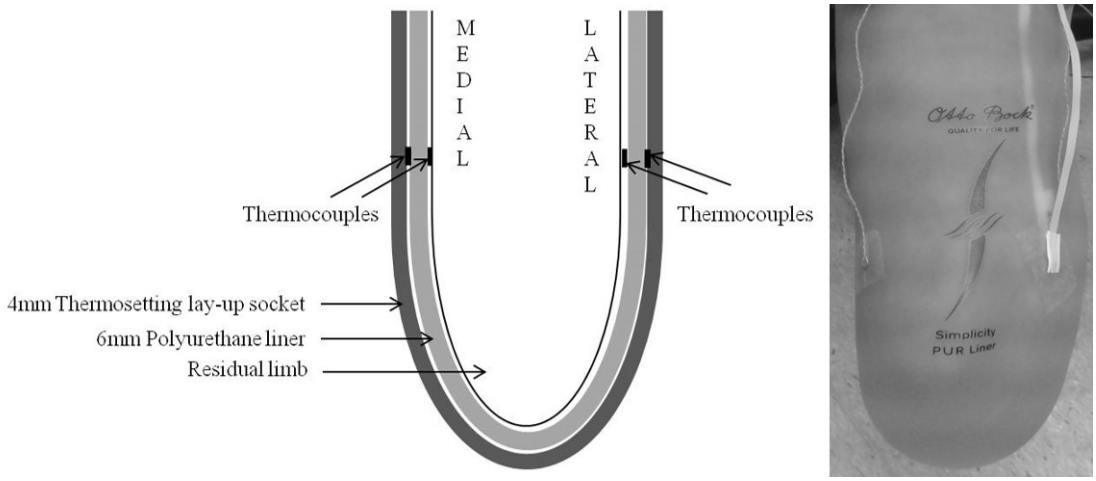

Figure 3.1: The anterior view indicating the placement of the thermocouples on the lateral and medial side of the residual limb skin and its corresponding positions on the liner of the amputee subject. (a) Schematic of the placement of the thermocouples in the prosthesis (b) Actual placement of the thermocouples for the experimental trials.

After the thermocouple heads were secured with tape, the prosthesis was donned with the thermocouple wires exiting the proximal edge of the socket. The subjects were asked to complete the following protocol: resting (sitting) for 10 minutes, walk at self-selected pace of 0.62 m/s on a treadmill for 10 minutes, and finally rest for 15 minutes. The residual limb skin and the socket temperatures were sampled at 0.5 Hz for the entire 35 minute protocol. For analysis purposes, three steady-state periods were defined as the last minute of each period: initial rest, walking, and final rest. The temperature profile of the residual limb skin and the liner was analysed at different ambient temperatures to see how closely they are correlated.Additionally the gait profile was also analysed for different ambient temperatures. This study was conducted in Scotland for the Spring/Summer profile where the ambient temperature ranges from approximately 10°C to 25°C. Hence, the temperatures from this range were picked. The experiment was conducted at 10°C and then repeated for 15°C, 20 °C, and 25°C (Dataset A). The experiments were conducted again after a time span of two months to confirm the influence of ambient temperature on the residual limb skin temperature and the

gait profile (Dataset B). This enabled in confirming the normal gait and residual limb temperature response of the subject at different ambient temperatures. All experiments were conducted in a climate-controlled chamber with zero wind velocity and 40% humidity level.

3.3 Gait Measurement

"The word gait describes 'the manner or style of walking', rather than the walking process itself" [62]. Thus, gait analysis is a the study of human locomotion. This involves measurement, quantification (introduction and analysis of the parameters of gait) and conclusions from the gait pattern. By gait analysis, the gait phases along with the kinematics associated can be identified. As a result, this is greatly being used in sports, rehabilitation and health diagnostics [63]. In lower limb prosthetics, analysing the gait pattern can be a useful indicator of residual limb health. Any discomfort within the prosthesis either due to volume fluctuation of the limb, inadequate prosthetic alignment or skin breakdown etc. can contribute to an abnormal gait in an amputee [64].

3.3.1 Human Gait Phases

The *gait cycle* is defined as the time interval between the exact same repetitive events of walking. Although the gait cycle can start at any event in walking, it is generally the instant when one foot contacts the ground ('initial contact'). If the cycle starts with right foot on the ground, then the cycle ends when the right foot makes contact again. The left foot follows the same cycle of events as the right foot, but is displaced in time by half a cycle [62]. There are two phases of the gait cycle - stance phase and swing phase. The stance phase comprises 60% of

the gait cycle whereas the swing phase comprises 40% of it. The human walking pattern can be analysed by phases more accurately as it signifies the functional effect of different motions on joints and segments. A normal walking gait cycle can be divided into eight different gait phases including initial contact, loading response, mid stance, terminal stance, pre-swing, initial swing, mid swing and terminal swing [65] as seen in Figure 3.2. Detailed description of the gait phases are described as follows [63, 66] .

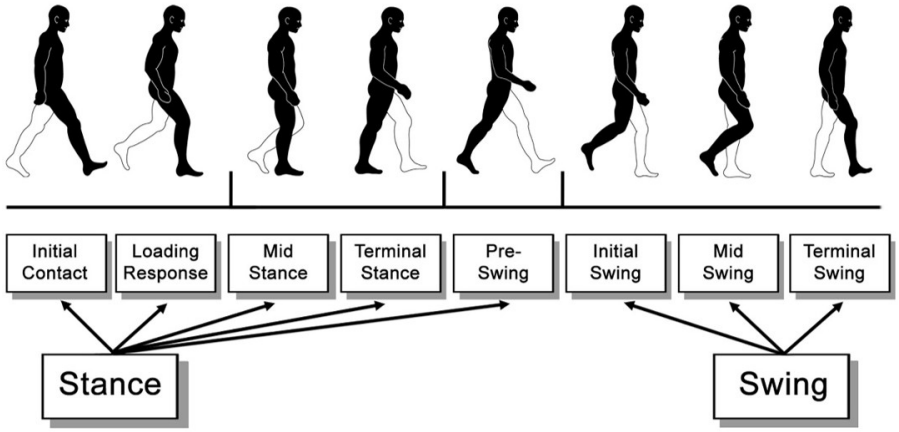

Figure 3.2: Gait phases in a normal gait cycle adapted from [66].

1. Initial Contact: This is the instant when the foot contacts the ground. This is important to observe as it affects the next phases.

2. Loading Response (0-10% of gait cycle): This is the initial double stance period. This begins with the initial contact and continues until the other foot is lifted up for swing.

3. Mid Stance (10-30% of gait cycle): This begins at the end of loading response, while the other foot is lifted from the ground and continues until the body weight is aligned over the forefoot.

4. Terminal Stance (30-50% of gait cycle): This period completes the period

of single support. It starts with heel rise and continues till the other foot strikes the ground.

5. Pre-swing (50-60% of gait cycle): This is the final phase of stance in the gait cycle. It begins with the initial contact of the opposite limb and ends with the ipsilateral toe-off. The objective of this phase is for positioning the limb for swing.

6. Initial swing (60-73% of gait cycle): This phase begins with lifting the foot from the floor and ending when the swinging foot is opposite the stance foot.

7. Mid swing (73-87% of gait cycle): This phase begins when the swinging foot is opposite the stance foot and ends when the swinging limb is forward and the tibia is vertical (i.e., hip and knee flexion postures are equal).

8. Terminal swing (87-100% of gait cycle): This final phase of swing begins with a vertical tibia and ends when the foot strikes the floor. During this phase, the limb advancement is completed (deceleration of the swing limb) and there is preparation for stance.

Each gait phase has a functional objective and the sequential motion of these phases enables the limb to attain the tasks of weight acceptance, limb support and limb advancement. Based on the analysis of gait phases, the movement of the limb based on the orientation of the leg segments can be deduced.

3.3.2 Techniques for Gait Analysis

In order to analyse human motion, the standard technique is by utilising high-speed cameras to capture the human motion. Studies have been done by integrating the three-dimensional motion using multi or single camera systems and

reaction force measurement to track the movement of human body parts in a complex [67–70]. However, this technique of optical motion analysis requires complex signal conditioning and is time consuming in nature. It also needs to be pre-calibrated, thereby making it expensive and limited to laboratory research. For the application in daily life with different environments, it is imperative for the gait monitoring system to be flexible, low-cost and wearable in nature. To implement this philosophy of home-based rehabilitation and tele-rehabilitation, many kinds of wearable (body-fixed) sensor system based on single or multiple accelerometer and gyroscope combinations can be utilised [71–74]. This would especially be useful for monitoring and detecting the early signs of tissue damage for lower limb amputees' activities outside of a laboratory [75–78].

Wearable sensor systems for biomedical applications in gait monitoring can be used in two different ways: one is about walking feature assessment for daily physical activities [79–86], wherein the data obtained from inertial sensors - accelerometer or gyroscope, are directly used as inputs of some inference techniques; and another direction is for determining the joint angle, body position and orientation accurately by fusing the data of different inertial sensors so as to decrease the errors of the quantitative human motion analysis [87]. In this research, the data from accelerometer and gyroscope is combined to estimate the shank angle of the amputee's residual limb, so our approach focuses on the second option for quantitative human motion analysis [87].

3.3.3 Accelerometer and Gyroscope Sensor Development

Inertial Measurement Unit (IMU)or inertial sensors, measure acceleration, angular rate and sometimes the magnetic field vector of a body in their own three-dimensional local coordinate system [65]. An IMU detects the current change

in position by using the accelerometer and detects changes in rotation like yaw, pitch, and roll by using the gyroscope. In this capacity, the IMU can be utilised in a number of applications like the inertial guidance systems, manned or unmanned landers on air and spacecraft and also serve as orientation sensors in the human field of motion. In this research, the InvenSense MPU-6050 sensor, as seen in Figure 3.3, was used to monitor the angular movement of the residual limb. This sensor contains a Microelectromechanical Systems (MEMS) accelerometer and a MEMS gyro in a single chip with 6 Degree of Freedom (DOF) with a footprint of 4 mm x 4 mm x 0.9 mm. This implies that there are 3 accelerometers, and 3 gyrosocopes inside the unit which are capable of measurement in the x, y and z direction. For precision tracking of both fast and slow motions, the parts feature a user-programmable gyro full-scale range of ± 250, ± 500, ± 1000, and $\pm 2000^{\circ}$/sec (dps), and a user-programmable accelerometer full-scale range of ± 2g, ± 4g, ± 8g, and ± 16g. Additional features include an embedded temperature sensor and an on-chip oscillator with $\pm 1\%$ variation over the operating temperature range [88].

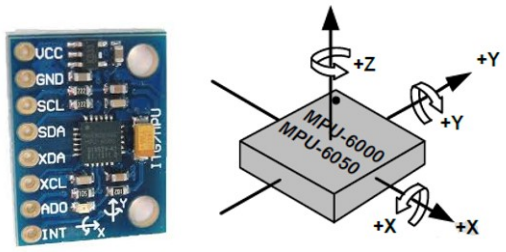

Figure 3.3: Schematic of the MPU-6050 sensor adapted from [89, 90].

Because the accelerometer measures all the forces working on the system, it is quite prone to noise. The data from the accelerometer is reliable in long term and so a low pass filter can be used. The gyroscope on the other hand, has a tendency to drift significantly over a period of time. Since the gyroscope data is reliable only on short term, a high pass filter can be utilised. Many algorithms for

determining the sensor orientation estimation have been proposed [91]; however in this work, in order to estimate the absolute angle is derived by combining the accelerometer and gyroscope data using a complementary filter. The integration of the output of a gyroscope θ_{gyro} feeds into a high pass filter and the output of an accelerometer θ_{accel} feeds into a low pass filter as seen in Figure 3.4.

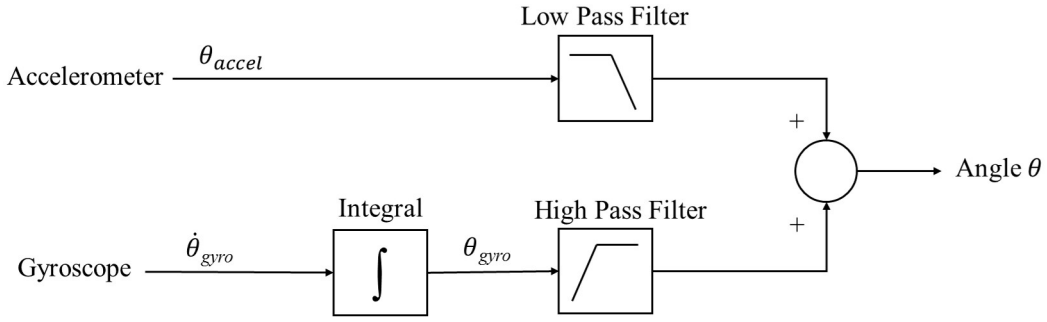

Figure 3.4: Schematic of the Complementary filter

The basic concept of this filter is to enhance advantages of each sensor. For example, the angular estimation using a gyroscope has a good accuracy in the sense of angular direction at high frequencies and the angular estimation using an accelerometer has a good accuracy at low frequencies. Hence for the complementary filter, if *G(s)* is the low pass filter for the accelerometer then the high pass filter for the gyroscope is *1-G(s)*. These can be written as in Equations 3.1 and 3.2 where τ is the time constant and determines the filter cut-off frequencies.

$$G(s) = \frac{1}{1+\tau s} \tag{3.1}$$

$$1 - G(s) = \frac{\tau s}{1+\tau s} \tag{3.2}$$

The transfer function of the angle θ of the complementary filter can be written as

$$\theta = \frac{1}{1+\tau s}\theta_{accel} + \frac{\tau s}{s(1+\tau s)}\dot{\theta}_{gyro} = \frac{\theta_{accel} + \tau\dot{\theta}_{gyro}}{1+\tau s} \tag{3.3}$$

Digitizing this and using backward difference yields Equation 3.4 as

$$1 + \tau s = (1 + \frac{\tau}{\Delta t}) - \frac{\tau}{\Delta t}z^{-1} \tag{3.4}$$

Substituting this in Equation 3.3 and rearranging leads to

$$\theta_k = \alpha(\theta_{k-1} + \dot{\theta}_{(gyro)k}\Delta t) + (1-\alpha)\theta_{(accel)k} \tag{3.5}$$

where $\alpha = {}^{\tau}/_{\tau + \Delta T}$. For this design, the optimum filter coefficient is 0.98 which is computed by running the filter at different time constants with a fixed sampling rate of 25 Hz. It should be noted that the lower the time constant, the more horizontal acceleration noise will be allowed to pass through.

3.3.4 Results and Analysis

For the gait analysis study, amputee subject 1 pulled out due to medical conditions. Hence, the gait cycle is studied for amputee subject 2 only. The determinants of gait are generally taken as either the hip angle, knee angle or the ankle angle. The placement of an IMU for an amputee on the hip, knee or ankle would be needed to be supported by a brace and would be thus obtrusive for their normal gait pattern. Therefore, in order to monitor the gait of the amputee subject, the IMU sensor was positioned on the shank of the prosthetic limb. The acceleration and the angular velocity in the x, y and z direction are recorded from

the IMU sensor at a frequency of 25 Hz when the amputee subject 2 followed the experimental protocol as described in section 3.2 at ambient temperatures of 10°C, 15°C, 20°C, and 25°C. Following this protocol where the residual limb skin temperature and the elevation angle at the shank were measured simultaneously will help in determining the gait pattern at varying activity and ambient temperature levels. Figure 3.5 shows the mounting of the IMU on the residual limb. The sensor's local coordinate axis were visually oriented to align with the anatomical axes. In this research because of the positioning of the IMU, the elevation angle of the shank was of interest for analysing the gait pattern. Shank angle θ_{shank} was defined as the angle between the shank segment and the vertical direction.

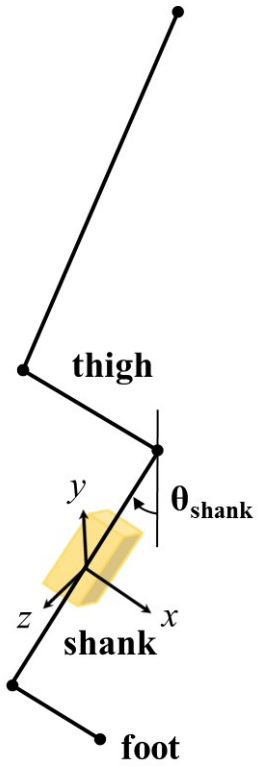

Figure 3.5: Shank angle definition for the lower limb kinematic model for an amputee subject.

Figure 3.6 indicates the acceleration, angular velocity and the computed shank

angle in the y direction of the amputee subject at an ambient temperature of 10°C during the 35 minute experimental protocol for Dataset B. The region of interest in the clinical trial is when the amputee subject 2 is walking on the treadmill for 10 minutes. Analysing this would give insight into the movement of the residual limb with the corresponding shank angle during the gait cycle. As seen in Figure 3.7, an off-line analysis was made to study the leg motion during the walking period for an 8 seconds timeframe at an ambient temperature of 10°C. In order to do so a complementary filter was designed (as described earlier) to estimate orientation of the shank. A MATLAB script was written to process the experimental data (detailed in Appendix A). Similarly, the orientation angle of the shank is computed for ambient temperatures of 15°C, 20°C, and 25°C as seen in Figures 3.8-3.10. The orientation of the shank angle during walking phase is always contained within $\pm 10^{\circ}$ which is what is expected from a amputee subject [92].

From Figures 3.7-3.10 it can be observed that, the shank angle profile of the amputee subject have been consistent in all ambient temperatures. Also the computed shank angle for all the ambient temperatures of Dataset A were very similar to those seen for Dataset B. This is important as it highlights that the performance of the IMU sensor with the complementary filter produces repeatable results for shank angle. The main advantage of this approach is its ability to provide 3D evaluation of the shank orientation. This can also be extended by attaching IMUs to the foot and the thigh of the amputee subject for an overall evaluation of knee kinematics which is seen in [76].

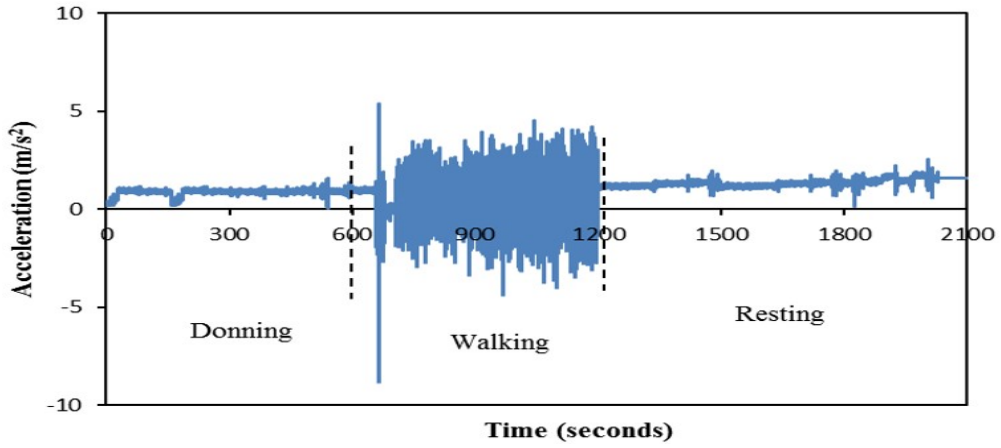

(a)

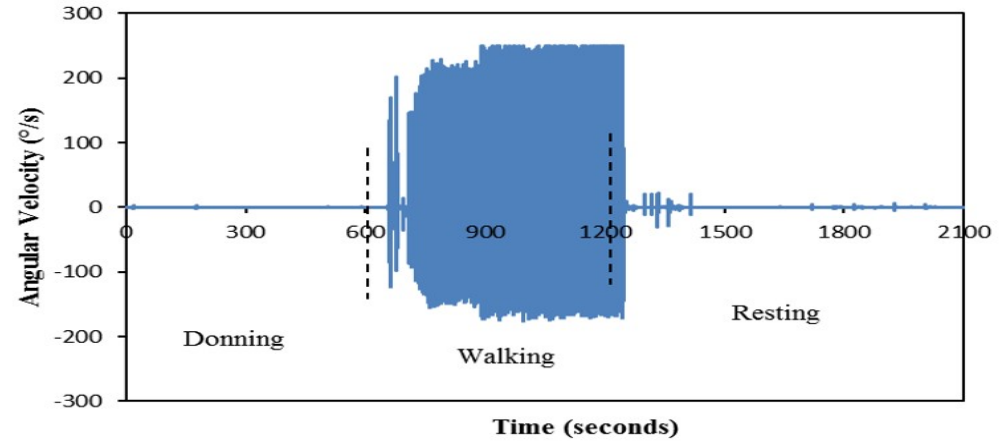

(b)

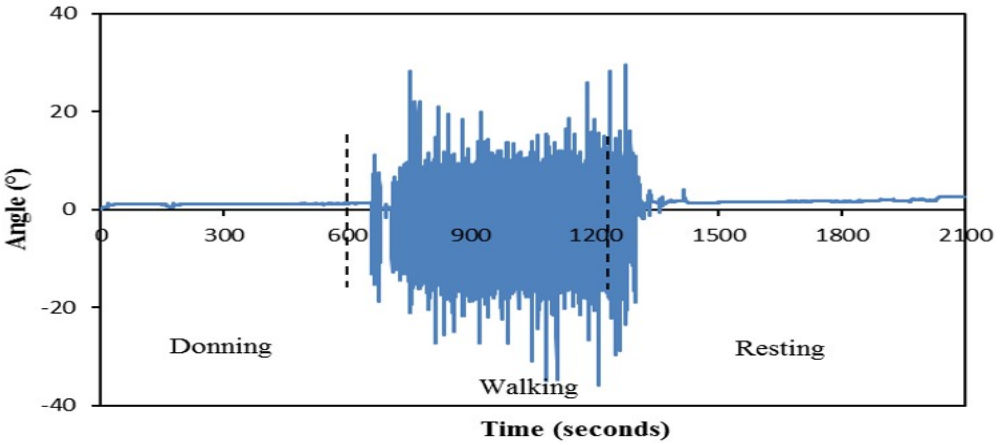

(c)

Figure 3.6: (a) Measured acceleration (b) Angular velocity (c) Shank angle obtained by the implementation of complementary filter at an ambient temperature of 10°C.

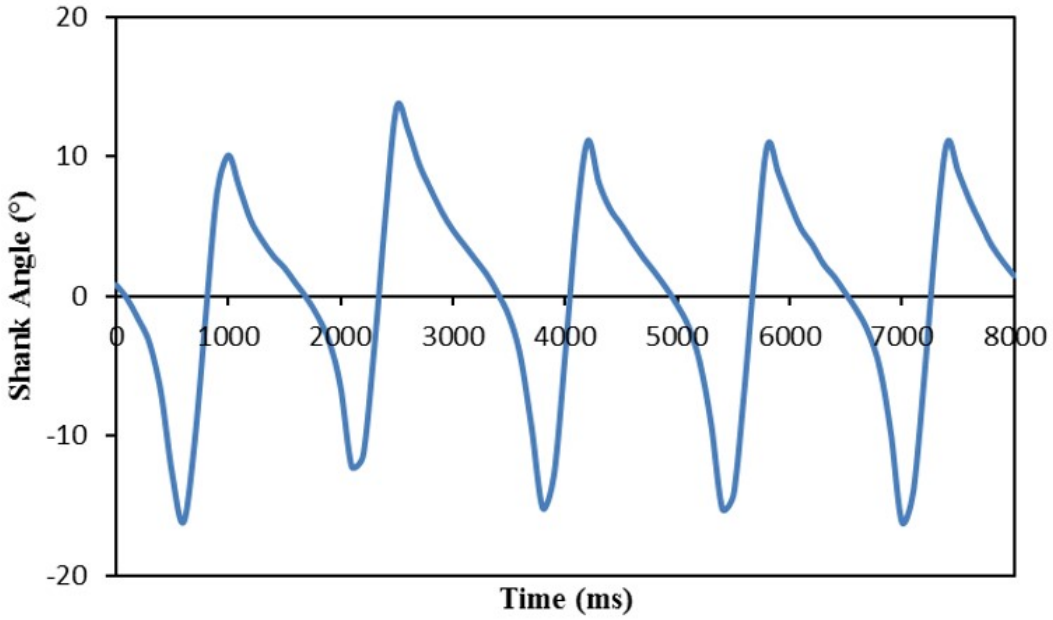

Figure 3.7: Estimation result of the rotational angle at the shank at an ambient temperature of 10°C.

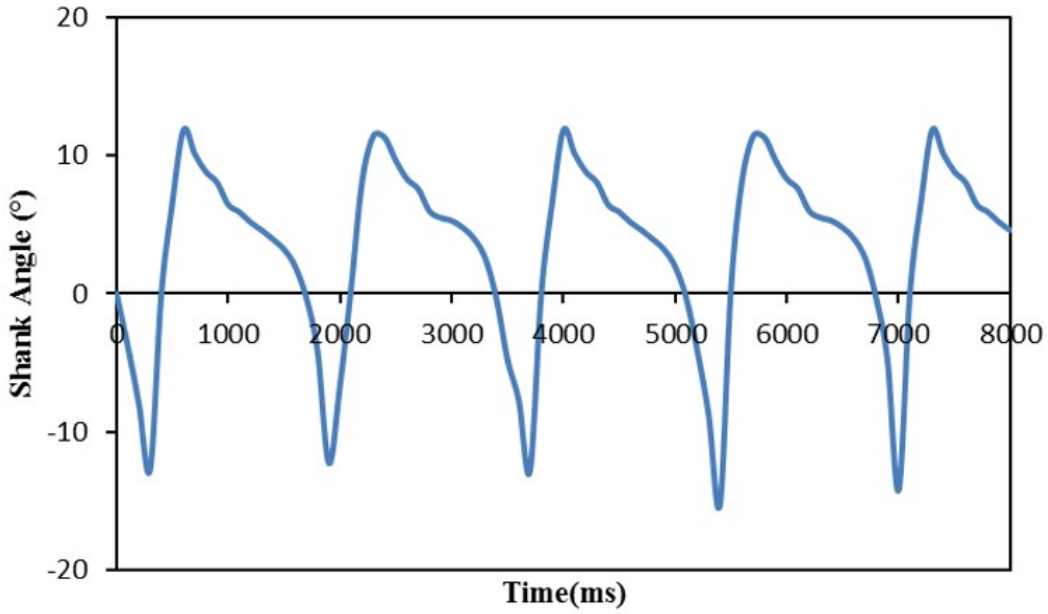

Figure 3.8: Estimation result of the rotational angle at the shank at an ambient temperature of 15°C.

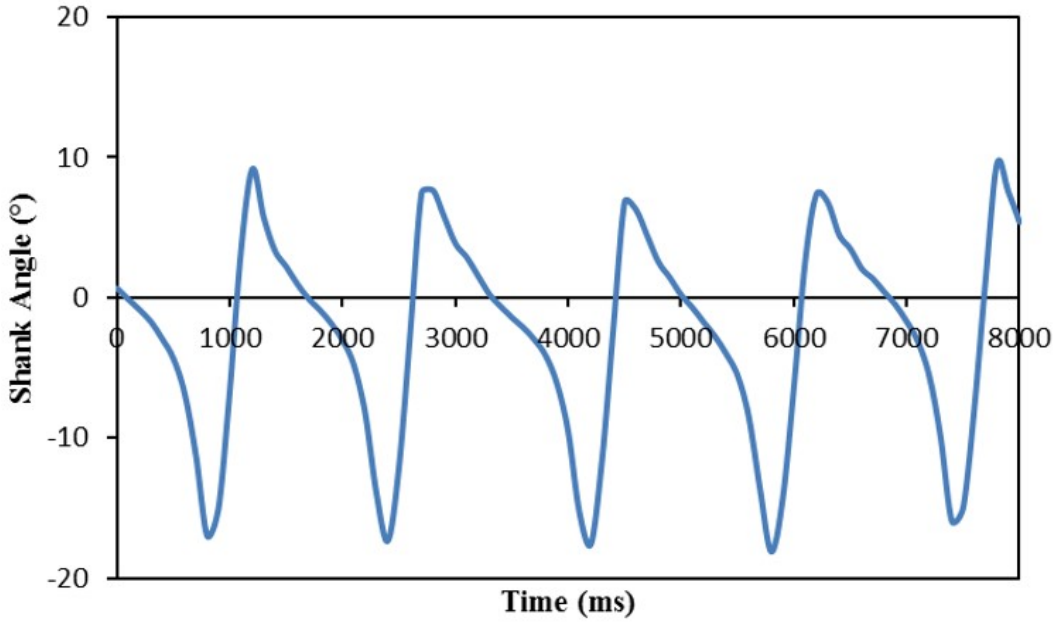

Figure 3.9: Estimation result of the rotational angle at the shank at an ambient temperature of 20°C.

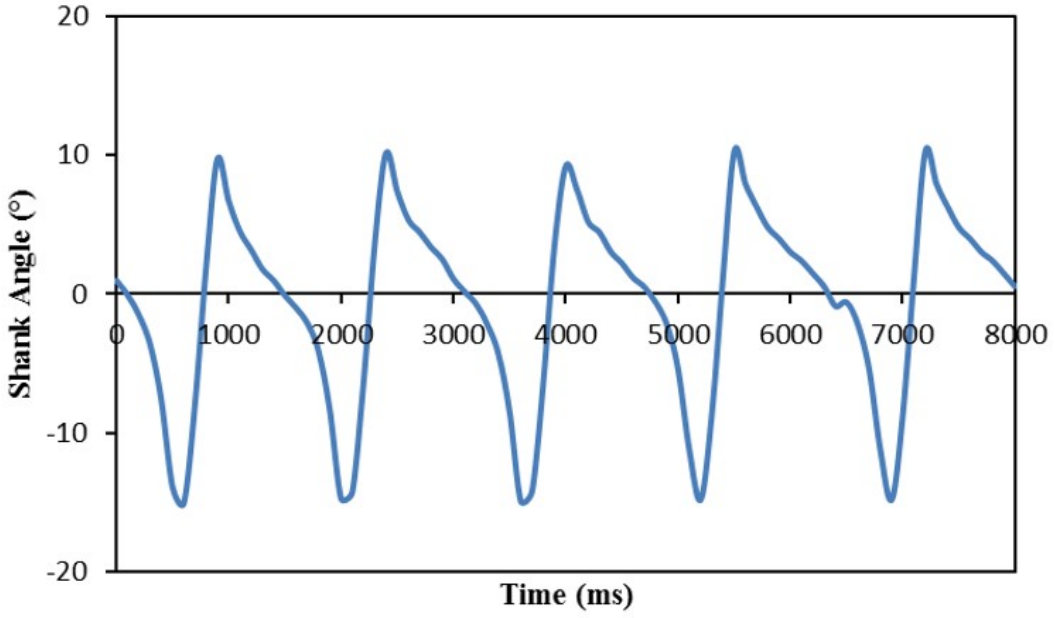

Figure 3.10: Estimation result of the rotational angle at the shank at an ambient temperature of 25°C.

The phases of the gait pattern on the IMU sensor were calibrated with mea-

surements of a commercial high-speed cameras. In order to determine the gait phase from the IMU sensor, the movement of the amputee's residual limb is captured using a 4K video capture using a high-speed camera. The camera is capable of shooting video at 120 frames per second in HD 720p. The climate-controlled chamber where the measurements were done was a medium lighted room to minimise noise due to high sun activity. The camera and the wearable system were synced in time, such that both the IMU data and the video from the camera could be correlated by their timestamps. The amputee subject with the positioned wearable platform while walking on the treadmill for 10 minutes was video recorded. For each measurement, a single video file was created using the camera software. Using video editing tools, videos were edited such that only one full gait cycle was left from the original file video. The shank angle so deduced by fusing the accelerometer and gyroscope data is then linked with the gait cycle video to correctly analyse and identify the gait phase. From Figure 3.11 it can been seen that using this technique, the Initial Contact (Toe Off) and Heel Strike can be identified.

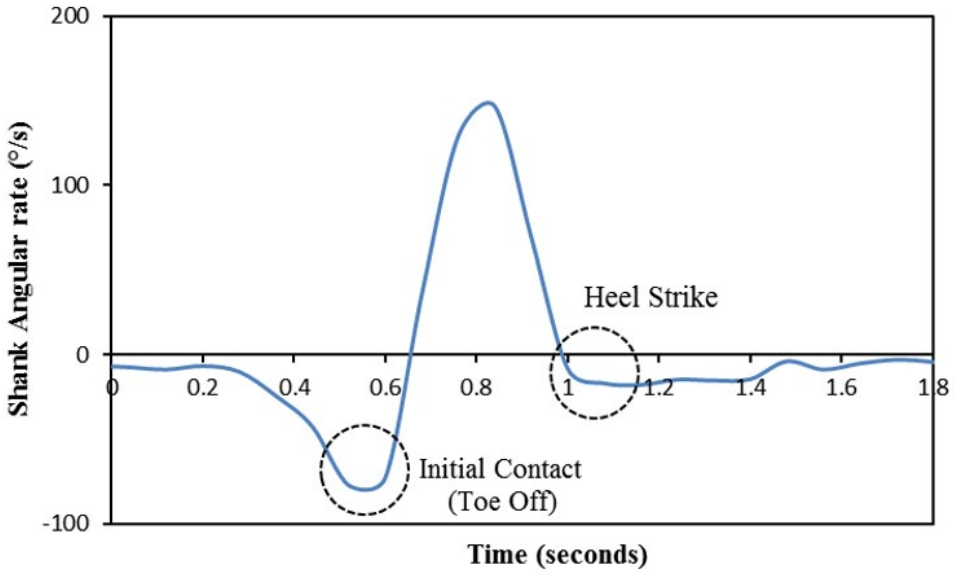

Figure 3.11: Gait cycle illustrating Toe Off and Heel Strike portions.

Further from Figure 3.12, various phases of the gait during one gait cycle can be correlated with the angular velocity obtained from the gyroscope and the shank angle computed by fusing the inertial sensor data.

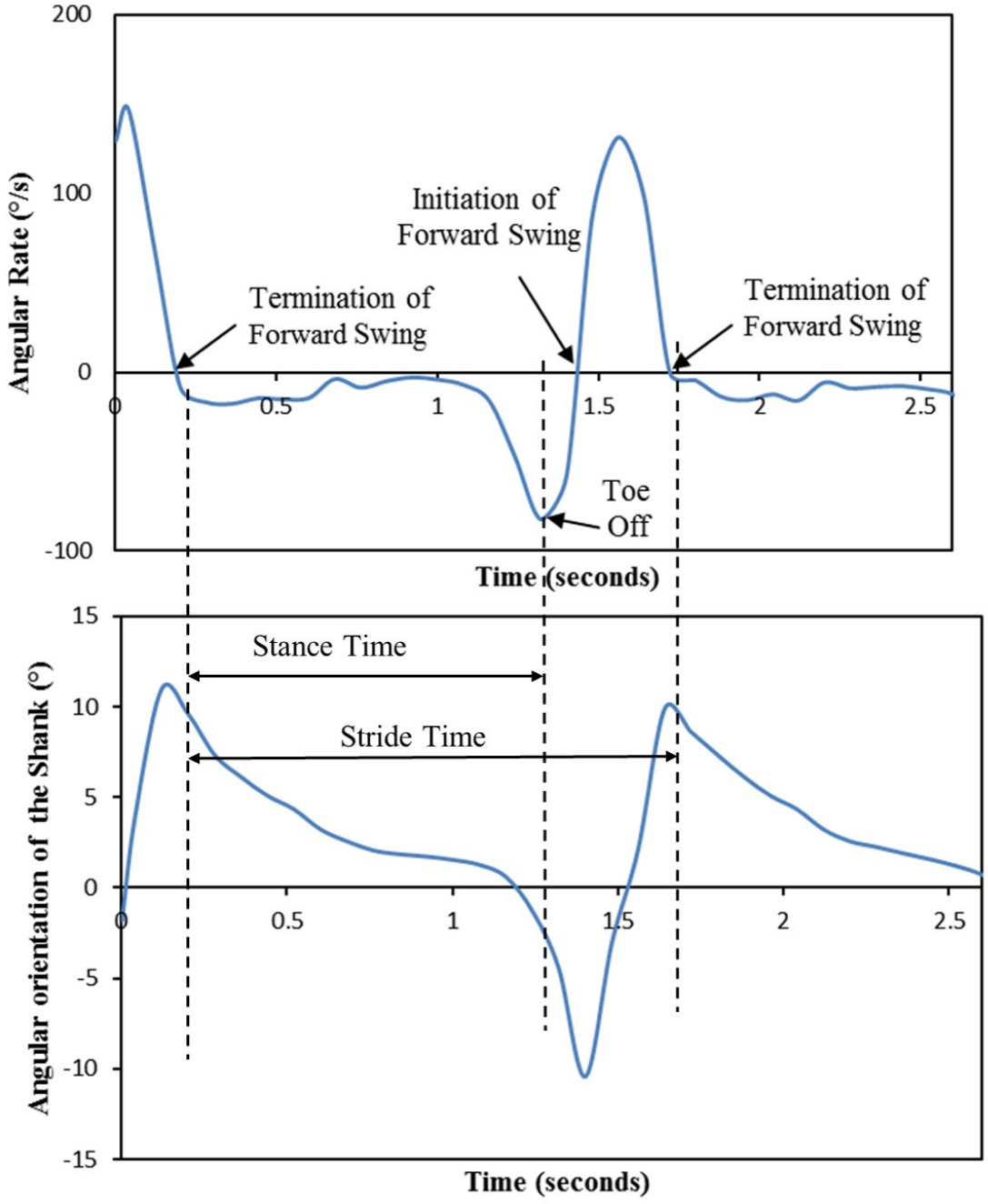

Figure 3.12: Identification of gait events for one gait cycle.

The usage of the IMU sensor along with the complementary filter, has helped in analysing and deducing the phases of the gait of amputee subject 2. The normal gait pattern was consistent for all ambient temperatures. This technique is capable to determine the abnormal gait pattern of the subject as the sensor has been calibrated for the same.

3.4 Residual Limb Skin Temperature Measurement

Monitoring and predicting the residual limb skin health in lower limb amputees is of principal importance as the socket of the prosthesis creates a warm and humid microenvironment that encourages growth of bacteria and skin breakdown [93,94]. Elevated residual limb skin temperature is considered one of the major factors that could affect the health of soft tissues in that region [95–99]. The results presented in [100] suggested that some prosthetic components can act as a barrier to conductive heat transfer due to low thermal conductivity. This implies that different liner and socket materials produce a different thermal environment and, hence, can lead to different residual limb skin temperatures [101,102]. This leads to a hypothesis that if the thermal properties of the socket and liner materials are known, then the in-situ skin temperature could be predicted by monitoring between socket and liner. The purpose of this is to assess whether or not a temperature measurement device can accurately measure the temperature of the residual limb when it is placed either on the inner or outer surface of a prosthetic socket. If that is achievable, then the monitoring of the residual limb skin temperature can be done without undesirable contact of any temperature sensor with the skin thus avoiding any increased skin irritation. The next sections

investigate how differing activity levels and ambient temperatures influence the in-socket temperature.

3.4.1 Data Analysis

The temperature profiles of the liner and residual limb skin at ambient temperatures of 10°C, 15°C, 20°C, and 25°C from set B for Subject 1 and Subject 2 are discussed in the following subsections respectively. From the studies on the amputee subjects, it is seen that donning causes a moderate temperature increase as also reported in [103], walking causes a significant increase, and the rest periods following activities must be substantially long to return the limb to temperatures before donning the prosthesis.

3.4.1.1 Results: Subject 1

Figures 3.13 and 3.14 indicate that the residual limb temperature profile for ambient temperatures of 10°C and 15°C has a similar pattern of being steady throughout the experiment. However, this temperature profile of the residual limb is significantly different from that at ambient temperatures of 20°C and 25°C as illustrated in Figures 3.15 and 3.16.

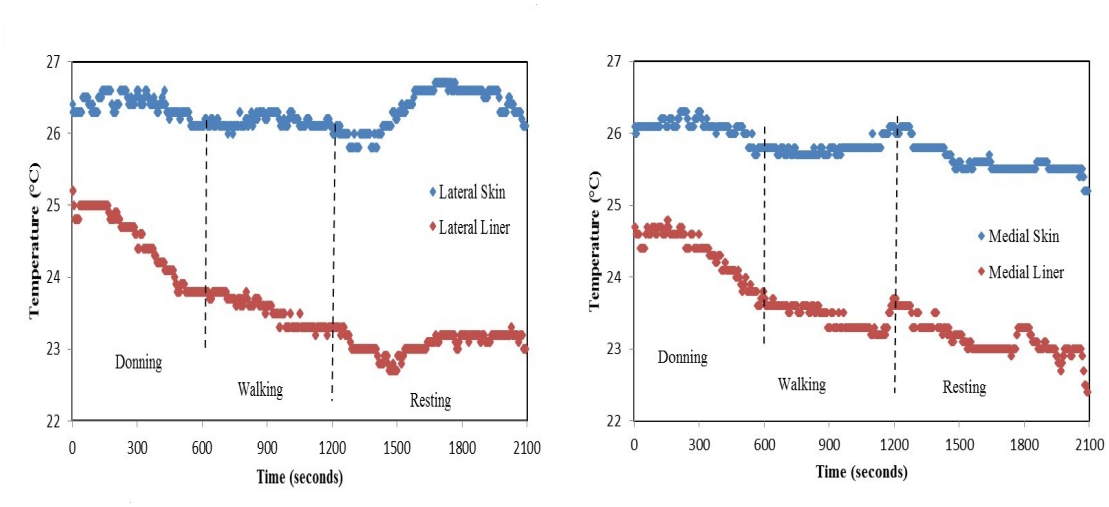

(a) (b)

Figure 3.13: Profiles of residual limb skin and liner temperature of Subject 1 at ambient temperature of 10°C at (a) lateral side (b) medial side.

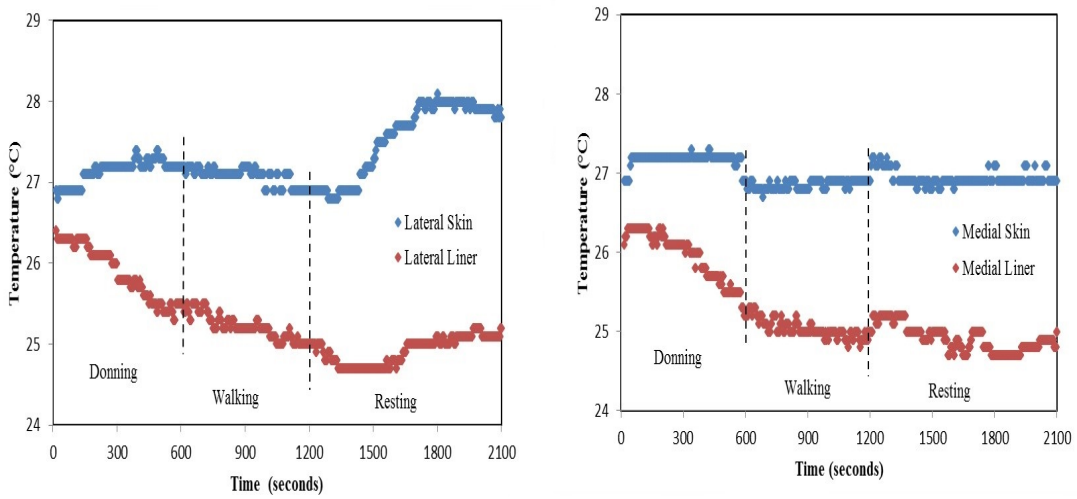

(a) (b)

Figure 3.14: Profiles of residual limb skin and liner temperature of Subject 1 at ambient temperature of 15°C at (a) lateral side (b) medial side.

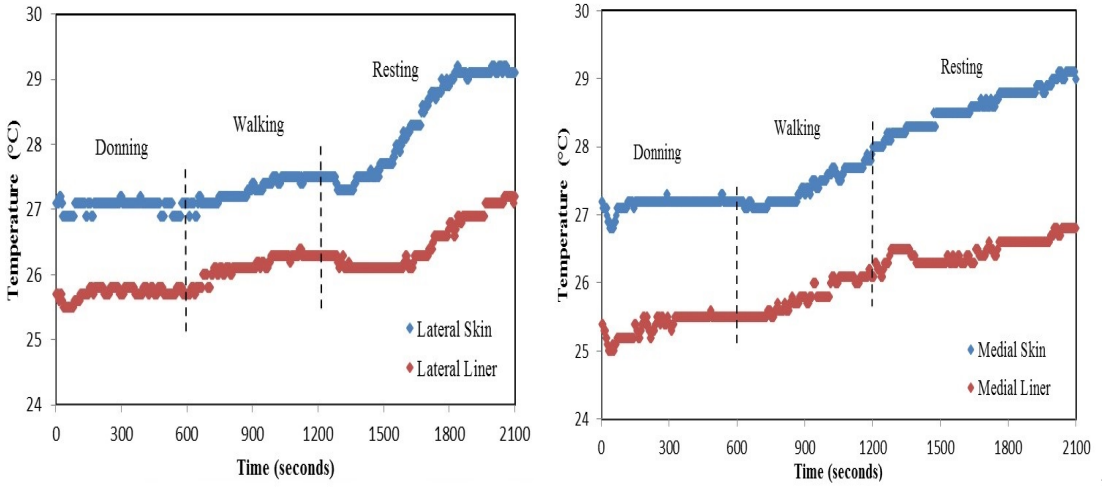

(a) (b)

Figure 3.15: Profiles of residual limb skin and liner temperature of Subject 1 at ambient temperature of 20°C at (a) lateral side (b) medial side.

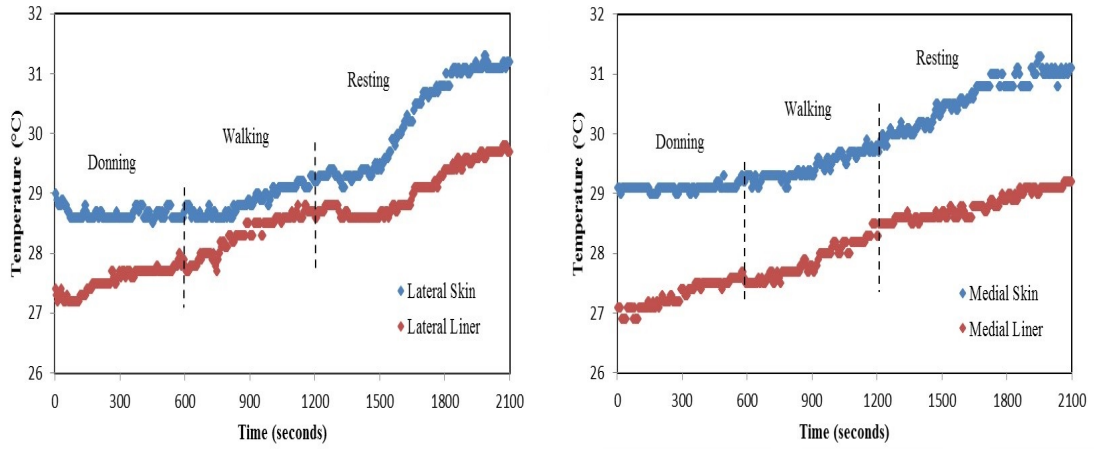

(a) (b)

Figure 3.16: Profiles of residual limb skin and liner temperature of Subject 1 at ambient temperature of 25°C at (a) lateral side (b) medial side.

Both the lateral and medial residual limb skin temperatures showed a steady increase in the temperature throughout the experiment. After the end of the experiment, the temperatures in both lateral and medial side were 2.1°C higher than the starting.

3.4.1.2 Results: Subject 2

Figures 3.17 and 3.18 indicate that the residual limb temperature profile for ambient temperatures of 10°C and 15°C have a similar pattern of being steady throughout the experiment. However, this temperature profile of the residual limb is significantly different from that at ambient temperatures of 20°C and 25°C as indicated in Figures 3.19 and 3.20.

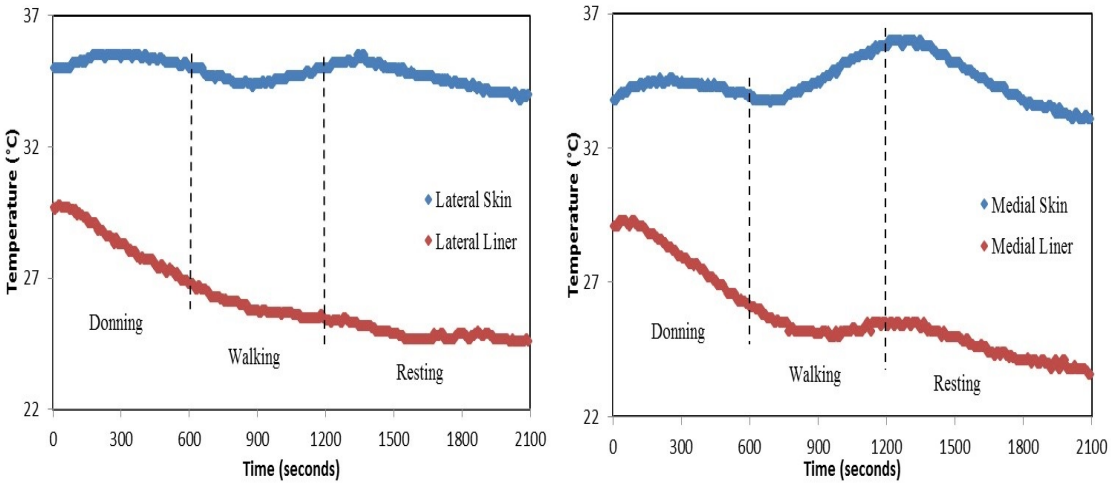

(a) (b)

Figure 3.17: Profiles of residual limb skin and liner temperature of Subject 2 at ambient temperature of 10°C at (a) lateral side (b) medial side.

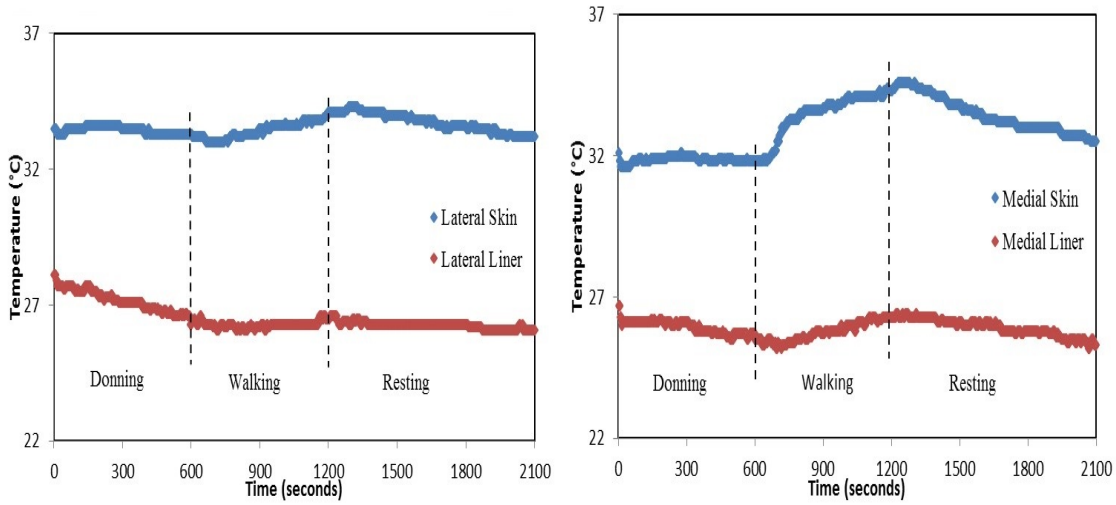

(a) (b)

Figure 3.18: Profiles of residual limb skin and liner temperature of Subject 2 at ambient temperature of 15°C at (a) lateral side (b) medial side.

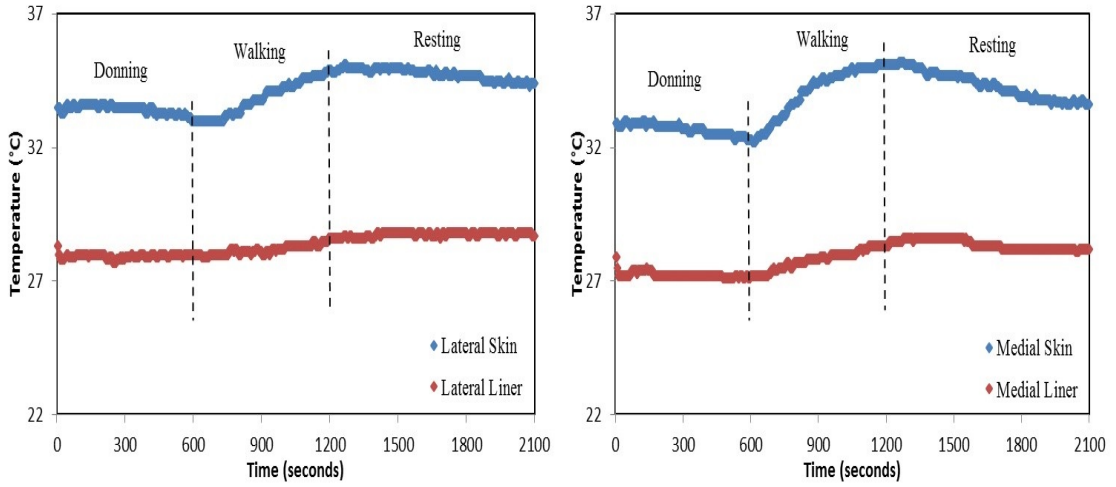

(a) (b)

Figure 3.19: Profiles of residual limb skin and liner temperature of Subject 2 at ambient temperature of 20°C at (a) lateral side (b) medial side.

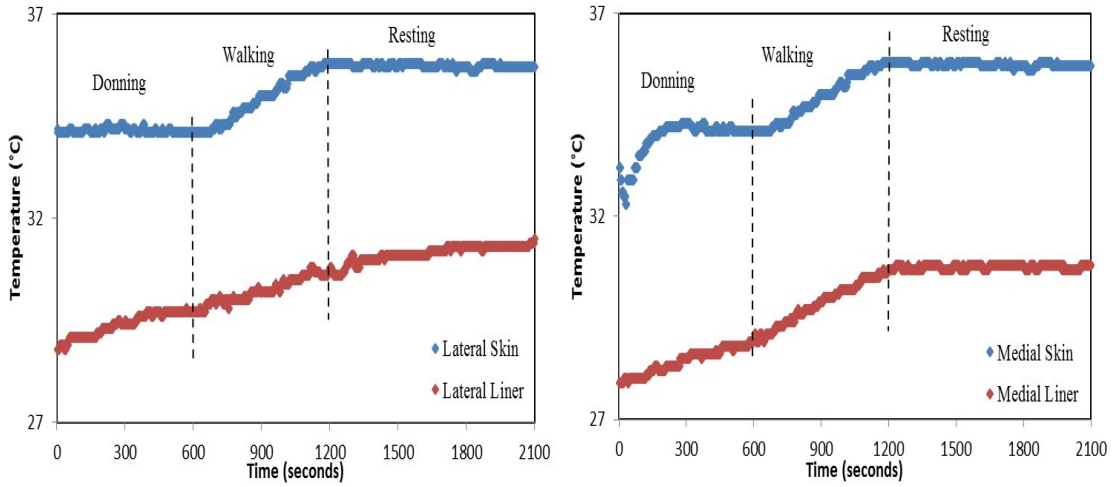

(a) (b)

Figure 3.20: Profiles of residual limb skin and liner temperature of Subject 2 at ambient temperature of 25°C at (a) lateral side (b) medial side.

3.4.2 Discussion

The above results are indicative of the fact that the residual limb skin temperature behaviour is a function of ambient temperature. However, as expected the residual limb temperature for both the amputees is different from each other. This is because every individual's physiological response to the ambient temperature change is different. This reflects that though the human body self regulates to maintain a stable internal environment despite changes in the external environment, in case of prosthetic users there are layers of liner and socket materials which inhibit the body's ability to thermoregulate effectively.

3.5 Summary

By monitoring the residual limb skin temperatures (for amputee subjects 1 and 2) and the gait pattern (for amputee subject 2), the state of residual limb health can be addressed. By performing the clinical trials in the environmental chamber at different ambient temperatures, it was established the residual limb skin temperature is a function of ambient temperature. However, the normal gait pattern remains unaffected by the same. This behaviour of the residual limb temperature can be exploited to design mathematical models like GPML and ANFIS which are detailed in the later chapters. Also, the gait pattern is calibrated for different phases and can be used to contrast between the normal and abnormal gait of amputee subject 2.

Chapter 4

Thermal Characterisation of Materials Used in Lower Limb Prosthetics

4.1 Introduction

The core temperature of the human body remains constant throughout the day by a process known as thermoregulation, despite internal heat production and variation of environmental temperature [104]. It comprises of a series skin, brain and visceral thermoreceptors, a control mechanism in the central nervous system and a series of different effectors [105]. This system works on negative feedback control, that is, the thermoreceptors sense an increase in temperature that is analysed by the control mechanism hypothalamus), which in turn causes a response from the effectors to lose more heat e.g. by vasodilation of blood vessels or by increasing the perspiration rate. The opposite happens if the thermoreceptors sense a decrease in skin temperature. The range of normal human body temperature is small and it varies between individuals [105]. Heat is generated

in the body through chemical (metabolism) and physical (shivering) processes. During Adenosine Triphosphate (ATP) production, around 75% of the energy is converted to heat [105]. Of the remaining 25%, the majority is also converted to heat except that which is used for voluntary muscle control [101]. This constant generation of heat within the body must be controlled correctly. If the heat loss does not occur at the same rate of heat production, then an increase in the core body temperature would occur. Conversely, if the heat loss occurs more rapidly than the heat production, then the core body temperature would decrease.

Heat generated within the core body must be transferred to the skin in order to be released to the environment. This is essential for maintaining a steady thermoregulatory state. In the human body this transfer occurs by blood convection and by tissue conduction [102] . This is the first stage in thermoregulation; the next step involves the transfer of this heat from the skin periphery to the environment. Heat is transferred from the body to the environment by conduction, convection, radiation and evaporation from the skin.

The mechanism that provides the main source of heat loss in the human body is evaporation. The previous three mechanisms lose heat by surrendering it to the environment, thus, effectively diminishing the temperature gradient that exists. Evaporation, however, can occur without a temperature gradient, so long as moisture is present on the skin. This prevents overheating in situations such as when the skin temperature and ambient temperature are equal [104]. Heat is lost from the skin as a result of moisture evaporating from the skin to the surrounding environment.

In lower limb prosthetic users, the skin plays a major role in thermoregulation of the body via radiation of heat. The prosthesis creates an environment where this heat transfer is influenced by the insulating properties of commonly used socket materials and liners. These materials inhibit the body's ability to radi-

ate heat effectively [100] and may be a cause of the reported thermal discomfort mentioned earlier. Although the mechanical properties of these materials have been well documented [106–108] less is known about how these materials transfer heat [55, 56, 100]. Before the issue of thermal discomfort can be studied, further investigation of the thermal properties of prosthetic materials is required. This would be useful in enabling the clinicians to identify which materials are the least effective at transferring the heat radiating from the human body to the outside environment.

The residual limb skin temperature and its corresponding liner temperature greatly depend upon the thermal properties of the prosthetic materials in use. The thermal conductivities of the different liner and socket materials have been investigated by Klute et al [100]. They assessed single layers of the prosthetic socket material and found that both thermoplastic and carbon fibre socket materials had very similar thermal conductivities. The above study investigated only individual layers of the socket and liner materials. However, prosthetic sockets are composed of two, sometimes three layers of differing materials and there is a need to define the effect of the thermal properties of these layers in combination. In this study, experiments were conducted to determine the thermal time constant of single layer of materials, and then those materials were combined in various combinations to give a more realistic representation of a prosthetic socket.

The advantage of evaluating the thermal time constant of the prosthetic materials over any other thermal properties like thermal conductivity, specific heat or heat transfer coefficient is the simplicity in its measurement and calculation and also implementation in the mathematical algorithms.

4.2 Thermal Time Constant Measurement

According to the law of thermodynamics, heat transfer F, from the heat source to the test material at a given time is proportional to the difference in temperature between the heat source and test material

$$-F = hA_s(T(t) - T_h) \tag{4.1}$$

where h is heat transfer coefficient,A_s is the surface area, *T(t)* is temperature of the test material at time t, and T_h is the constant temperature of the heat source. The addition of heat leads to the rise in temperature of test material which is given by

$$\rho c_p V(\frac{dT}{dt}) = F \tag{4.2}$$

where ρ is the density, c_p is the specific heat and V is the volume of the test material. Equating these two equations for heat transfer,

$$\rho c_p V(\frac{dT}{dt}) = -hA_s(T(t) - T_h) \tag{4.3}$$

This can be further rewritten as

$$\frac{dT}{dt} = \frac{1}{\tau}(T(h) - T) \tag{4.4}$$

Here the time constant τ can be defined as

$$\tau = \frac{\rho c_p V}{hA_s} \tag{4.5}$$

This implies that the time constant is indicative of temperature response of the material. When the temperature of the heat source is constant, the rate of change

of the test material temperature is given by

$$\frac{d\Delta T}{dt} = -\frac{1}{\tau}\Delta T \tag{4.6}$$

where $\Delta T = T - T_h$. Solving this equation gives the difference between the temperature of the test material and the heat source ΔT as a function of time t

$$\Delta T(t) = \Delta T_0 e^{-t/\tau} \tag{4.7}$$

where ΔT_0 is the initial temperature difference between the test material and the heat source, at time $t = 0$. This indicates that the rate at which the temperature of the test material approaches the heat source temperature slows exponentially. Thus, the time constant that is derived from the principles of heat transfer provides a much simpler method to envision the thermal behaviour of a material. In order to measure the degree of thermal responsiveness of the prosthetic material, the thermal time constant τ is evaluated which is defined as the time required for the material at a certain temperature to reach 63.2% of the specified final temperature.

To explore the thermal properties of these materials when used individually and in combination, a number of liner and socket materials of dimension 100 mm x 100 mm were selected to provide a range representing those commonly used by lower limb amputees. Table 4.1 lists the socket and liner specimens along with their thickness used in the study. The experimental setup included a heat source (heating tape Omega Engineering: 13 mm x 1.22 m, 312 W, 240 V) whose temperature could be controlled through a Proportional-Integral-Derivative (PID) controller. The other equipments used were Solid State Relay (SSR) to provide safety to the circuit; 10-pin terminal block to allow connection of all devices; K-type thermocouples and a 4-channel thermocouple thermometer. The idea is to

duplicate the cross section of the prosthesis by arranging the heating tape (which would be maintained at a steady temperature by the PID controller and would be emulating a section of residual limb of the amputee), liner and socket materials on top of each other.

Table 4.1: Socket and Liner materials used for the study

Name	Material	Thickness (mm)
Alpha Locking (Liner)	Co-polymer	6
Iceross Comfort (Liner)	Silicone	6
Iceross Original (Liner)	Silicone	3
OttoBock Technogel (Liner)	Polyurethane	6
Pe-lite (Liner)	Closed cell foam	5
Stump sock	Terry	0.7
Thermoplastic (Socket material)	Co-polymer polypropylene	4.7
Thermosetting lay-up (Socket material)	Compound of materials	4
Carbon fibre lay-up (Socket material)	Compound of materials	4.8

The heat source was the heating tape which lay flat on a 15 cm x 15 cm sheet of aluminium with an identical sized sheet of aluminium then placed on top of the heating tape forming a sandwich. The two sheets of aluminium were secured to each other by string from the heating tape. This circuit also incorporated a SSR and a terminal block. The SSR was used as a switch in the circuit receiving a small input voltage from the PID controller and controlling a larger output voltage of the heating source. The terminal block was required to make all the connections possible. The temperature of the heating tape was measured using a type K thermocouple that was also connected to the PID controller. This thermocouple provided feedback to the PID controller of the temperature on its surface, and the controller could make the necessary adjustments to the system to get the desired heating tape temperature. Figure 4.1 indicates the schematic

of the experimental setup described above.

In order to determine the reliability of the experimental setup, the system was switched on and a set point of 29°C was selected. It was noted that the experimental setup reached this temperature steadily and held it there successfully. Additionally, when the temperature was increased by 1°C to 30°C, the circuit increased the temperature and also held it at the new set point of 30°C. This process was repeated, increasing by 1°C until 40°C was reached. From this process it was decided that the heating tape and PID controller provide sufficient control of the temperature for the experiment to proceed.

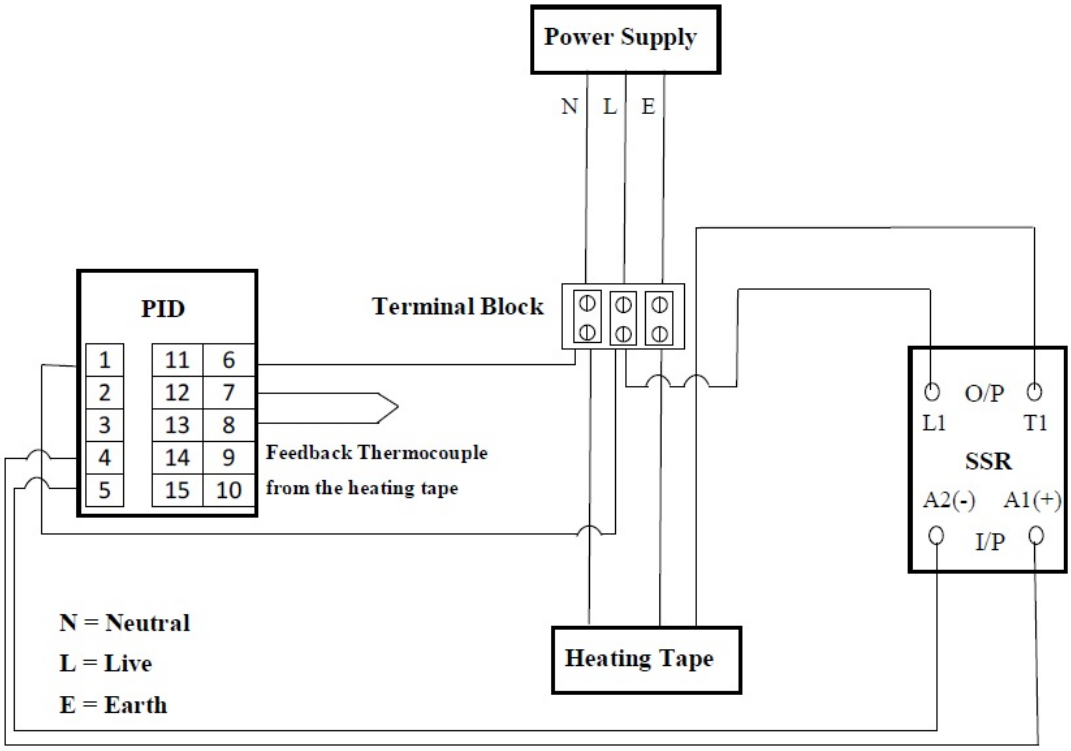

Figure 4.1: Schematic of the experimental setup utilised for measuring the thermal time constant of prosthetic materials.

4.3 Experimental Process

The heating tape was to be heated to 30°C and the circuit given sufficient time to come to rest. The temperature of the heating tape T_1 was measured using one of the type K thermocouples. Full contact of the thermocouple was ensured by using using polyimide adhesive tape labels (rated to 100°C). All data was collected on a computer connected to the thermocouple data logger and analysed using software provided with it. The prosthetic materials (liner and socket) were first tested individually to study their thermal behaviour in terms of the time constant. Along with the thermocouple on the heating tape, a second thermocouple was placed on the outer surface of the test material to measure the temperature at this point T_0. Figure 4.2 is a diagrammatic representation of this set up. Recording began at 30°C and only stopped when $T_1 = T_0$, or T_0 had come to a steady temperature. The material was removed from the heating tape and allowed to cool to the room temperature. Simultaneously the temperature of the heating tape was increased by 2°C and allowed to reach a steady temperature. The material was then placed back on the heating source and the data was recorded again. This process was repeated for increasing values of T_1 by 2°C until 40°C was reached. Data collected by the thermocouple data logger and software was the temperature of the heating tape T_1, the temperature of the outer surface of the prosthetic material under test T_0 and the length of experiment (time). This routine was repeated until all the materials (as in Table 4.1) had been tested individually. Once all the materials had been individually tested, the next stage involved measuring the temperature profile of the liner and socket material when used together. This was done by placing the socket material on top of the liner material and then putting this stack of materials on the heating tape.

Similar to the testing individual materials, thermocouples were placed on the outer surface of the each of materials liner and socket. Figure 4.3 shows a

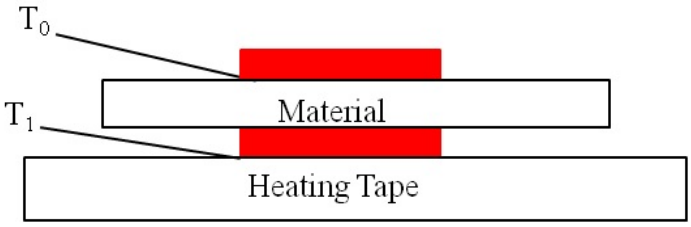

Figure 4.2: Schematic of the experimental setup utilised for measuring the thermal time constant of prosthetic materials.Schematic illustrating the placement of the prosthetic material (either liner or socket) on the heating tape. Interface temperatures T_1 and T_0 are measured by thermocouples.

diagrammatic representation for testing of these two stacked materials. Data collection was only stopped this time when $T_1 = T_3$, or T_3 ceased to increase in temperature. Data collected was temperature of the heating tape T_1, temperature of the outer surface of the liner material T_2, temperature of the outer surface of the socket material T_3 and duration of experiment. A number of two-layer prosthetic material combinations were tested. Measurement followed the same procedure as described above i.e. beginning at 30°C and rising by 2°C until 40°C, then the materials were changed and measurement was repeated again for combinations listed in Table 4.3. All the experimentation was done in an ambient temperature of 22°C.

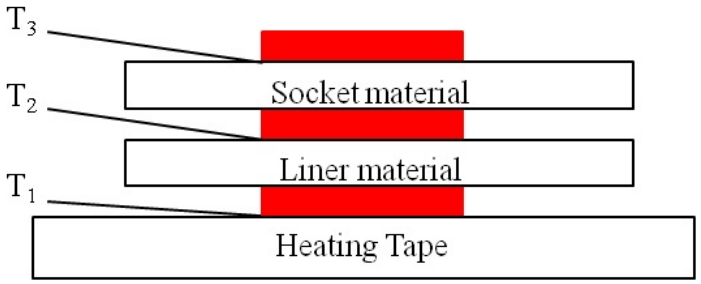

Figure 4.3: Schematic illustrating the placement of the liner and socket material on the heating tape. Interface temperatures T_1, T_2 and T_3 are measured by thermocouples.

When the prosthetic materials were tested individually, it was noted that as the set point temperature of the heating tape T_1 was increased, the maximum tem-

perature reached by the material T_0 increased and so did the difference between the set point temperature and material temperature $T_1 - T_0$. This is indicative of the fact that with increasing temperature T_1, more heat is transferred through the material, but the amount of heat lost in the process is also increased. Similarly, it was observed that when liner-socket materials are tested together, then with the increase in the set point temperature of the heating tape T_1, the maximum temperature reached by the liner material T_2 and socket material T_3 increased. Moreover, the difference between the set point temperature and material temperatures namely $T_1 - T_2$ and $T_1 - T_3$ recorded a rise as well. It also took them longer to reach a steady temperature than when they were tested individually. This indicates that the rate of heat transfer decreases when prosthetic materials are used in combinations.

4.4 Determination of Thermal Time Constant

The thermal profile of the prosthetic materials when tested individually or in combination with another material was obtained from the thermocouple data logger. The results indicated that the heat transfers through the prosthetic materials in a logarithmic fashion. There is an initial increase in the rate of heat transfer which decreases as time increases - and reaches a steady state at a temperature lower than that of the heating tape temperature.

Of all the two layer combinations that were tested, the combinations that were of most interest were the 6 mm thick polyurethane liner along with 4 mm thick thermosetting lay-up socket material and the 5 mm pelite liner with thermoplastic socket material as these are the most widely used liner-socket pair in practice. From Table 3.1 it can be noted that these combination of materials were used in the prosthesis set up of the two amputee subjects recruited for this study. The

thermal graphs recorded for the above mentioned materials when used individually and in combination are indicated in Figures 4.4 - 4.7. Figures 4.4 and 4.6 indicates the temperature profile of the respective liner and socket material when tested individually using the layup shown in Figure 4.2. It is observed that the interface temperatures T_0 when plotted against time follow a logarithmic profile and reaching steady state in the end.

The thermal response T_2 and T_3 of the above mentioned liner-socket combination when tested together using layup as shown in Figure 4.3, are indicated in Figures 4.5((a) and (b)) respectively. From the graphs it is evident that the thermal response of the materials is slower when they are used in combination than when they are used individually. These graphs were then used to calculate the thermal time constant of the prosthetic materials which would indicate the how quickly the heat flows from the source to the opposite end of the material.

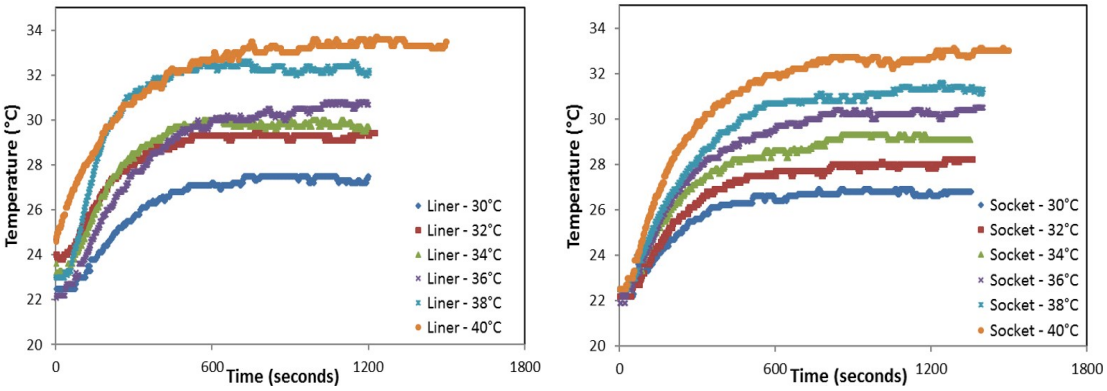

(a) (b)

Figure 4.4: Temperature profile of (a) Polyurethane Liner (b) Thermosetting Socket material at different heat source temperatures when tested individually using the experimental setup.

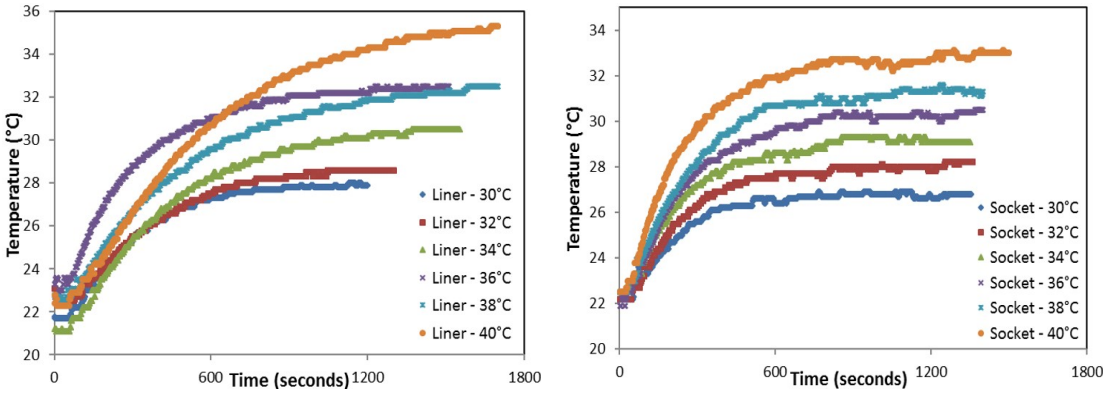

(a) (b)

Figure 4.5: Temperature profile of (a) Polyurethane Liner (b) Thermosetting Socket material at different heat source temperatures when tested in combination (by being placed on top of the other) using the experimental setup.

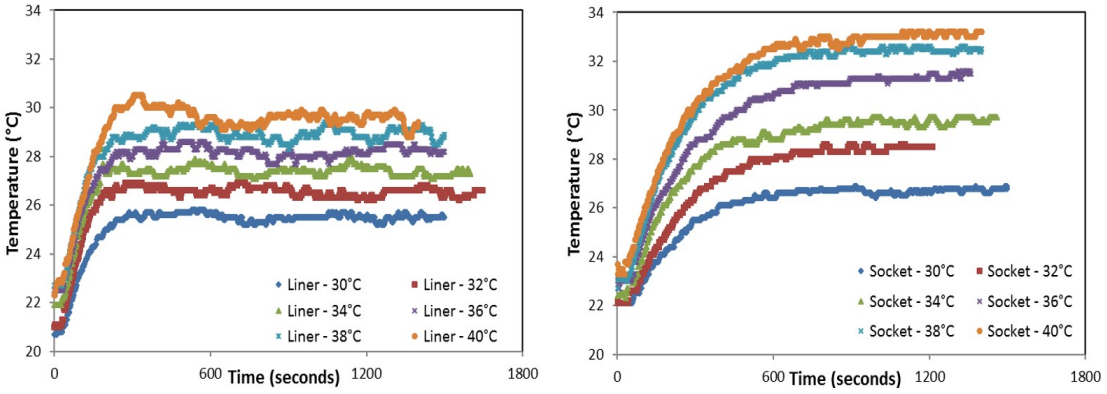

(a) (b)

Figure 4.6: Temperature profile of (a) Pelite Liner (b) Thermoplastic Socket material at different heat source temperatures when tested individually using the experimental setup.

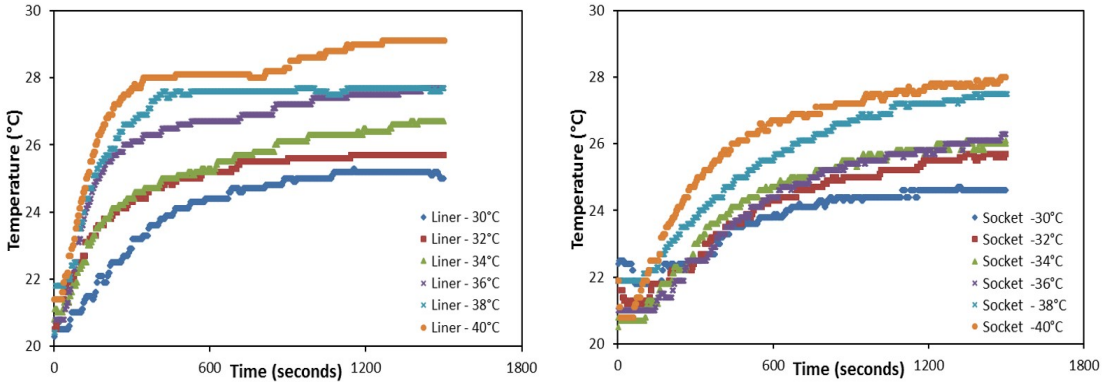

(a) (b)

Figure 4.7: Temperature profile of (a) Pelite Liner (b) Thermoplastic Socket material at different heat source temperatures when tested in combination (by being placed on top of the other) using the experimental setup.

Utilising this behaviour of the prosthetic materials, the thermal time constant τ is computed using the logarithmic method. Time constants are parameters of systems that obey first order, linear differential equations. Consider that the equation for the thermal response curve of the prosthetic test material is

$$x(t) = x(0)e^{-t/\tau} \tag{4.8}$$

where *x(t)* is the temperature of the test material at ambient time *t*, *x(0)* being the initial temperature response and τ being the thermal time constant indicating how quick is the system response. Taking the natural log of the response curve given by Equation 4.8,

$$ln[x(t)] = ln[x(0)] - \frac{t}{\tau} \tag{4.9}$$

Equation 4.9 can be thought of as a straight line with the thermal response plotted against time. This implies that if the temperature of the test material is plotted w.r.t time, then the slope of the line is the time constant and the intercept is the natural log of initial value. Using this concept, the temperature profile of the material when tested individually or in combination with another material as recorded by the data logger, can be utilised to compute the thermal time constant.

The steps below detail the logarithmic method technique used to determine the thermal time constant when a prosthetic material is tested individually.

1. The steady state temperature of the material T_{0ss} is determined.

2. The temperature at ambient time T_0 is subtracted from the steady state value so that an exponentially decaying dataset is created.

3. The natural log of the exponentially decaying data as computed in step 2 $ln[x(T_{0ss}) - x(T_0)]$ is taken and plotted w.r.t time. Using regression, a line of best fit is generated and the slope is computed. The slope is a measure of the thermal time constant.

Similar procedure is adopted when a prosthetic material is used in combination with another material i.e. when a liner and socket material are used together. However, it should be noted that for the same, the steady state temperature at the liner interface of the combination T_{2ss} is used and not T_{3ss}. This is because the mathematical model that is used for non-invasive measurement, predicts the residual limb temperature by measuring the liner temperature and hence, the thermal time constant at the liner interface of the combination is of interest. Hence, the generation of an exponentially decaying data is done by subtracting the liner temperature at ambient time T_2 from T_{2ss}.

As in step 3, $ln[x(T_{2ss}) - x(T_2)]$ is plotted w.r.t. time and the slope of line is indicative of the thermal time constant of the liner-socket material combination measured at the liner interface. Figures 4.4(a) and 4.5(a) illustrate the temperature profile of the polyurethane liner when used individually and in combination (with thermosetting socket material) respectively which is then utilised to compute the thermal time constant by the method described above.

4.5 Results

Thermal time constant is essentially the same for all starting temperatures. The process to determine the thermal time constant as described above, is repeated for different heat source temperatures (from 30°C - 40°C, with increasing intervals of 2°C). This is done in order to confirm the accuracy of time constant value of the liner when used individually or in combination of a socket material and rule out any experimental errors. Hence Tables 4.2 and 4.3 indicate the value of τ for polyurethane liner when used individually as well as when it is tested in combination with a thermosetting socket material respectively at different heat source temperatures. Similarly, Tables 4.4 and 4.5 indicate the value of τ for pelite liner when used individually as well as when it is tested in combination with a thermoplastic socket material respectively at different heat source temperatures. The thermal time constant for 6 mm polyurethane liner when used in combination with thermosetting lay-up socket material is approximately 5.4 minutes whereas when it is tested individually the average value of is 2.8 minutes. Additionally, the thermal time constant for 5 mm pelite liner when used in combination of thermoplastic socket material is approximately 6.7 minutes whereas when it is tested individually the average value of is 1.6 minutes.

Table 4.2: Time Constant of Polyurethane Liner when used individually at different test temperatures

Source Temperature (°C)	Steady State Temperature (°C)	Time Constant (minute)
30	27.5	2.9
32	29.3	2.9
34	29.7	2.7
36	30.0	2.9
38	32.4	2.7
40	32.6	2.8

Table 4.3: Time Constant of Polyurethane Liner when tested in combination with Thermosetting Socket material at different test temperatures

Source Temperature (°C)	Steady State Temperature (°C)	Time Constant (minute)
30	27.9	5.3
32	28.6	5.4
34	30.5	5.4
36	32.5	5.2
38	32.2	5.4
40	34.1	5.7

Table 4.4: Time Constant of Pe-lite Liner when used individually at different test temperatures

Source Temperature (°C)	Steady State Temperature (°C)	Time Constant (minute)
30	25.8	1.7
32	26.9	1.6
34	28.0	1.5
36	28.6	1.6
38	29.4	1.6
40	30.5	1.7

Table 4.5: Time Constant of Pelite Liner when tested in combination with Thermoplastic Socket material at different test temperatures

Source Temperature (°C)	Steady State Temperature (°C)	Time Constant (minute)
30	25.7	6.7
32	26.1	6.6
34	26.7	6.6
36	27.7	6.7
38	28.3	6.7
40	29.4	6.7

The thermal time constants for the prosthetic materials (when used individually), as listed in Table 4.1, were also determined using the procedure described. The results of the same as in Table 4.6 do confirm to [100] and suggest that the prosthetic materials can act as a barrier to conductive heat transfer due to their low thermal conductivity or high thermal time constants. From the results it can be observed that there is substantial variation in the time constants of liner materials, whereas the prosthetic socket materials have similar time constants.

Thus, it can be concluded that the selection/combination of prosthetic materials have a considerable impact on the residual limb skin temperature as they can produce different thermal environments. This can be further seen in Table 4.7 where the time constants of some of the widely used liner socket combinations are detailed.

The results indicated that as the temperature of the heat source was increased, the rate of heat transfer and the maximum value of heat transfer also increased. Along with this, the amount of heat loss increased as the temperature of the heat source increased. It was also found that different prosthetic materials transfer heat at different rates and that they also transfer different amounts of heat. Further to this, when these materials are placed in combinations, the rate of heat transfer is slower and the maximum amount of heat transferring through the materials is also decreased.

Table 4.6: Time Constants for Liner and Socket materials when evaluated individually

Material	Thermal Time Constant τ (minute)
Alpha Locking (Liner)	3.6
Iceross Comfort (Liner)	3.1
Iceross Original (Liner)	2.6
Ottobaock Technogel (Liner)	2.8
Pe-lite(Liner)	1.6
Stump sock	0.6
Thermoplastic (Socket material)	4.0
Thermosetting lay-up (Socket material)	4.1
Carbon fibre lay-up (Socket material)	4.5

Table 4.7: Time Constants of the Liner and Socket materials when evaluated in a combination

Combination of Prosthetic Materials	Thermal Time Constant τ (minute)
OttoBock Technogel (Polyurethane liner 6mm) with Thermosetting lay-up (socket material 4mm)	5.4
Iceross Comfort (Silicone liner 6mm) with Carbon fibre lay-up (socket material 4.8mm)	5.5
Iceross Original (Silicone liner 3mm) with Carbon fibre lay-up (socket material 4.8mm)	4.1
Iceross Comfort (Silicone liner 6mm) with Thermosetting lay-up (socket material 4mm)	5.8
Alpha Locking (Co-polymer liner 6mm) with Carbon fibre lay-up (socket material 4.8mm)	6.2
Pe-lite (Closed cell foam liner 5mm) with Thermoplastic (socket material 4.7mm)	6.7

4.6 Summary

The residual limb skin temperature depends on the ambient temperature and the activity level of the subject. Moreover, a major factor is the thermal time constant of the materials used in the prosthesis. Owing to the low thermal conductivity of the prosthetic materials, it can restrict the heat transfer from the residual

limb and create a warm microenvironment within the prosthesis [**109**]. Hence, it becomes all the more imperative to build in the existing mathematical model the thermal time constant so obtained from the thermal studies. Therefore, if the thermal properties of the socket and liner materials are known, then the in-socket residual limb temperature can be accurately predicted. This can be achieved by monitoring the temperature between the socket and liner (rather than skin and liner) and thereof using mathematical algorithms like Gaussian Processes technique and Artificial neuro fuzzy inference system.

Chapter 5

Residual Limb Skin Temperature Prediction using Gaussian Processes for Machine Learning

5.1 Introduction

This chapter describes the development of a supervised mathematical algorithm - Gaussian Processes for Machine Learning (GPML) to predict the residual limb temperature of the amputee. Predicting the in-socket residual limb temperature by monitoring the temperature between socket and liner rather than skin and liner could be an important step in alleviating complaints on increased temperature and perspiration in prosthetic sockets. Additionally, this technique of contactless monitoring of the residual limb skin temperature would be without any practicality issues with prosthetic use in a domestic situation such as, protruding lead wiring, consistent positioning of sensors and possible skin irritation and discomfort. The aim of this chapter is to verify the hypothesis that if the thermal properties of the socket and liner materials are known, then the *in-situ* skin tem-

perature could be predicted by monitoring between the socket and the liner. The purpose of this is to assess whether or not a temperature measurement device can accurately measure the temperature of the residual limb when it is placed either on the inner or outer surface of a prosthetic socket. If that is achievable, then the monitoring of the residual limb skin temperature can be done without undesirable contact of any temperature sensor with the skin thus avoiding any increased skin irritation. The accuracy of the predictive GPML model was compared to the actual residual limb skin temperature which by virtue of its operating principle offers greater accuracy and precision. An overview of the Gaussian processes model is firstly presented followed by a description of its predictive capability and the results of data analysis.

5.2 Gaussian Processes for Machine Learning

Gaussian Process (GP) models are extensively used to perform Bayesian nonlinear regression and classification - tasks that are central to many machine learning problems. In the regression task, the goal of the Gaussian Process technique is to infer a continuous function *f(x)* from a training set of input-output pairs in supervised learning context. A Gaussian Process is a collection of random variables, any finite number of which have joint Gaussian distributions [110]. The key assumption in Gaussian Process modelling is that the data can be represented as a sample from a multivariate Gaussian distribution. Therefore, it could be totally specified by the mean and covariance function as seen in Equation 5.1.

$$p(f|X) = \chi(\mu, C) \tag{5.1}$$

Here $p(f|X)$ is the conditional probability of the inferring function f if the corresponding input is X. $\chi(\mu, C)$ denotes a Gaussian distribution with mean μ and covariance C. A Gaussian Process model can be thought of as a prior probability distribution over functions in Bayesian inference. This enables deducing the hyperparameters for the model which are an indication of the precision and relevance of the input parameters for predicting the output. Thus, a Gaussian process regression model is a fully probabilistic Bayesian model by nature unlike most other regression techniques, which only provide a best estimate of *f(x)*. This is a high level overview of GP, which uses probabilistic predictions of possible interpolating functions f to solve the regression problem [111].

5.2.1 Gaussian Process Definition

A Gaussian process model infers a joint probability distribution over all possible outputs for all inputs. This form enables the implementation of Bayesian framework in a simple way [110, 111]. Bayes' theorem states that the posterior probability of a condition is given by the product of the prior probability and the likelihood in the light of the evidence. This can be written as

$$\overset{posterior}{P(B|A,H)} = \frac{\overset{likelihood}{P(A|B,H)}\overset{prior}{P(B|H)}}{\underset{evidence}{P(A|H)}} \tag{5.2}$$

$P(B|A,H)$ is the posterior probability that statement B is true, given that condition A is observed and that hypothesis H is correct. $P(A|B,H)$ is the probability of observing A if B is true and H is correct, which is called the likelihood. $P(B|H)$ is the prior probability of B being true, without having made any observations. $P(A|H)$ is the evidence: the probability of observing A if hypothesis H is correct [111].

The inference of a joint probability distribution function involves deducing a number of quantities called the hyperparameters Θ. These hyperparameters are an indication of the precision and relevance of the input parameters for predicting the output. Thus, the aim in a Gaussian process model is to choose model parameters for which the probability of the training data is maximised [110].

5.2.2 Covariances

To specify a particular GP prior, we need to define the mean μ and covariance C of Equation 5.1. The GP model used in this study assumes that the priors in use have a zero mean. If the training data contains N points comprising of outputs y_N with its corresponding inputs x_N, then the Gaussian model is defined by N dimensional covariance matrix C_N. The covariance matrix is basically indicative of the closeness to each other outputs for different inputs, taking into account the model parameters. This allows predictions of outputs y_* to be made, based on the difference between the new inputs x_* and those seen in the training data. Each element of C_N is defined by covariance function C_f, which is a function of inputs and hyperparameters [110–112]. For the element ij in covariance matrix $C_{ij} = C_f(x_i, x_j, \Theta)$. The covariance function can be user defined. The particular choice of covariance function determines the properties of sample functions drawn from the GP prior (e.g. smoothness, length scales, amplitude etc.). Therefore, it is an important part of GP modelling to select an appropriate covariance function for a particular problem. In this study, the Squared Exponential (SE) covariance function was used. The SE covariance function is the most widely used in machine learning. It provides very smooth sample functions that are infinitely differentiable:

$$C_f(x_i, x_j, \Theta) = \theta_1 e^{-\frac{(x_i - x_j)^2}{2l^2}} + \sigma_n^2 \delta_{ij} \tag{5.3}$$

where the set of hyperparameters $\Theta = \{\theta_1, l, \sigma_n\}$ and δ_{ij} is the kronecker delta function. The value of $\delta_{ij} = 1$ if $i = j$ and is zero for all $i \neq j$. The first term in the above equation allows the closeness of two outputs to be related to the closeness of the inputs. The length scale l for an input parameter indicates how much the output will vary relative to changes in an input.

5.2.3 Gaussian Process Regression

To prepare for Gaussian process regression, the covariance function as seen from Equation 5.3 is calculated for all possible combinations of inputs. This is summarised as matrices in the following equations:

$$C_N = \begin{bmatrix} C_f(x_1, x_1) & C_f(x_1, x_2) & \cdots & C_f(x_1, x_N) \\ C_f(x_2, x_1) & C_f(x_2, x_2) & \cdots & C_f(x_2, x_N) \\ \vdots & \vdots & \ddots & \vdots \\ C_f(x_N, x_1) & C_f(x_N, x_2) & \cdots & C_f(x_N, x_N) \end{bmatrix} \tag{5.4}$$

$$C_{N*} = \begin{bmatrix} C_f(x_*, x_1) & C_f(x_*, x_2) & \cdots & C_f(x_*, x_N) \end{bmatrix} \tag{5.5}$$

$$C_{N**} = C_f(x_*, x_*) \tag{5.6}$$

Since the key assumption in Gaussian process modeling is that the data can be represented as a sample from a multivariate Gaussian distribution, we have

$$\begin{bmatrix} y \\ y_* \end{bmatrix} \sim \chi \left(0, \quad \begin{bmatrix} C_N & C_{N*}^T \\ C_{N*} & C_{N**} \end{bmatrix} \right) \tag{5.7}$$

where T indicates the matrix transposition. The conditional probability $p(y_*|y)$: "given the data, how likely is certain prediction for y_*", follows a Gaussian distribution as in Equation 5.8.

$$y_*|y \sim \chi(C_{N*}C_N^{-1}y, C_{N**} - C_{N*}C_N^{-1}C_{N*}^T) \tag{5.8}$$

The reliability of the regression depends upon on the covariance function and in turn the hyperparameters. Typically, the values of the hyperparameters would not be known *a priori*. To get the optimal hyperparameters, Equation 5.2 can be written as

$$P(\Theta|y_N, x_N, C_f) = \frac{P(y_N x_N, C_f, \Theta)P(\Theta)}{P(y_N|x_N, C_f)} \tag{5.9}$$

Referring to Equation 5.9, it is apparent that the evidence is independent of hyperparameters and is constant for a given dataset. To find the optimal hyperparameters, the posterior probability is maximised as the prior maybe non-informative. This corresponds to minimizing the Negative Log Marginal Likelihood (NLML) as in Equation 5.10. Hence, for a particular training set and covariance function, the Gaussian process would select the best hyperparameters that give the best predictions for training data [111, 112].

$$logp(y|x, \Theta) = -\frac{1}{2}y^T C_N^{-1}y - \frac{1}{2}log|C_N| - \frac{N}{2}log2\pi \tag{5.10}$$

Several multivariate optimisation algorithms can be utilised to calculate the hyperparameters, such as Laplace's approximation, Markov Chain Monte Carlo sampling, KullbackLeibler optimal approximation, or the Variational Bayes' approximation. In the present study, kernel hyperparameters were optimised by the exact inference technique. For real-valued outputs, it combines the Gaussian process prior with a Gaussian likelihood and perform an exact posterior inference in closed form.

5.3 Gaussian Process Model Generation and Prediction

The data from the data logger indicated that at any given ambient temperature, the trace of the liner temperature follows that of the residual limb skin as observed in Chapter 3. This suggested a possibility to model the liner temperature as a function of the skin temperature and create a mathematical model of the same. The Matlab Gaussian Process Regression and Classification Toolbox [113] was used to write a script for processing (detailed in Appendix B). The model designed takes the liner temperature as the input x and the predicted output is the residual limb skin temperature y. To test the predictive capability of a model, it is trained on one set of data and tested on previously unseen data. It is seen from Chapter 3 that the skin temperature is dependent on ambient temperature. Hence, individual Gaussian process models for the lateral and medial side of the residual limb were designed, using the principle as described in the previous section for ambient temperatures of 10°C, 15°C, 20°C and 25°C. Consider the ambient temperature 10°C, first the lateral side model was trained on different scenarios to investigate the optimal training required. Table 5.1 presents the

different testing and training cases presented to the model for Subject 1. Initially the model was trained by 250 data points from set A. The training points are inclusive of the three stages of protocol (initial rest, walking, and final rest) and are picked in the ratio of time intervals used for the respective protocol periods. Hence, the first 70 points from initial rest, first 70 points from walking, and first 110 points from the final rest were taken for training. The predictive capability of the model is gauged by computing the training error, test error, and the normalized log likelihood by testing with 100 data points (not seen by the model during training) from set A which are again drawn in the ratio of time intervals used for the respective protocol periods. This process is continued by increasing the number of training data points from set A. The normalized log likelihood for each set of test data is also given, calculated by dividing the value of marginal likelihood by the number of points in the test set. It can be seen that as the number of training points increases, the error value decreases and the likelihood of the data increases. This implies that with greater training points, the new model either predicts data closely or has higher confidence due to a higher density of training points.

When the model is trained on all the values of set A and tested with 100 points (randomly picked from set A), the training error does decrease while the likelihood also decreases slightly. This might be an indication that too much of training to the model might lead to over fitting the data. Next the model trained on the entire set A was tested on 100 points in set B which were unseen by the model. The results indicated that the test error has a substantial increase, but the likelihood function is still consistent with the uncertainty predictions of the Gaussian model. This may be because the Dataset B is similar to Dataset A, leading to points closer to the smooth relationship predicted by the Gaussian process. A similar testing and training approach as described above is employed for deducing the optimum model for Subject 2. The summary of it can be seen

in Table 5.2.

Table 5.1: Summary of GPML for various testing and training scenarios for Subject 1

Training Set	Test Set	Training error (RMSE)	Test error (RMSE)	Number of training points	Number of test points	Normalized log likelihood
A	A	0.142	0.142	250	100	0.786
A	A	0.0924	0.0924	500	100	0.893
A	A	0.0913	0.0913	750	100	0.897
A	A	0.0910	0.0910	1050	100	0.895
A	B	0.0910	0.102	1050	100	0.896

Table 5.2: Summary of GPML for various testing and training scenarios for Subject 2

Training Set	Test Set	Training error (RMSE)	Test error (RMSE)	Number of training points	Number of test points	Normalized log likelihood
A	A	0.156	0.156	250	100	0.708
A	A	0.0987	0.0987	500	100	0.881
A	A	0.0927	0.0927	750	100	0.889
A	A	0.0912	0.0912	1050	100	0.886
A	B	0.0911	0.110	1050	100	0.888

In order to deduce the optimum hyperparameters, their initial values were selected as [0, 0, 0.1]. For the predictions to be in 95% confidence interval, the number of iterations that the model made is 435. However, if the length scale l for an input parameter is correlated to the heat transfer in prosthetic material by means of the thermal time constant, the GPML model converges at 100 iterations to generate the optimum hyperparameters. Hence, if the length scale in the covariance function is set to the thermal time constant of the materials used in the prosthetic limb, it would optimise the Gaussian process model and generalise it for amputee subjects with similar prosthesis setup. For Subject 1, the value of length scale is specified as 5.4, which is equal to the time constant of the materials used in his prosthesis setup. Similarly, for Subject 2, the length scale is defined to be 6.7. When l is specified, less number of iterations are required for the computation of other hyperparameters. This in turn minimises the log marginal likelihood function to give the best predictions. The results from this model (with the length scale equal to the thermal time constant) lie in 95% confidence interval which translates to an accuracy of $\pm 0.5^{\circ}$C. With the introduction of the thermal time constant as the length scale in the covariance function, the physical properties of the prosthetic material are accounted for in the model as being a purely empirical model. The flowchart depicting the process of GPML is seen in Figure 5.1.

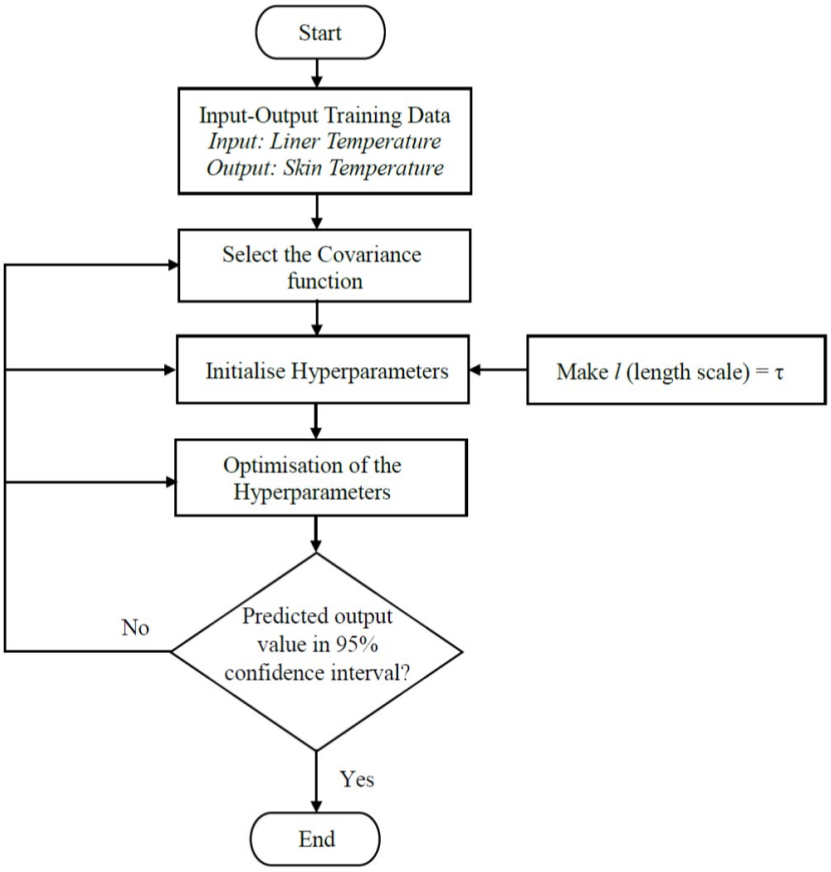

Figure 5.1: Process of the GPML for predicting the residual limb temperature from the liner-socket interface temperature.

5.3.1 Predictive Ability of the Model - Subject 1

From the scenarios described in Table 5.1, it was deduced that when the model is trained on whole Dataset A and the initial hyperparameters selected as [0, 5.4, 0.1] which are optimised using Equation 5.10, then its predictions for Dataset B lie in the 95% confidence interval (± 2 standard deviations). This is indicated in Figures 5.2-5.5 for the ambient temperatures of 10°C, 15°C, 20°C, and 25°C for Subject 1. After hyperparameter optimisation, the covariance hyperparameters for the lateral side at 10°C were $[-1.27, 2.92, -1.41]$ and the likelihood hyper-

parameter was −1.79. The final negative log marginal likelihood (optimised) was 285.84. Table 5.3 presents the hyperparameters for the predictive model at different ambient temperatures for Subject 1 [**114**].

Table 5.3: Summary of hyperparameters for predictive Gaussian model for Subject 1

Scenario	Optimised hyperparameters	Initial NLML	Final NLML	Initial likelihood	Final likelihood
Lateral side at 10°C	[-1.27, 2.92, -1.41]	786.11	285.84	-1.78	-1.79
Medial side at 10°C	[-1.20, -0.86, 1.29]	747.63	352.61	-2.17	-2.21
Lateral side at 15°C	[-1.43, 1.88, -1.62]	657.23	211.89	-1.85	-1.89
Medial side at 15°C	[-1.38, 1.76, 1.66]	643.73	310.54	-1.63	-1.70
Lateral side at 20°C	[-1.49, 1.52, -1.31]	662.47	274.09	-1.89	-1.92
Medial side at 20°C	[-1.37, 1.22, 1.45]	629.81	152.61	-1.99	-2.24
Lateral side at 25°C	[-1.86, -1.37, -1.04]	538.43	323.78	-1.78	-1.80
Medial side at 25°C	[-1.35, -1.57, 1.06]	520.86	109.68	-1.96	-1.99

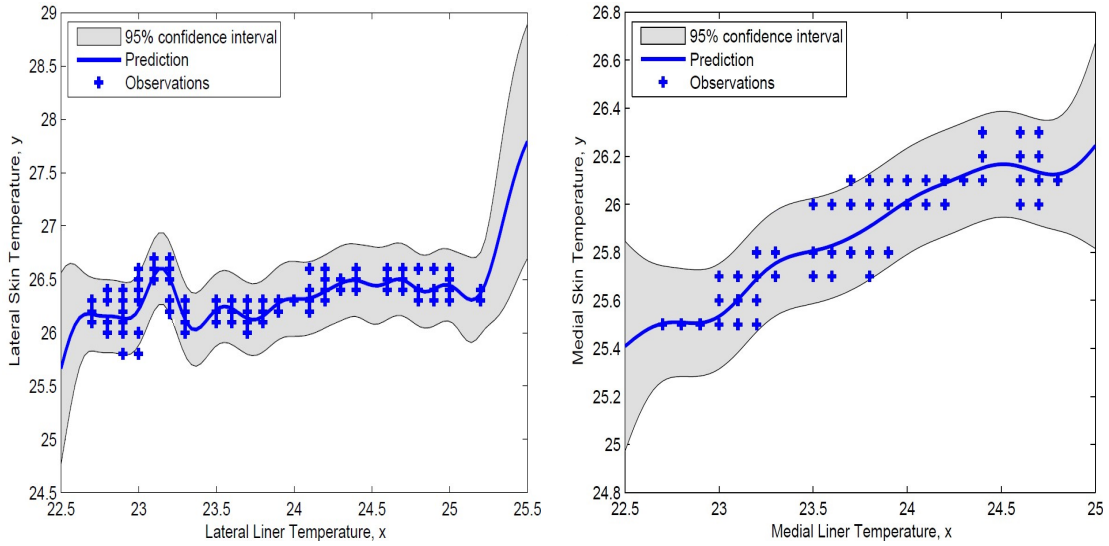

(a) (b)

Figure 5.2: Illustration of prediction with Gaussian Process regression for ambient temperature of 10°C at (a) lateral side (b) medial side of Subject 1. The test data points are given by crosses. The shaded area represents the point wise 95% confidence region of the predictive distribution.

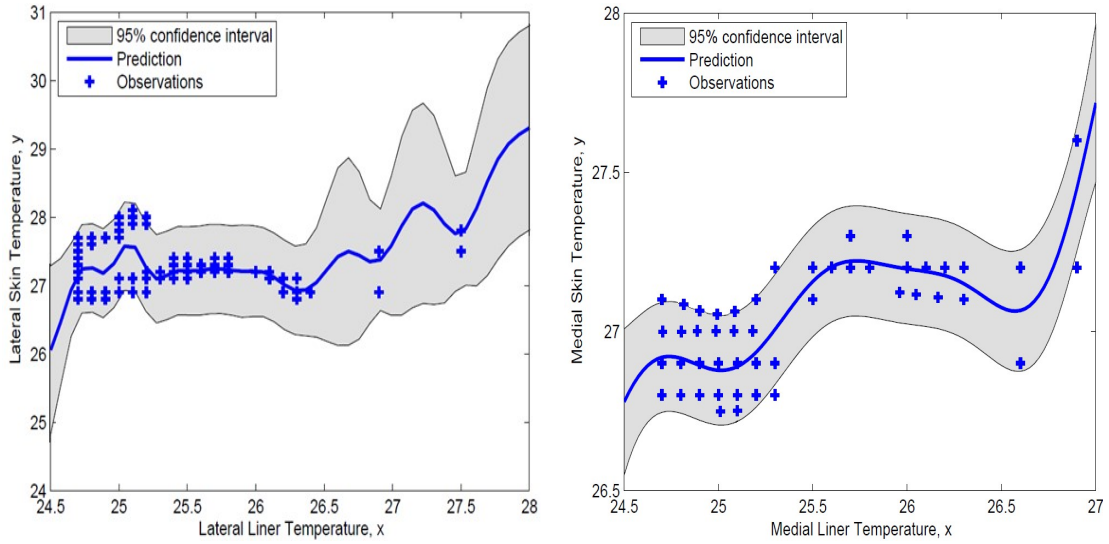

(a) (b)

Figure 5.3: Illustration of prediction with Gaussian Process regression for ambient temperature of 15°C at (a) lateral side (b) medial side of Subject 1. The test data points are given by crosses. The shaded area represents the point wise 95% confidence region of the predictive distribution.

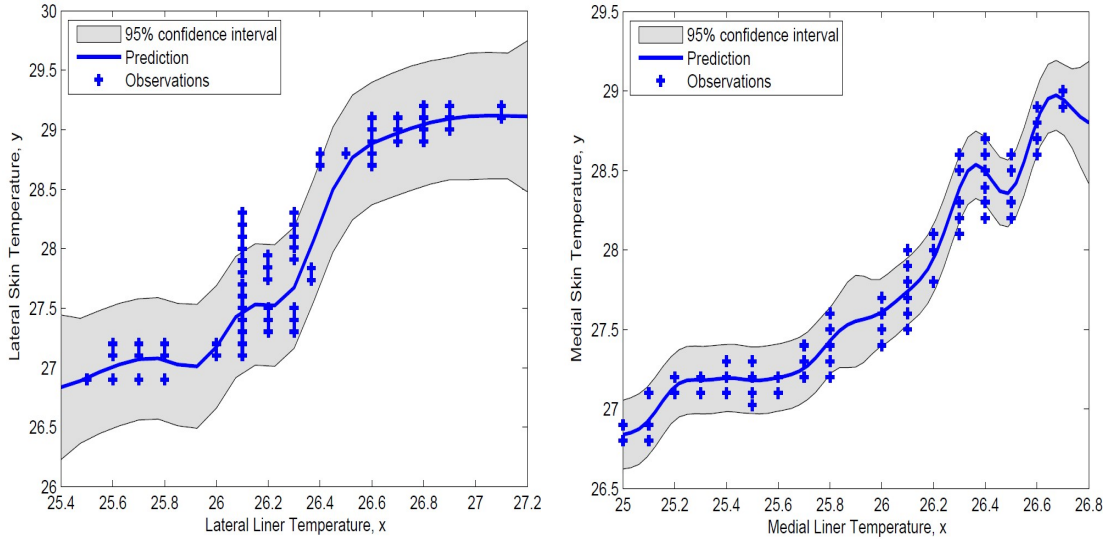

(a) (b)

Figure 5.4: Illustration of prediction with Gaussian Process regression for ambient temperature of 20°C at (a) lateral side (b) medial side of Subject 1. The test data points are given by crosses. The shaded area represents the point wise 95% confidence region of the predictive distribution.

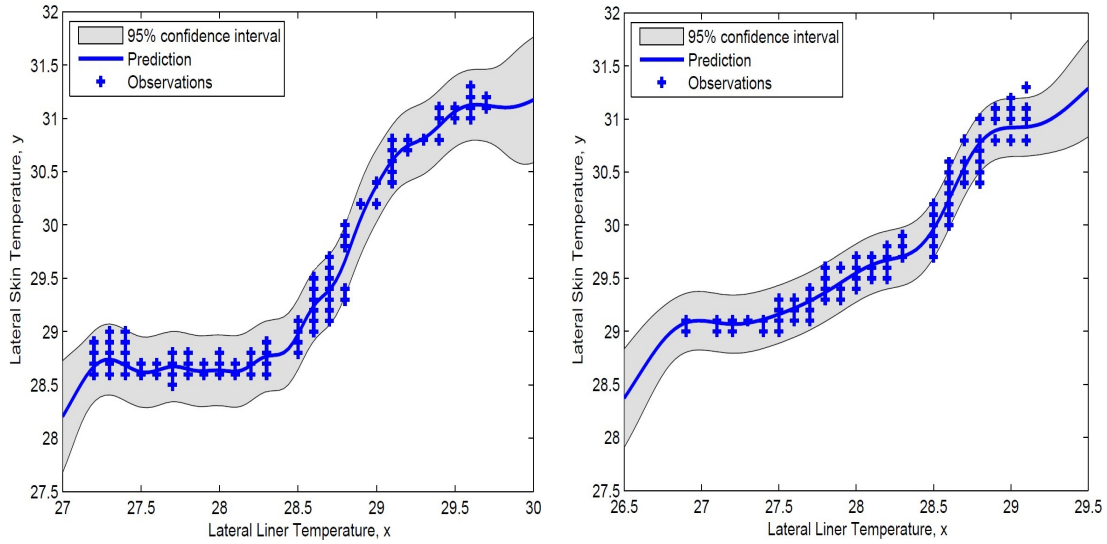

(a) (b)

Figure 5.5: Illustration of prediction with Gaussian Process regression for ambient temperature of 25°C at (a) lateral side (b) medial side of Subject 1. The test data points are given by crosses. The shaded area represents the point wise 95% confidence region of the predictive distribution.

5.3.2 Predictive Ability of the Model - Subject 2

The initial hyperparameters are selected as [0, 6.7, 0.1] and optimised by training the model on the entire Dataset A. The predictions for Dataset B are indicated in Figures 5.6-5.9 for Subject 2. The optimised hyperparameters for different scenarios are detailed in Table 5.4.

Table 5.4: Summary of hyperparameters for predictive Gaussian model for Subject 2

Scenario	Optimised hyperparameters	Initial NLML	Final NLML	Initial likelihood	Final likelihood
Lateral side at 10°C	[-1.31, 2.11, -1.59]	708.19	221.04	-1.66	-1.72
Medial side at 10°C	[-1.46, 2.34, 1.66]	754.16	352.19	-1.75	-1.81
Lateral side at 15°C	[-1.33, 2.62, -1.70]	735.88	282.90	-1.62	-1.73
Medial side at 15°C	[-1.41, 2.55, 1.58]	623.58	340.24	-1.71	-1.89
Lateral side at 20°C	[-1.38, 2.29, -1.43]	737.41	229.83	-1.69	-1.77
Medial side at 20°C	[-1.24, 2.61, 1.81]	686.13	379.43	-1.84	-1.89
Lateral side at 25°C	[-1.49, 2.78, -1.52]	729.54	297.87	-1.97	-2.12
Medial side at 25°C	[-1.28, 2.59, 1.79]	645.82	366.67	-1.86	-1.95

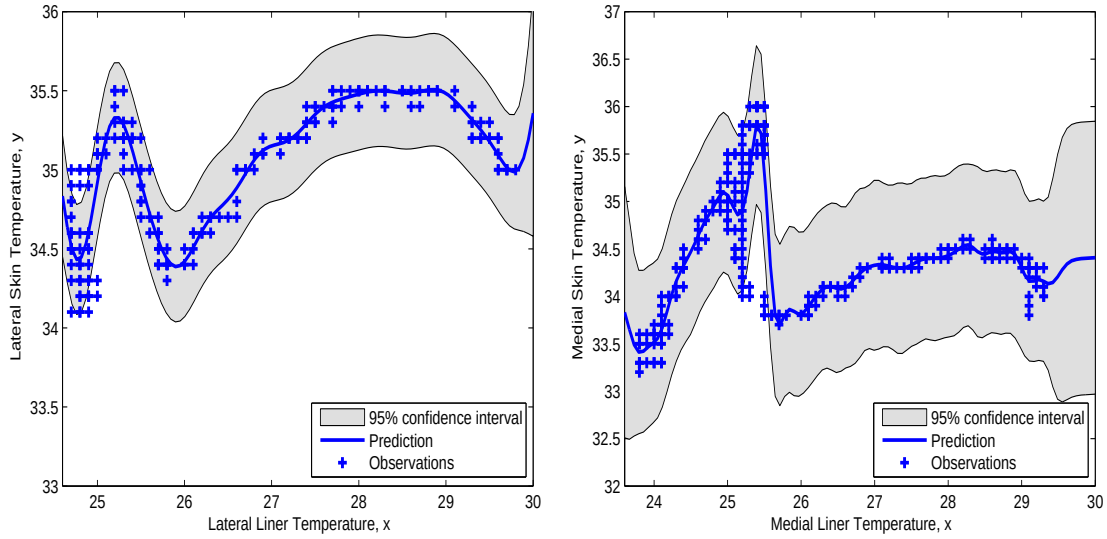

(a) (b)

Figure 5.6: Illustration of prediction with Gaussian Process regression for ambient temperature of 10°C at (a) lateral side (b) medial side of Subject 2. The test data points are given by crosses. The shaded area represents the point wise 95% confidence region of the predictive distribution.

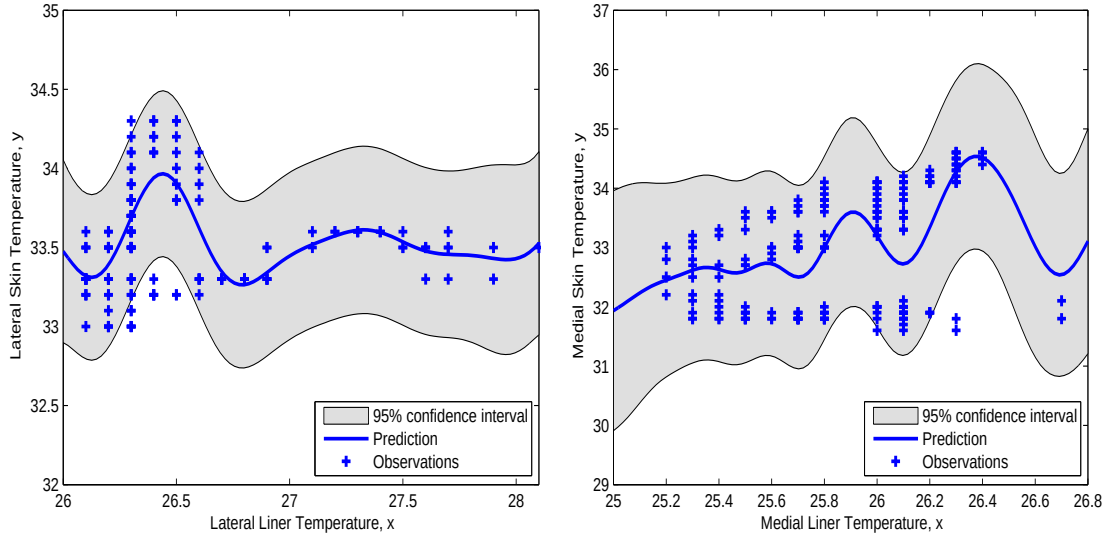

(a) (b)

Figure 5.7: Illustration of prediction with Gaussian Process regression for ambient temperature of 15°C at (a) lateral side (b) medial side of Subject 2. The test data points are given by crosses. The shaded area represents the point wise 95% confidence region of the predictive distribution.

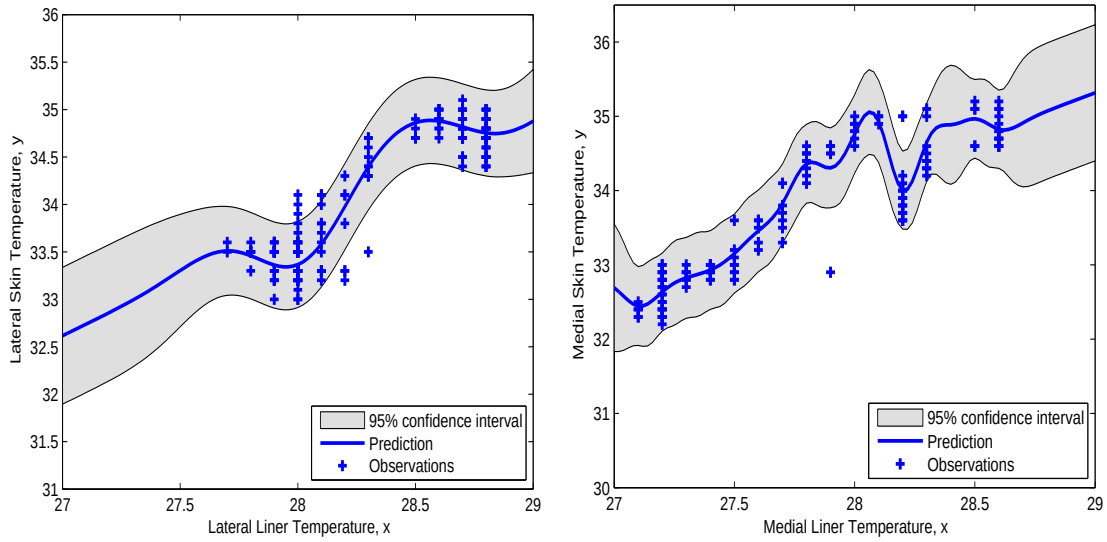

(a) (b)

Figure 5.8: Illustration of prediction with Gaussian Process regression for ambient temperature of 20°C at (a) lateral side (b) medial side of Subject 2. The test data points are given by crosses. The shaded area represents the point wise 95% confidence region of the predictive distribution.

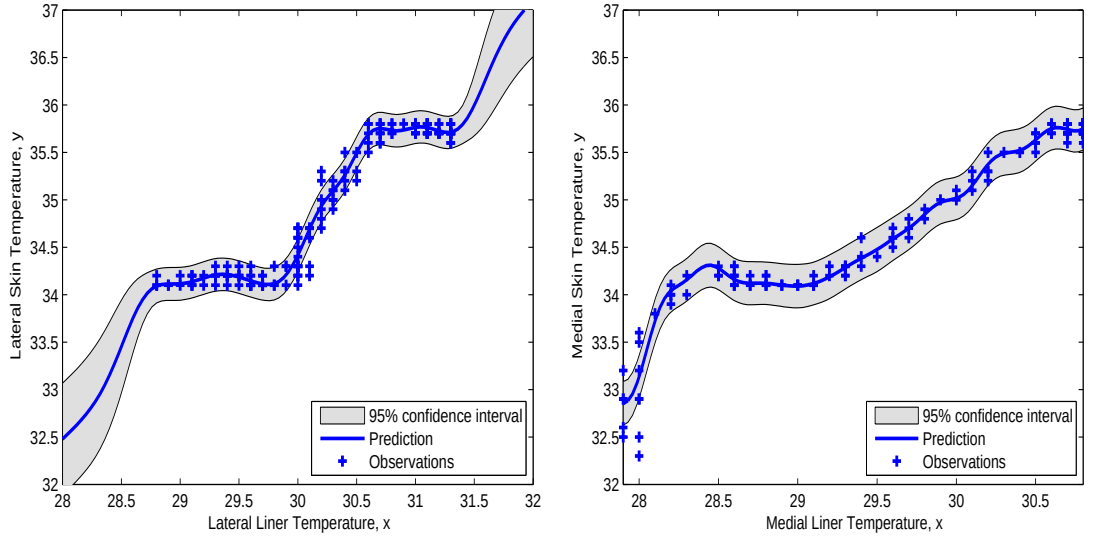

(a) (b)

Figure 5.9: Illustration of prediction with Gaussian Process regression for ambient temperature of 25°C at (a) lateral side (b) medial side of Subject 2. The test data points are given by crosses. The shaded area represents the point wise 95% confidence region of the predictive distribution.

5.4 Result Analysis of the Gaussian Model

From the Figures 3.13-3.20 in Chapter 3, it can be seen that since the volume of the datasets are big, the overall trend of the temperature profile is difficult to gauge. In order to reduce the random noise while retaining a sharp step response, a moving average filter is designed. This is basically a simple low pass Finite Impulse Response (FIR) filter used for smoothing out a sampled array of data. As the name implies, the moving average filter works by averaging a number of specified points from the input signal to produce each point in the output signal [115]. In the mathematical form, this can be written as

$$y[i] = \frac{1}{M} \sum_{j=0}^{M-1} x[i+j] \tag{5.11}$$

where x is the input signal, y is the output signal, and M is the number of points in the average. This equation uses points only on one side of the output data sample being calculated. The moving average filter performs a convolution of the input data $x[i]$ with a rectangular pulse of length M and height $1/M$ (to make the area of the pulse, and hence, the gain of the filter, one). As the filter length increases (value of M) the smoothness of the output increases, with the sharp transitions in the dataset made increasingly blunt. Therefore, after the predictive algorithm was formulated, the actual and predicted data is averaged after every 5 samples to create a single mean, and done till the end of all data points. This helps in filtering out short-term fluctuations and highlighting the longer-term trends. It also improves the joint probability function resulting in an enhanced fit of the Gaussian to the data; so that more points are more accurately predicted. The actual skin temperature obtained by the Gaussian predictive model for both the amputee subjects are shown in the subsequent subsections the test ambient temperatures of 10°C, 15°C, 20°C, and 25°C.

5.4.1 Subject 1

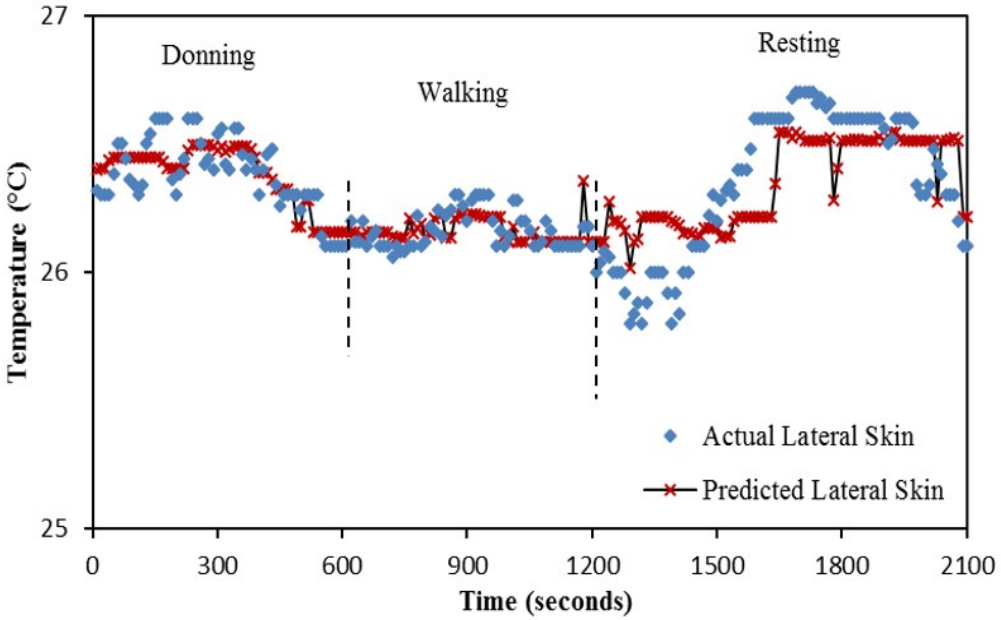

(a)

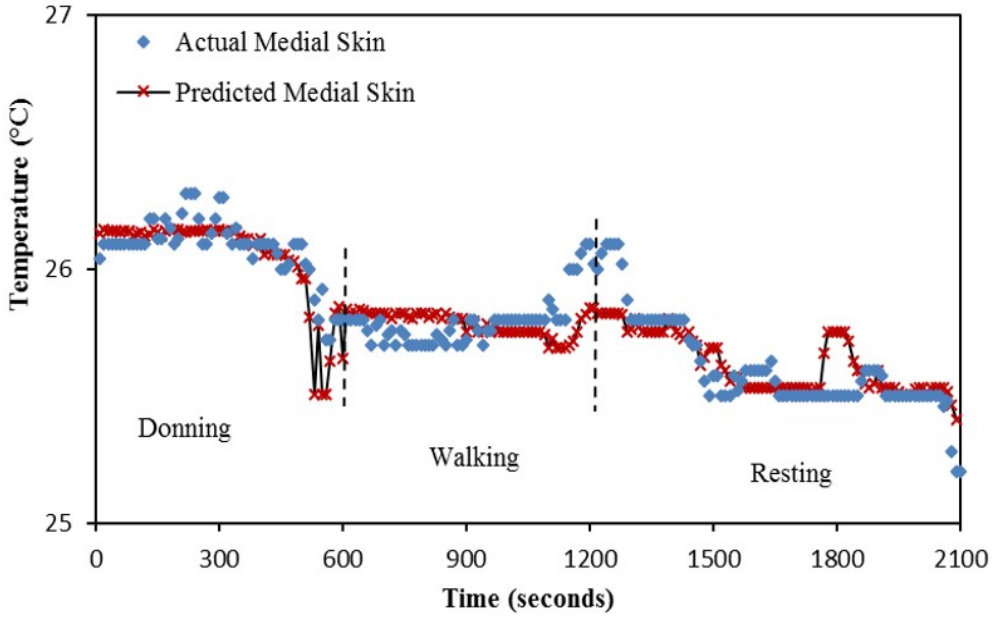

(b)

Figure 5.10: The predicted residual limb skin temperature from the time averaged Gaussian Process Model is shown along with the actual skin temperature at lateral and medial sides in (a) and (b) respectively at ambient temperature of 10°C.

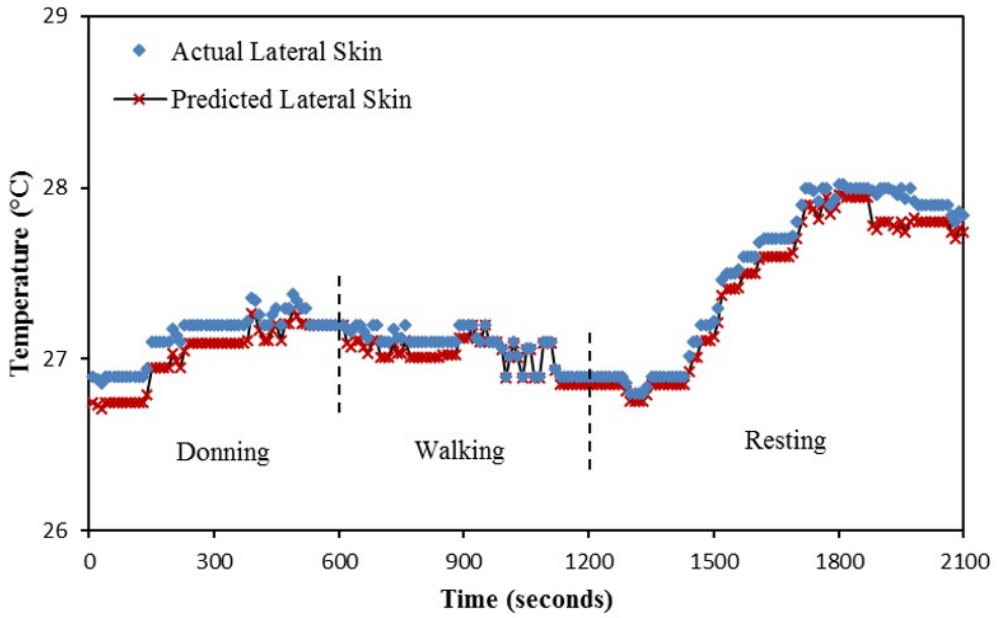

(a)

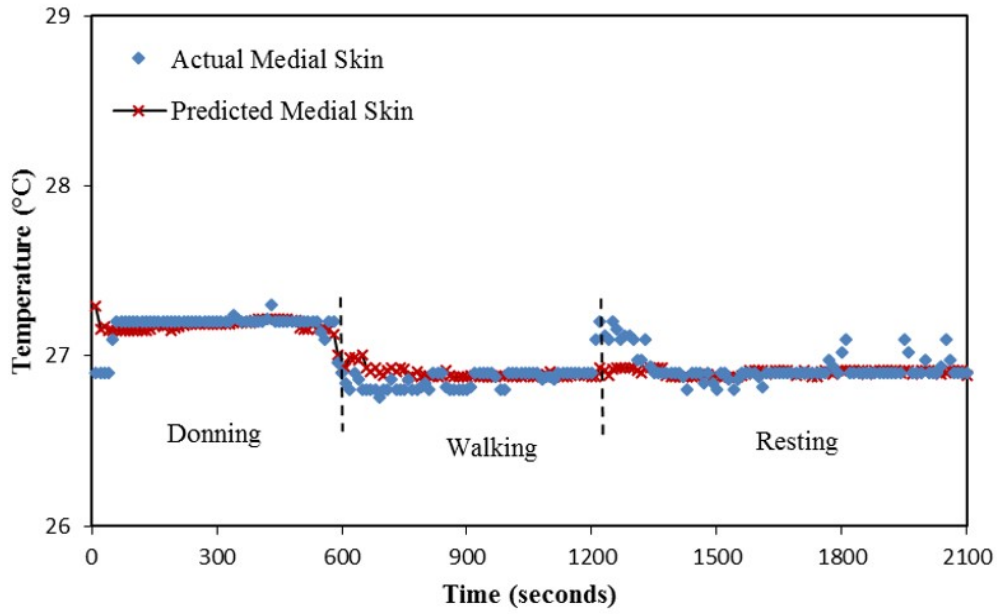

(b)

Figure 5.11: The predicted residual limb skin temperature from the time averaged Gaussian Process Model is shown along with the actual skin temperature at lateral and medial sides in (a) and (b) respectively at ambient temperature of 15°C.

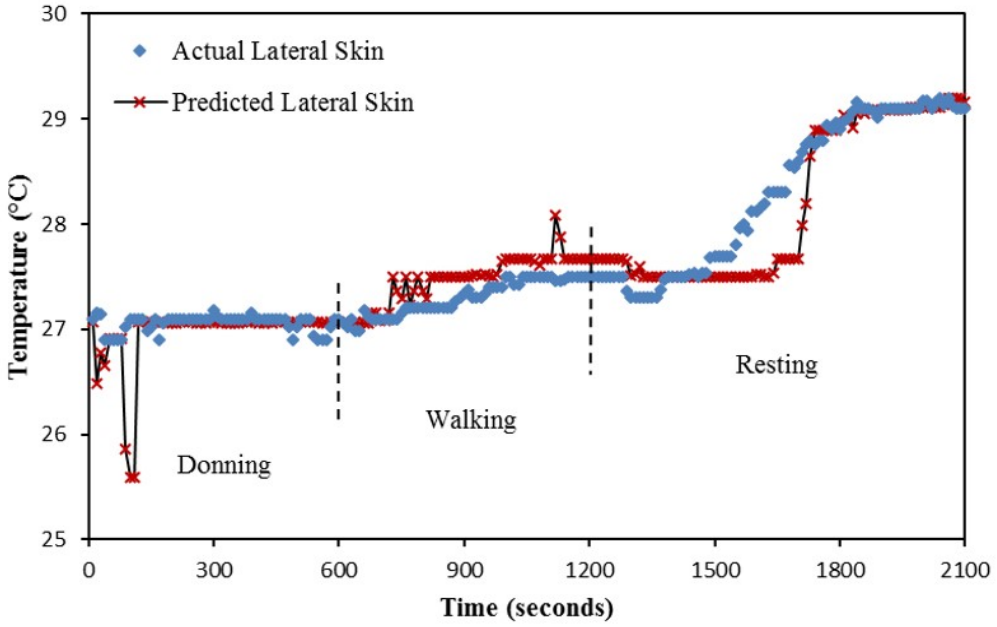

(a)

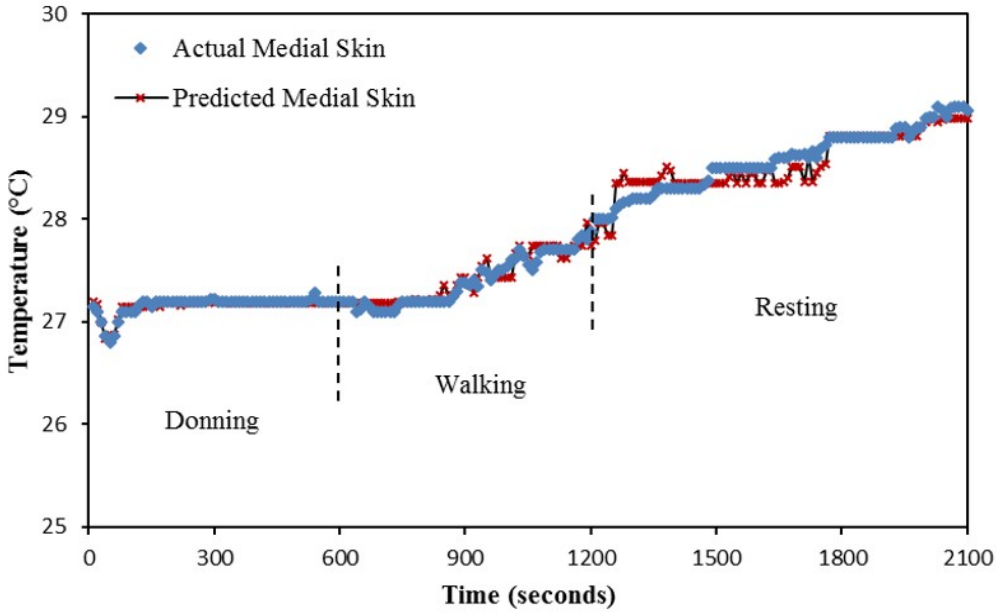

(b)

Figure 5.12: The predicted residual limb skin temperature from the time averaged Gaussian Process Model is shown along with the actual skin temperature at lateral and medial sides in (a) and (b) respectively at ambient temperature of 20°C.

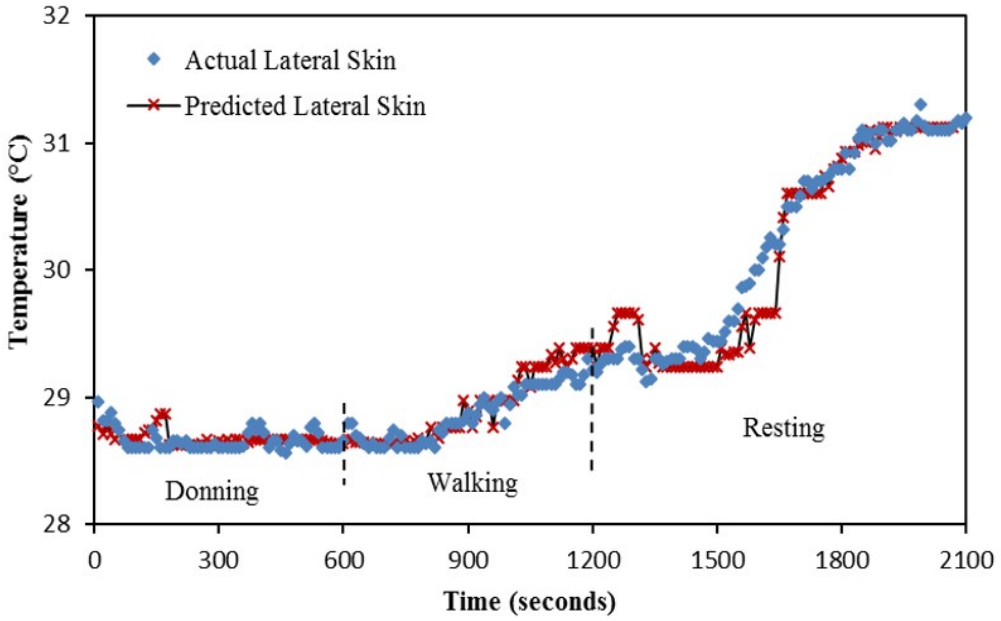

(a)

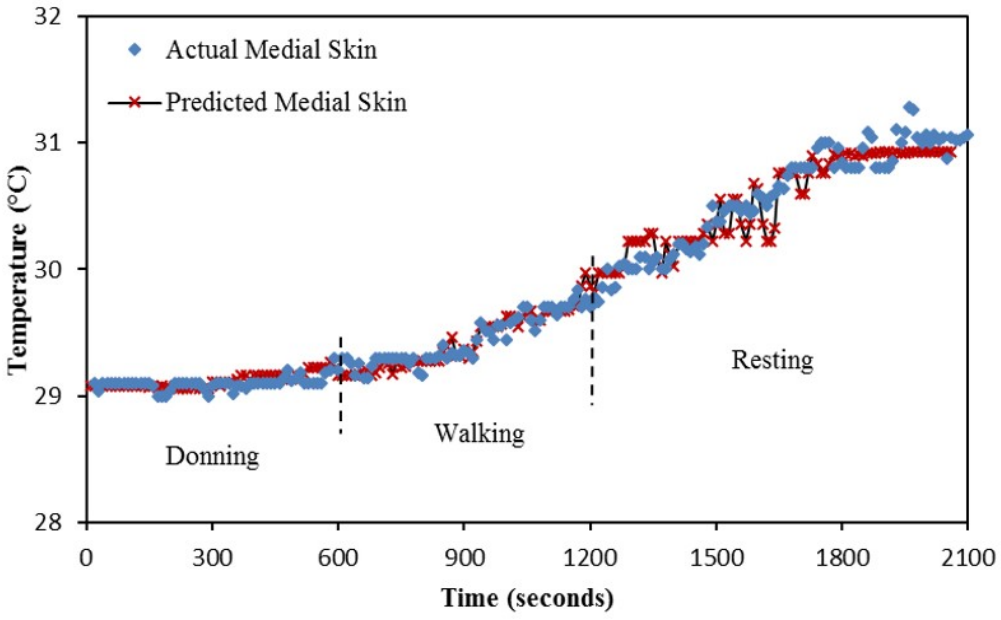

(b)

Figure 5.13: The predicted residual limb skin temperature from the time averaged Gaussian Process Model is shown along with the actual skin temperature at lateral and medial sides in (a) and (b) respectively at ambient temperature of 25°C.

5.4.2 Subject 2

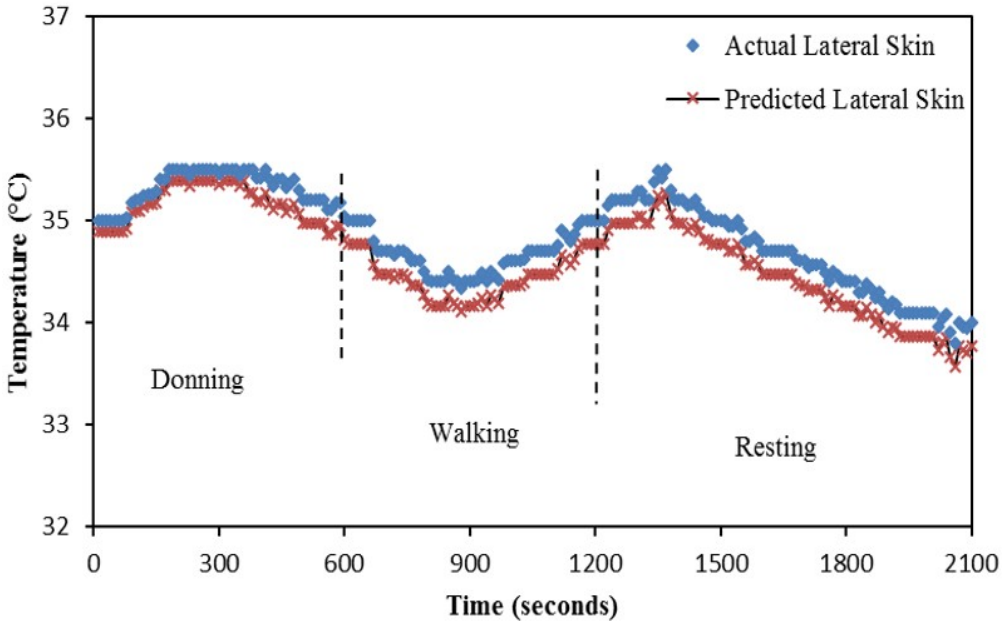

(a)

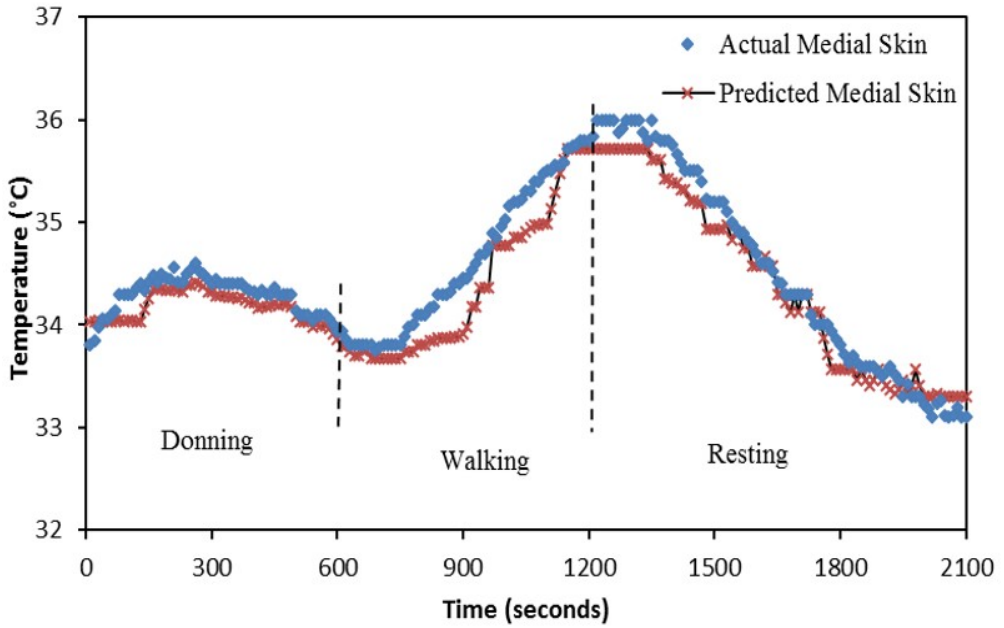

(b)

Figure 5.14: The predicted residual limb skin temperature from the time averaged Gaussian Process Model is shown along with the actual skin temperature at lateral and medial sides in (a) and (b) respectively at ambient temperature of 10°C.

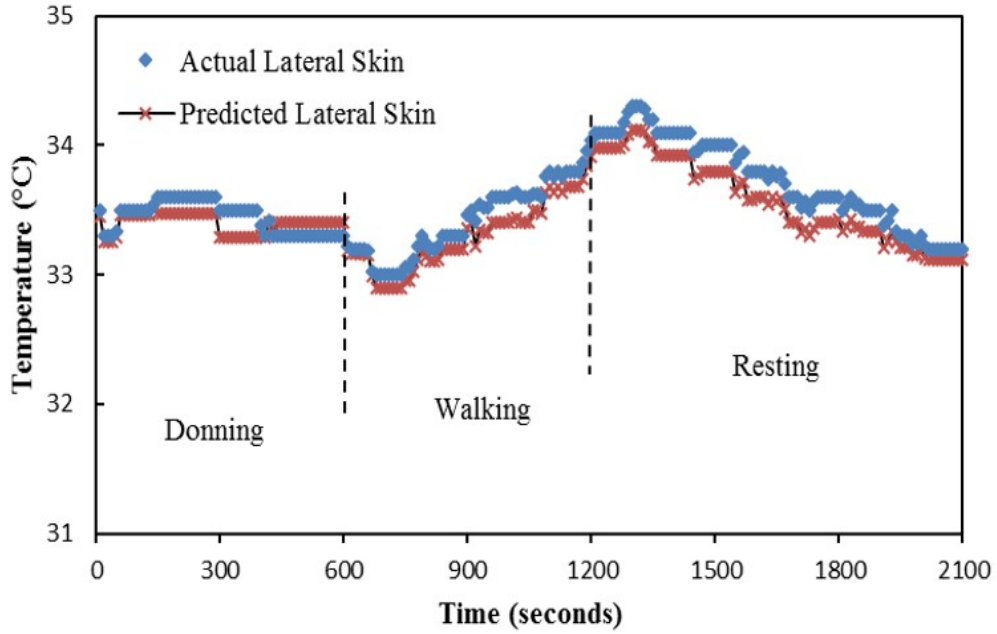

(a)

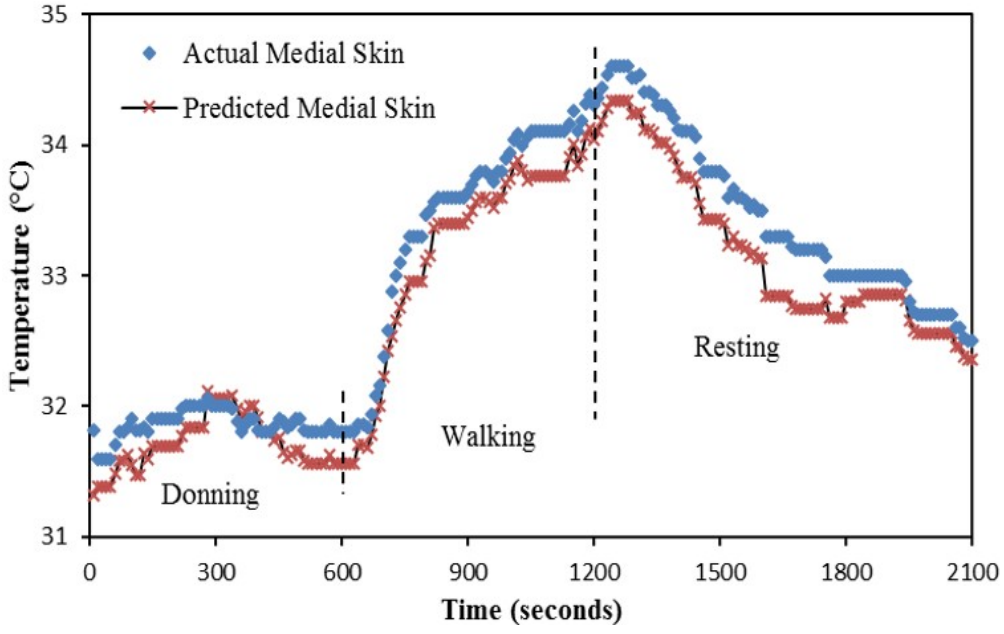

(b)

Figure 5.15: The predicted residual limb skin temperature from the time averaged Gaussian Process Model is shown along with the actual skin temperature at lateral and medial sides in (a) and (b) respectively at ambient temperature of 15°C.

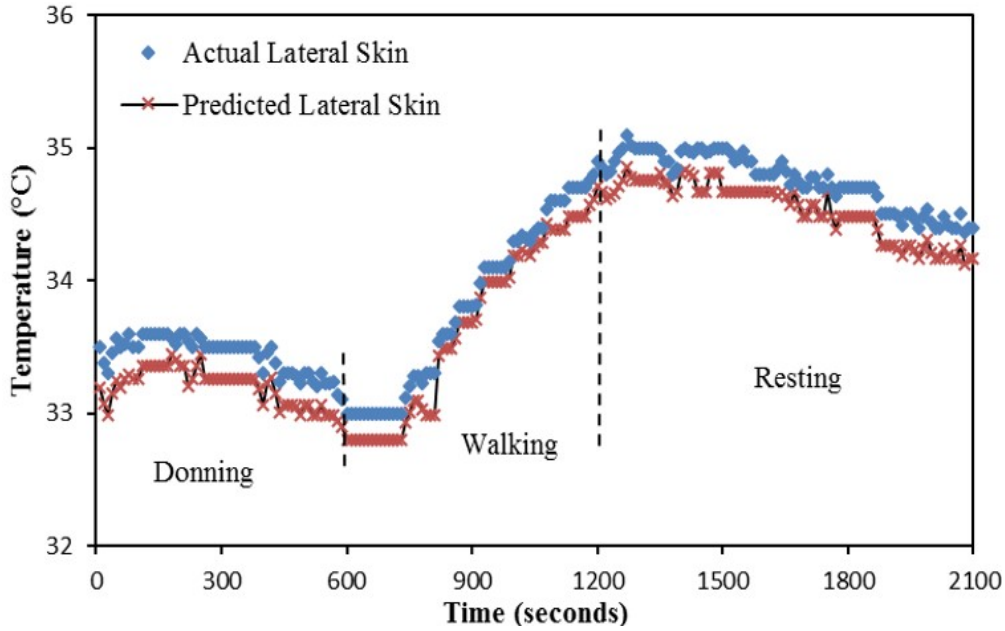

(a)

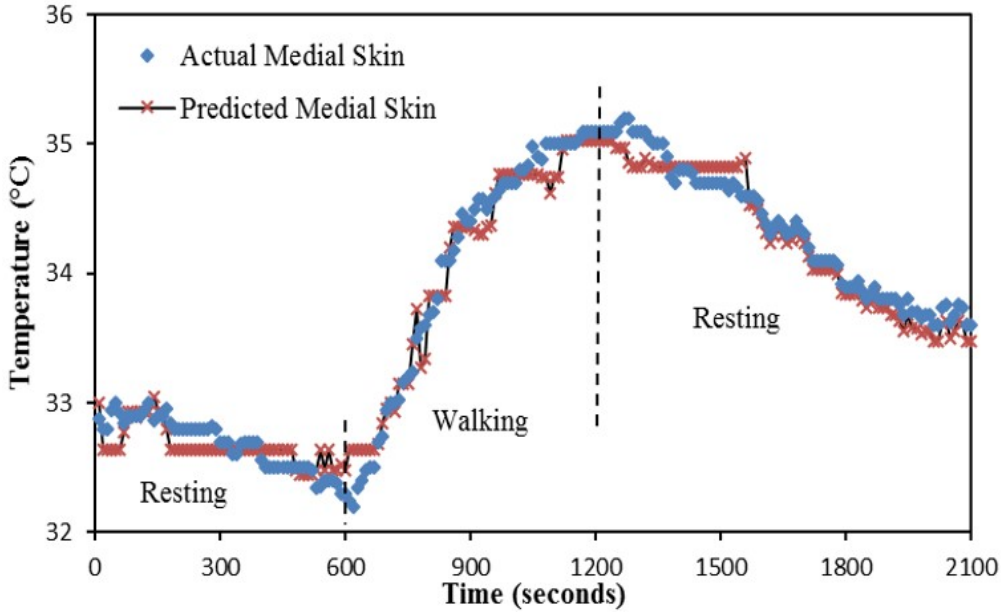

(b)

Figure 5.16: The predicted residual limb skin temperature from the time averaged Gaussian Process Model is shown along with the actual skin temperature at lateral and medial sides in (a) and (b) respectively at ambient temperature of 20°C.

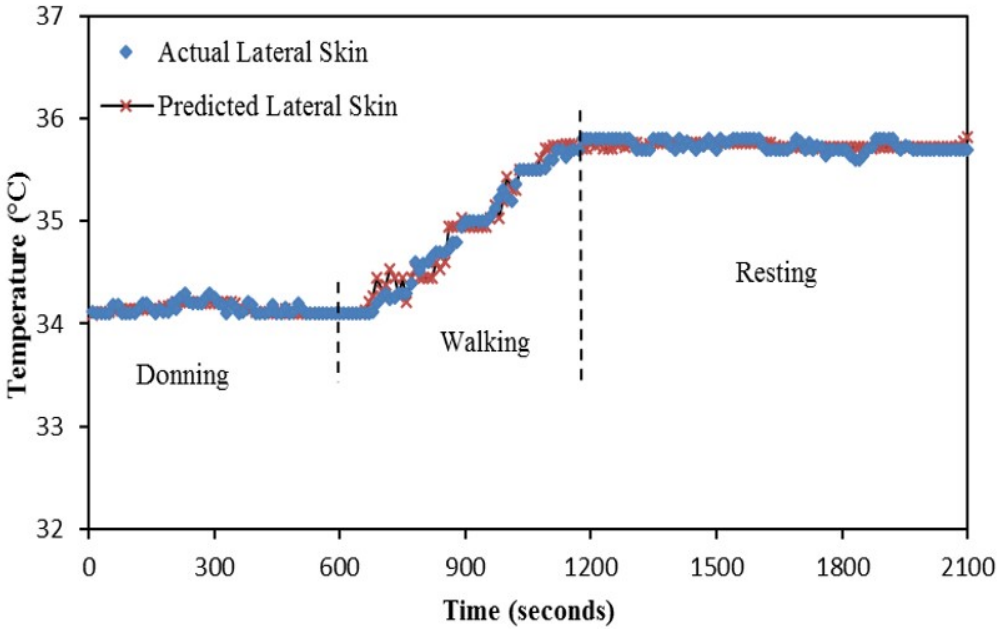

(a)

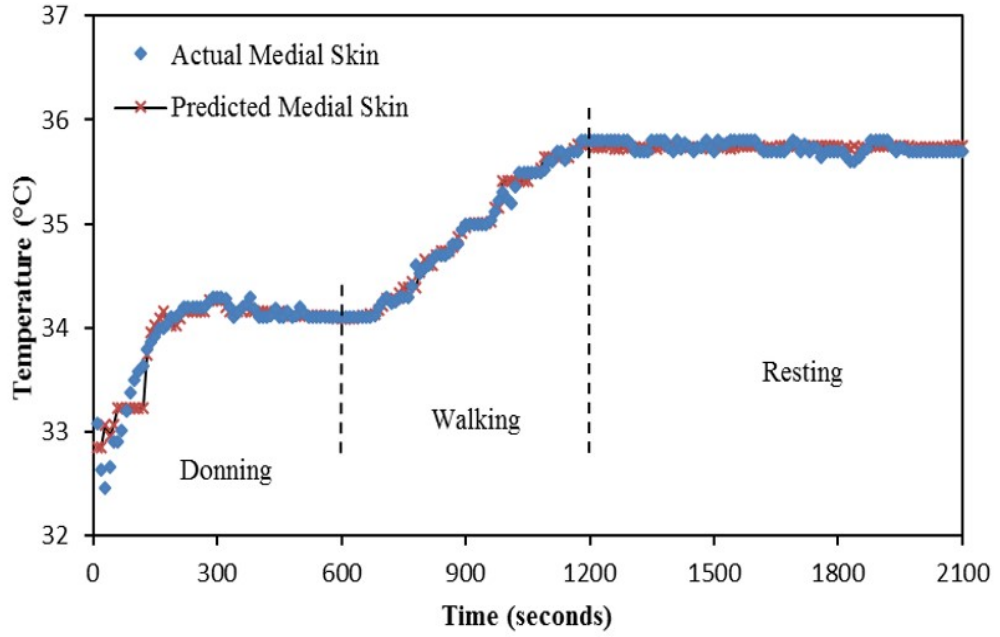

(b)

Figure 5.17: The predicted residual limb skin temperature from the time averaged Gaussian Process Model is shown along with the actual skin temperature at lateral and medial sides in (a) and (b) respectively at ambient temperature of 25°C.

5.5 Discussion

The challenge of monitoring the residual limb skin temperature of lower limb amputees contactlessly can be addressed by using the Gaussian Processes approach. It was observed that residual limb skin temperature and the liner temperature are majorly affected by both the ambient temperature and the activity level of the subject. Hence, the Gaussian models were individually trained for each of the ambient temperatures on which the tests were done. Also, it was noted (from Chapter 3) that the residual limb skin temperature and the liner temperature profile of the two amputee subjects are significantly different from each other for the same ambient test temperatures. This could be attributed to the difference in the physiological response of every individual and therefore, separate GPML models were developed for each subject using their respective datasets for training and testing. In order to filter out the random fluctuations, time averaging of 5 seconds is done using an FIR filter. This along with the introduction of thermal time constant in the hyperparameters of the Gaussian model for both the subjects leads to results which are in 95% confidence interval.

5.6 Summary

The accuracy of the model developed to non-invasively monitor the residual limb temperature of an amputee is ± 0.5°C. It is observed from the study that the residual limb temperature depends on the ambient temperature and the activity level of the subject. Moreover, a major factor is the thermal time constant of the prosthetic materials used. Because of the low thermal conductivity of the prosthetic materials, it can restrict the heat transfer from the residual limb and create a warm micro-environment within the prosthesis. Hence, it becomes all the more imperative to build in the existing GPML model the thermal time constant

so obtained from the thermal studies.

Thus, this highlights the relevance of thermal time constant of prosthetic materials in Gaussian Processes technique. With the introduction of thermal time constant in the model, the accuracy increases, thereby making predictions more reliable [**116**]. Also, this approach is quite useful in extending the model to a wider amputee population to define a generic behaviour. Future scope of the work includes studying the interplay between temperatures and sweating response in prosthesis of amputees with different pathologies.

Chapter 6

Residual Limb Skin Temperature Prediction using Adaptive Neuro Fuzzy Inference System (ANFIS)

6.1 Introduction

This chapter describes the development of a supervised mathematical algorithm ANFIS to predict the residual limb temperature of the amputee by monitoring the temperature between socket and liner. Similar to Chapter 5, the aim is to demonstrate the implementation of ANFIS for contactless monitoring of residual limb temperature. This technique utilises backpropagation learning method, wherein the fuzzy inference system is implemented in a framework of neural networks which are adaptive by nature. The architecture and the underlying learning procedure of ANFIS is presented, which is then followed by a description of its predictive capability and the results of the data analysis. The motivation for development of this model was to analyse and compare the machine learning algorithms - GPML and ANFIS, the principles of which are quite different from

each other. Gaussian process models which are non-parametric in nature can be optimised exactly, given the values of the hyperparameters. ANFIS, on the other hand is mostly parametric as it uses neural networks properties. Therefore, for convergence the model relies hugely on the training parameter and the input function. The comparisons on the predictive ability of ANFIS and GPML are also listed and discussed [**117**].

6.2 Adaptive Neuro Fuzzy Inference System

ANFIS are a class of adaptive networks that incorporate both neural networks and fuzzy logic principles. Neural networks are supervised learning algorithms which utilise a historical dataset for the prediction of future values. In fuzzy logic, the control signal is generated from firing the rule base. This rule base is drawn on historical data and is random in nature. This implies that the controller's output is also random which may prevent then optimal results. The use of ANFIS can make the selection of the rule base more adaptive to the situation. In this technique, the rule base is selected utilising the neural network techniques via the back propagation algorithm. To enhance its applicability and performance, the properties of fuzzy logic, i.e. approximating a non-linear system by setting IF-THEN rules is inherited in this modeling technique. This integrated approach, makes ANFIS to be a universal estimator [118].

6.2.1 ANFIS Strategy

ANFIS belongs to a family of hybrid system, called as the term 'neuro fuzzy networks' [119] inheriting the properties of both neural networks and fuzzy logic. Neural networks can easily learn from the data. However, it is difficult to interpret the knowledge acquired by it, as the meaning associated with each neuron

and each weight is quite complex to comprehend. In contrast, fuzzy logic itself cannot learn from the data. But fuzzy-based models are easily understood as they utilise linguistic terms rather than numeric and the structure of IF-THEN rules. Linguistic variables are defined as variables whose values are words or sentences in a natural language with associated degrees of membership. The fuzzy set in which linguistic variables belongs is an extension of a 'crisp' set where an element could have full or no membership. However, fuzzy sets allow partial membership as well, which implies that an element may partially belong to more than one set [120]. In other words, for a crisp set, the membership level of an element x in set A can be expressed by a characteristic function $\mu_A(x)$, such that if

$$\mu_A(x) = \begin{cases} 1 & if x \in A \quad \text{implying full membership} \\ 0 & if x \notin A \quad \text{implying non-membership} \end{cases} \tag{6.1}$$

But for a fuzzy set A the membership function $\mu_A(x)$ can take values in the interval [0,1]. The basic structure of the developed ANFIS controller for the prediction of residual limb skin temperature consists of four parts, which are, fuzzification, rule base, inference engine and the de-fuzzification blocks as seen in Figure 6.1.

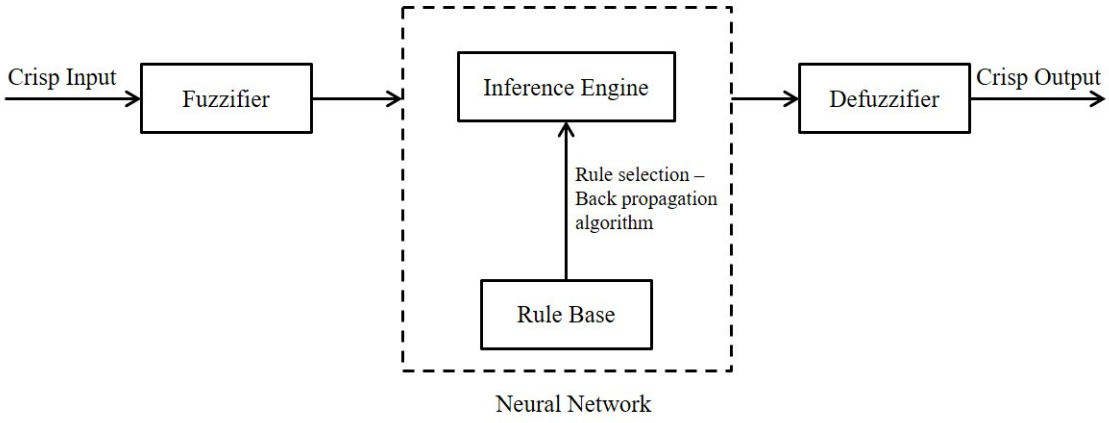

Figure 6.1: Block diagram of a Neuro- Fuzzy (ANFIS) controller

In the ANFIS controller, the crisp input signal (liner temperature in our case) is converted to fuzzy inputs by the Membership Function (MF). The membership function pattern of the ANFIS model used in study is defined to be Gaussian. The fuzzy inputs along with the Gaussian membership function are then fed into the neural network block. The neural network block consists of a rule base which is connected to the inference engine. Back propagation algorithm is used to train the inference engine for the proper selection of rule base. Once trained, proper rules can be generated and fired from the neural network block to yield optimal output. The linguistic output from the neural network block is then converted into crisp output (residual limb skin temperature) by the defuzzifier unit [121]. The structure of the neuro-fuzzy model consists of different adaptive layers. Each of these layers has nodes with an associated network of transfer functions, through which the fuzzy inputs are processed. The output from these nodes are then combined to yield a single crisp output as the configuration of the ANFIS permits only one output of the model. This crisp output is fedback as input to the model and compared with the set value. If there is any deviation, the error signal so generated becomes the input to the ANFIS controller, thereby maintaining stability in the system [122].

6.2.2 ANFIS Structure

ANFIS supports the Takagi-Sugeno based systems [123]. The rule base for it can be expressed as follows:

$$\text{If } x \text{ is } A \text{ then } y \text{ is } B$$

where the linguistic variables A and B defined by the fuzzy sets on the ranges X and Y, respectively. The if-part of the rule "x *is* A" is called the antecedent or premise, while the then-part of the rule "y *is* B" is called the consequent or

conclusion. The structure of the adaptive network is composed of five network layers i.e. layer 1 to layer 5 (with nodes and connections) as shown in Figure 6.2.

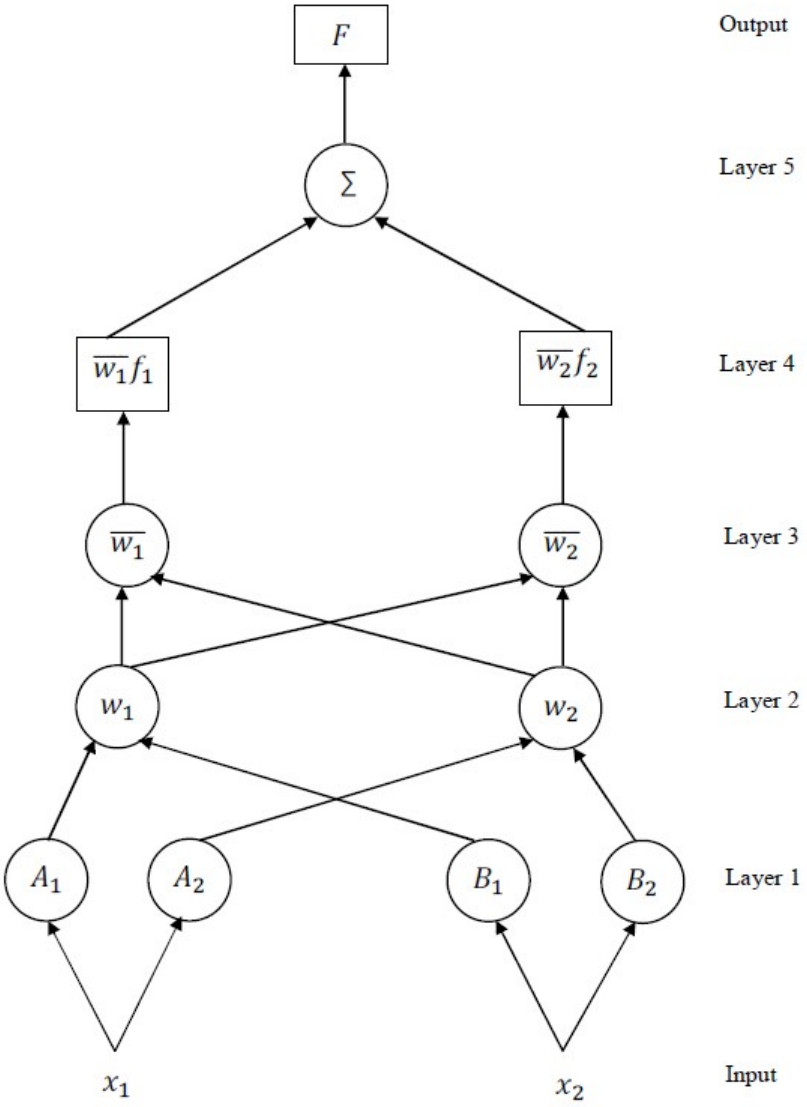

Figure 6.2: Architecture of a first order two rule Takagi-Sugeno type ANFIS.

Assuming that the system is defined to have two inputs x_1 and x_2, one output z and fuzzy set A_1, A_2, B_1, B_2; then for a first order Takagi-Sugeno fuzzy model, having two IF-THEN rules in the common rule set, the system can be defined

using Equations 6.2 and 6.3 [124].

$$If\ \ x_1\ \text{is}\ A_1\ \text{and}\ x_2\ \text{is}\ B_1\ \text{then}\ \ f_1 = p_1x_1 + q_1x_2 + r_1 \tag{6.2}$$

$$If\ \ x_1\ \text{is}\ A_2\ \text{and}\ x_2\ \text{is}\ B_2\ \text{then}\ \ f_2 = p_2x_1 + q_2x_2 + r_2 \tag{6.3}$$

Layer 1: This layer is called as the fuzzification layer. Here the crisp input signal is fed to the node i which is associated with a linguistic label A_i or B_{i-2}. Thus, the node function $O_{1,i}(X)$ determines the membership level (full, none or partial) of the given input. The output of each node is calculated using Equations 6.4 and 6.5 where x is the input to node i, A_i is the linguistic variable associated with this node function and μ_{Ai} is the membership function (MF) of A_i.

$$O_{1,i} = \mu_{Ai}(x_1)\ \text{ for } i = 1{,}2 \tag{6.4}$$

$$O_{1,i} = \mu_{Bi-2}(x_2)\ \text{ for } i = 3{,}4 \tag{6.5}$$

μ_{Ai} is chosen as the generalised Gaussian shaped membership function in this model development as seen in Equation 6.6.

$$\mu_{Ai}(x) = exp\Big\{ -\frac{1}{2}\Big(\frac{x - c_i}{a_i}\Big)^2\Big\} \tag{6.6}$$

where x is the input and $\{a_i, c_i\}$ is the premise parameter set. c determines the centre of the corresponding membership function whereas a determines the width. These parameters can be specified and adjusted by the learning algorithm in the training process. The Gaussian membership function achieves smoothness as well as possess the useful property of invariance under multiplication (i.e. the product of two Gaussians is a Gaussian with a scaling factor) and Fourier transform (i.e. the Fourier transform of a Gaussian is also a Gaussian).

Layer 2: The nodes in this layer are fixed and labeled as $O_{(2,i)}$. The output of

each node is the product of all the incoming signals as in the Equation 6.7.

$$O_{(2,i)} = w_i = \mu_{Ai}(x_1)\mu_{Bi}(x_2) \text{ for } i = 1,2 \tag{6.7}$$

The output of each node represents the firing strength w_i of a rule. Also, known as the membership layer, it acts on the input variables from layer 1 as membership functions to represent them in their fuzzy sets.

Layer 3: Each node in this layer calculates the ratio of the individual rule's firing strength to the sum of all rules firing strengths as in the Equation 6.8. $\overline{w_i}$ represents the normalized firing strength. Hence, this layer is also known as the rule layer.

$$O_{(3,i)} = \overline{w_i} = \frac{w_i}{w_1 + w_2} \text{ for } i = 1,2 \tag{6.8}$$

Since, each node in this layer calculates the normalized weights, the output signal can be thought of as the normalized firing strength of a given rule.

Layer 4: This layer known as the defuzzification layer. It calculates the individual output values y by inferring the rules from the rule base. Individual nodes of this layer are connected to the respective normalization node in layer 3 and also receive the input signal. Each node of this layer is adaptive in nature with the node function given by the Equation 6.9 where $\{p_i, q_i, r_i\}$ is a set of consequent parameters of rule i.

$$O_{(4,i)} = \overline{w_i} f_i = \overline{w_i}(p_i x_1 + q_i x_2 + r_i) \tag{6.9}$$

Layer 5: This layer is known as the output layer. It has only one node and it calculates the sum of all the outputs coming from the nodes of the defuzzification

layer to produce the overall ANFIS output as in Equation 6.10.

$$overall\ \ output = O_{(5,i)} = \sum_i \overline{w_i} f_i = \frac{\sum_i w_i f_i}{\sum_i w_i} \tag{6.10}$$

This architecture of the adaptive network is used to develop the ANFIS model for the prediction of in-socket residual limb temperature and the learning algorithm is described in the next section.

6.2.3 Training the ANFIS Model

From the ANFIS structure, it can be noted that the final output can be expressed as linear combination of the consequent parameters if the premise parameters are known as seen in Equation 6.11. The output F of the model as seen in Figure 6.2 can be written as

$$\begin{aligned} F &= \frac{w_1}{w_1 + w_2} f_1 + \frac{w_2}{w_1 + w_2} f_2 \\ &= \overline{w_1} f_1 + \overline{w_2} f_2 \\ &= (\overline{w_1} x) p_1 + (\overline{w_1} x) q_1 + (\overline{w_1} x) r_1 + (\overline{w_2} x) p_2 + (\overline{w_2} x) q_2 + (\overline{w_2} x) r_1 \end{aligned} \tag{6.11}$$

where F is seen to be linear in the consequent parameters $\{p_1, q_1, r_1, p_2, q_2, r_2\}$.

In order to learn from the training dataset the ANFIS model can either use the hybrid or the back propagation algorithm. In this study for model development, the back propagation algorithm is utilised as it is one of the simplest methods for supervised learning of neural networks. The algorithm is provided with the training dataset where the relation between the input-output pair is known. The actual output from the network is compared to the expected output and an error

signal is computed for each of the output nodes. Since all the nodes to some extent have contributed to the errors in the output layer, the output error signals are transmitted backwards from the output layer to each node in the hidden layer. This is repeated for every layer, until each node has received an error signal equal to its relative contribution in the overall error. These error signals are then used by the individual nodes to update their connection weights until the error function of the network becomes minimum. The method used in the back propagation algorithm is gradient descent. The aim is thus to reduce the error until the neural network learns the training data.

6.3 Model Generation and Prediction

The basic idea behind this neuro-adaptive technique is to provide a method for the Fuzzy Inference System (FIS) to learn from the dataset. This enables to compute the membership function parameters that can best allow the FIS to infer the relation between the input-output pairs. These parameters can be adjusted in the learning process as described in the previous section.

6.3.1 ANFIS as an Estimator

The design of ANFIS as an estimator is twofold - constructing and training. In order to start the modeling process, an initial fuzzy model needs to be constructed. For deducing the final fuzzy model, certain parameters such as the number of inputs, the number of linguistic variables, the type of membership function and the number of rules are applied to the initial fuzzy model. The initial fuzzy model can be drawn by either grid partitioning method or the subtractive clustering technique. Effective portioning of the input space is vital as it can decrease the

rule number and thus improve the rate of learning and application phase. As mentioned in the previous section, the Input MF is chosen to be of Gaussian form. The Output MFs can be either a constant or a linear form. The Constant form is chosen to be the output MF in this study. After specifying the number and type of input MFs, the estimator rule base is constituted. The automatic rule generation (grid partition) method is preferred [125]. The grid partition form takes all possible combinations of membership functions of all inputs. For example, an ANFIS model with two inputs and three MFs on each input would result in $3^2 = 9$ Takagi-Sugeno fuzzy if-then rules automatically. A drawback of this method is that it requires much computational knowledge in systems that are defined by many inputs; however, it is used in this study due to advantage of processing in MATLAB. Once the initial ANFIS structure is constructed, learning algorithm and training parameters are chosen. ANFIS model can be generated either from the command line, or through the ANFIS editor GUI. In this study, ANFIS Editor GUI is used to generate the ANFIS models with the chosen design parameters in construction phase. A MATLAB script is written to train the ANFIS structure in the training step as seen in Appendix C. The steps involved in the ANFIS estimator design by utilising the Matlab Fuzzy Logic Toolbox [126] are as follows:

1. The training data is loaded to the Editor Graphical User Interface (GUI).
2. Design parameters, number of input MF, type of input and output MF, are chosen. Thus, the initial ANFIS structure is formed.
3. The code for the training is run with initial structure.
4. ANFIS structure is constituted after the training is saved to be used as an estimator.

6.3.2 Predictive Ability of ANFIS

The architecture of the realised ANFIS model had the following specifications; number of nodes: 84, number of training data pairs: 210, number of test data pairs: 100 and number of membership functions: 3. The adaptive network utilises the back propagation method to optimise the membership functions and the parameters so that the prediction error is minimised. Dataset A is used to train the model and the predictive ability of ANFIS is tested on Dataset B. During the training process of the model, the input data is mapped a number of times to minimise the prediction error. The number of iterations required for mapping is known as epochs. It is observed that in all the scenarios of testing, 50 iterations (epochs) are required to train the model on Dataset A with a minimal error. The trained model is then tested on 100 data points from Dataset B to validate it. The following subsections demonstrate the predictive ability of ANFIS for ambient temperature of 10°C, 15°C, 20°C and 25°C at lateral and medial side of residual limb for both the amputee subjects.

6.3.2.1 Predictive Ability of ANFIS - Subject 1

Table 6.1 summarises the predictive ability of the model tested for various ambient temperatures at the lateral and medial side of residual limb for Subject 1. It is seen that in all the scenarios, the results from the ANFIS model were encouraging with the test errors being significantly lower than the training errors. This is an exception in the scenario for lateral side testing at 15°C where the test error is more than the training error and its impact can be seen in the Figure 6.4(a).

Table 6.1: Summary of ANFIS for various testing and training scenarios for Subject 1

Scenario	Training error (RMSE)	Test error (RMSE)
Lateral side at 10°C	0.1543	0.07814
Medial side at 10°C	0.09894	0.07378
Lateral side at 15°C	0.3098	0.6985
Medial side at 15°C	0.0750	0.0742
Lateral side at 20°C	0.2236	0.1265
Medial side at 20°C	0.0873	0.0443
Lateral side at 25°C	0.0145	0.0696
Medial side at 25°C	0.1234	0.1519

6.3.2.2 Predictive Ability of ANFIS - Subject 2

Table 6.2 summarizes the predictive ability of the model tested for various ambient temperatures at the lateral and medial side of residual limb for Subject 2. It is seen that with the design settings of the ANFIS as described in section 6.3.2, the results from the model were not very consistent; with the test errors being significantly lower and sometimes higher than the training errors. It can be seen from Figures 6.7-6.10 that the predicted output does try to follow the actual skin temperature but it offsets and has fluctuations which does not fit the model to

the data accurately.

Table 6.2: Summary of ANFIS for various testing and training scenarios for Subject 2

Scenario	Training error (RMSE)	Test error (RMSE)
Lateral side at 10°C	0.1629	0.0515
Medial side at 10°C	0.3762	0.4333
Lateral side at 15°C	0.2392	0.2634
Medial side at 15°C	0.6911	0.8139
Lateral side at 20°C	0.2101	0.2372
Medial side at 20°C	0.2464	0.1499
Lateral side at 25°C	0.0684	0.0801
Medial side at 25°C	0.0910	0.1171

6.4 Result Analysis of the ANFIS Model

Similar to Section 5.4, a FIR filter was implemented to average the actual and predicted data after every 5 samples for smoothing out the short term fluctuations.

6.4.1 Subject 1

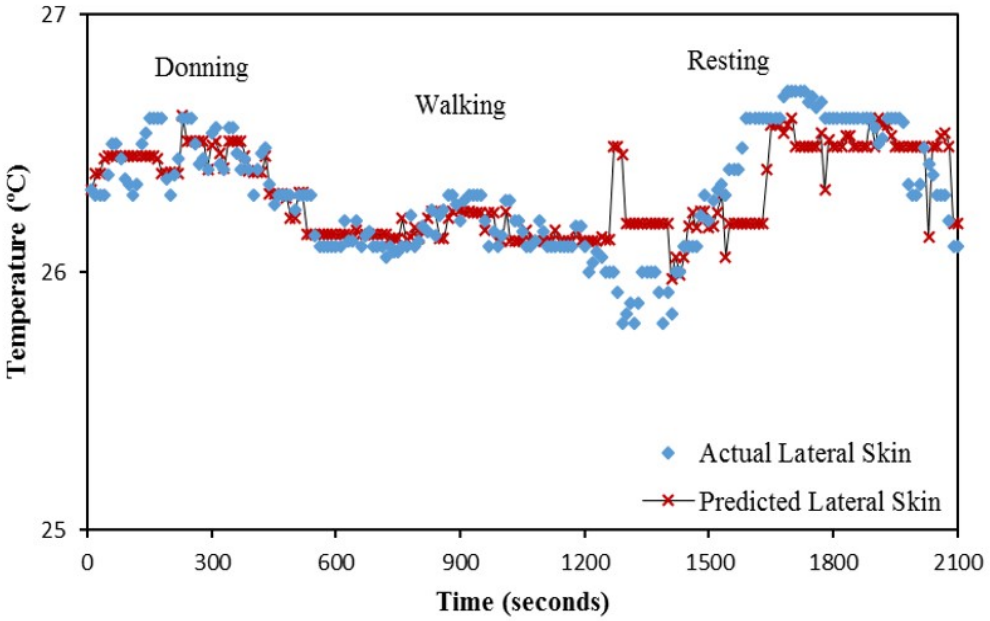

(a)

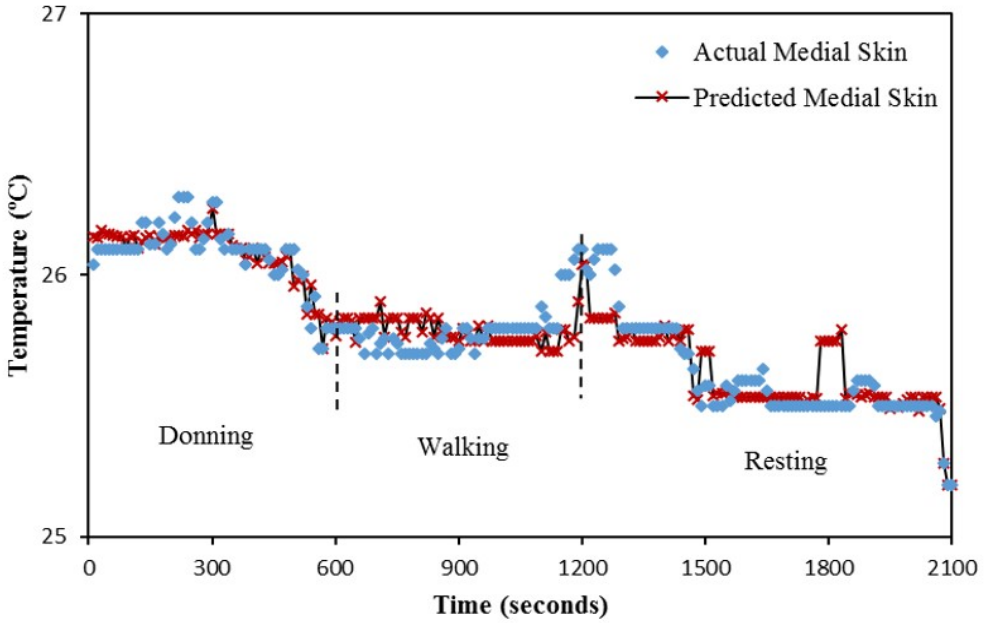

(b)

Figure 6.3: The predicted residual limb skin temperature from the ANFIS Model is shown along with the actual skin temperature at lateral and medial sides in (a) and (b) respectively at ambient temperature of 10°C.

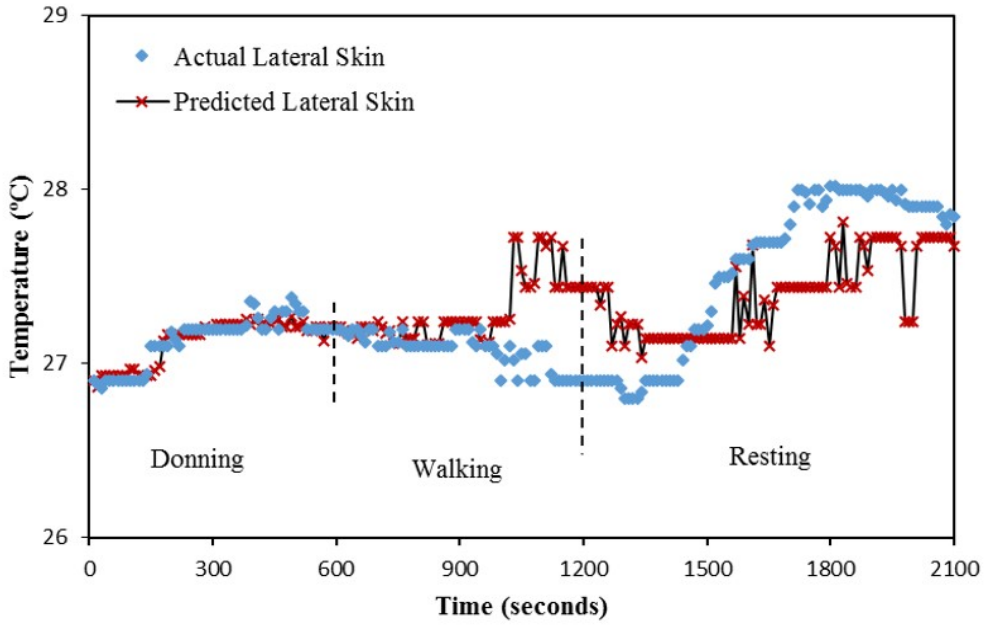

(a)

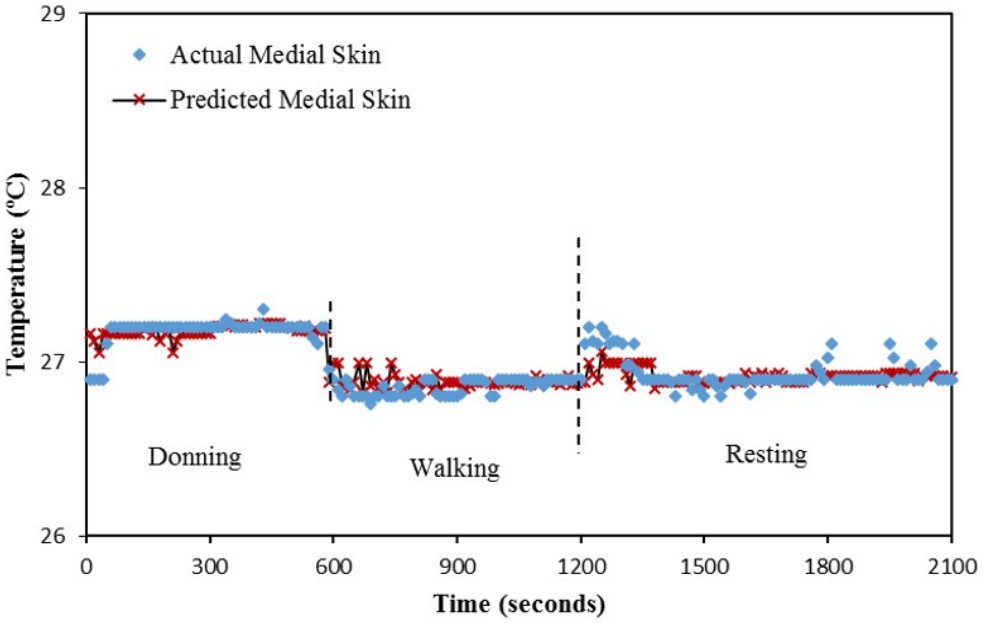

(b)

Figure 6.4: The predicted residual limb skin temperature from the ANFIS Model is shown along with the actual skin temperature at lateral and medial sides in (a) and (b) respectively at ambient temperature of 15°C.

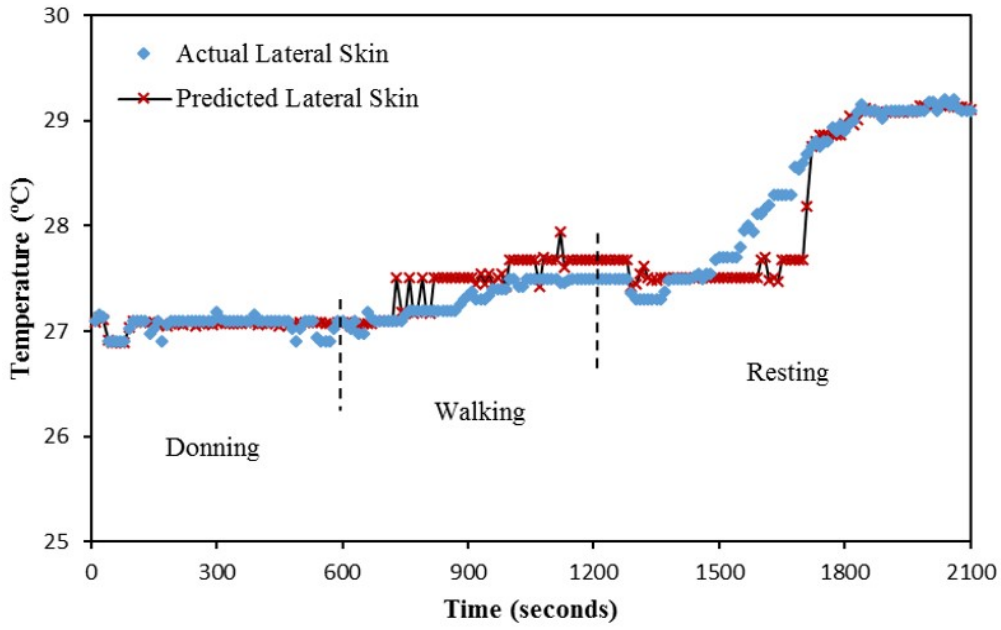

(a)

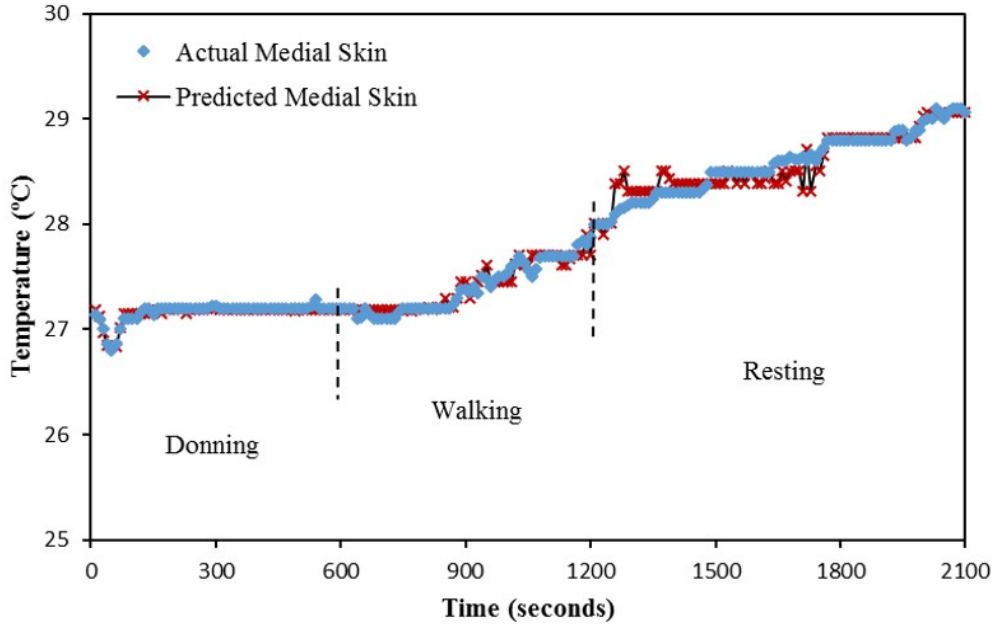

(b)

Figure 6.5: The predicted residual limb skin temperature from the ANFIS Model is shown along with the actual skin temperature at lateral and medial sides in (a) and (b) respectively at ambient temperature of 20°C.

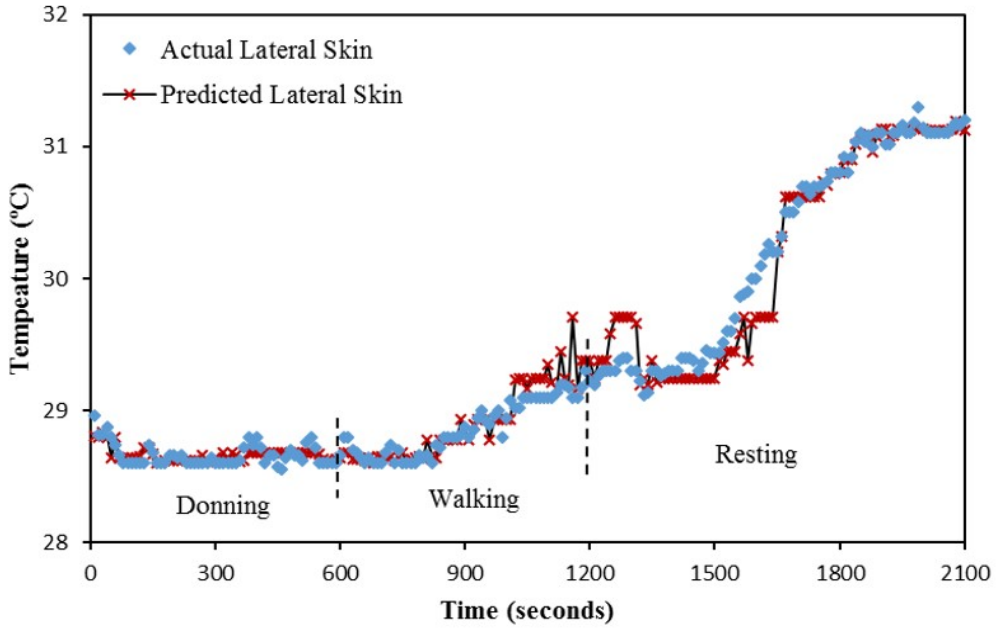

(a)

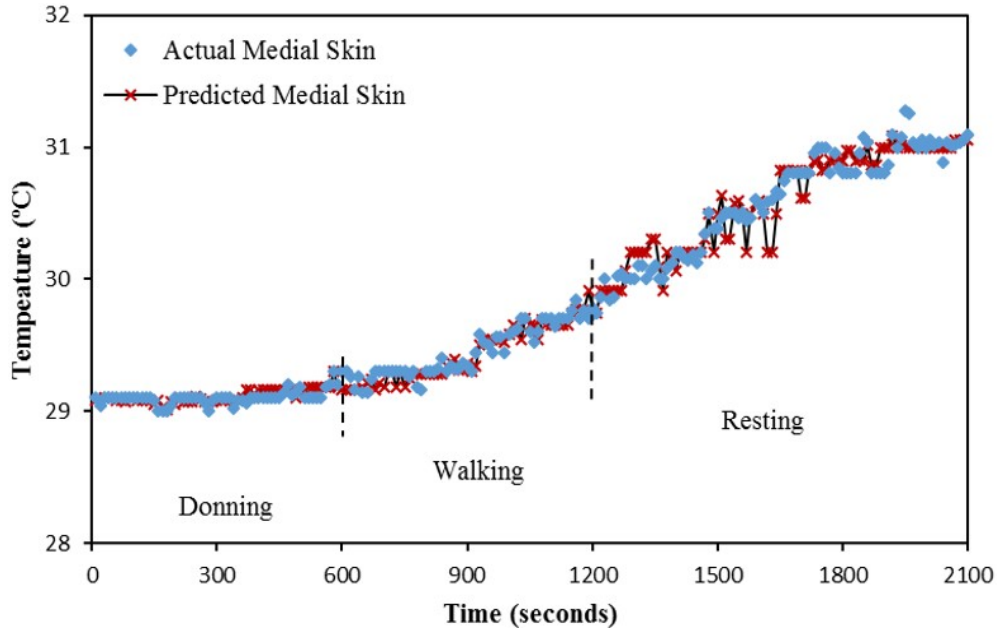

(b)

Figure 6.6: The predicted residual limb skin temperature from the ANFIS Model is shown along with the actual skin temperature at lateral and medial sides in (a) and (b) respectively at ambient temperature of 25°C.

6.4.2 Subject 2

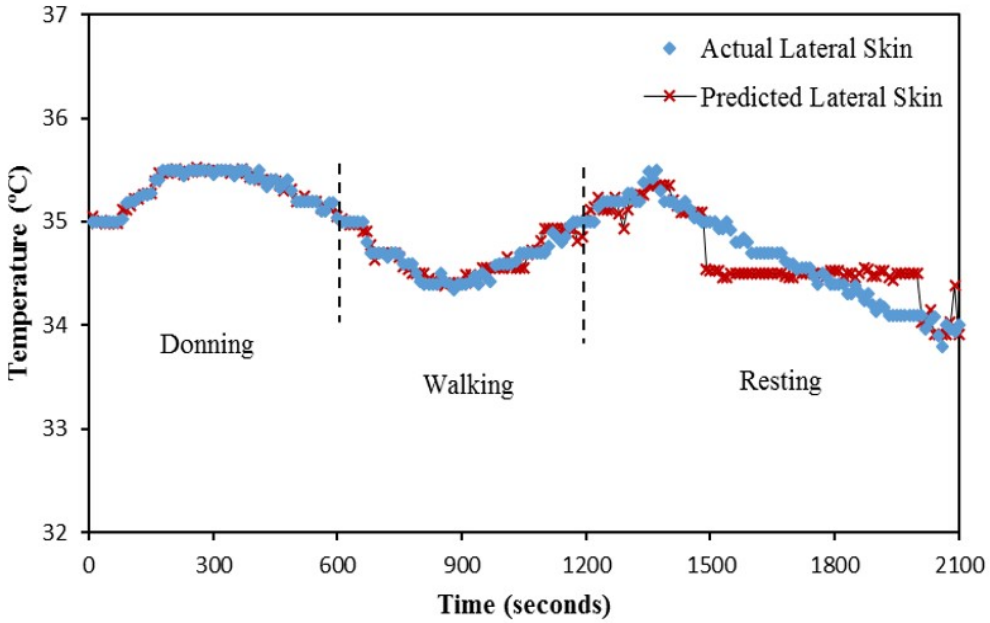

(a)

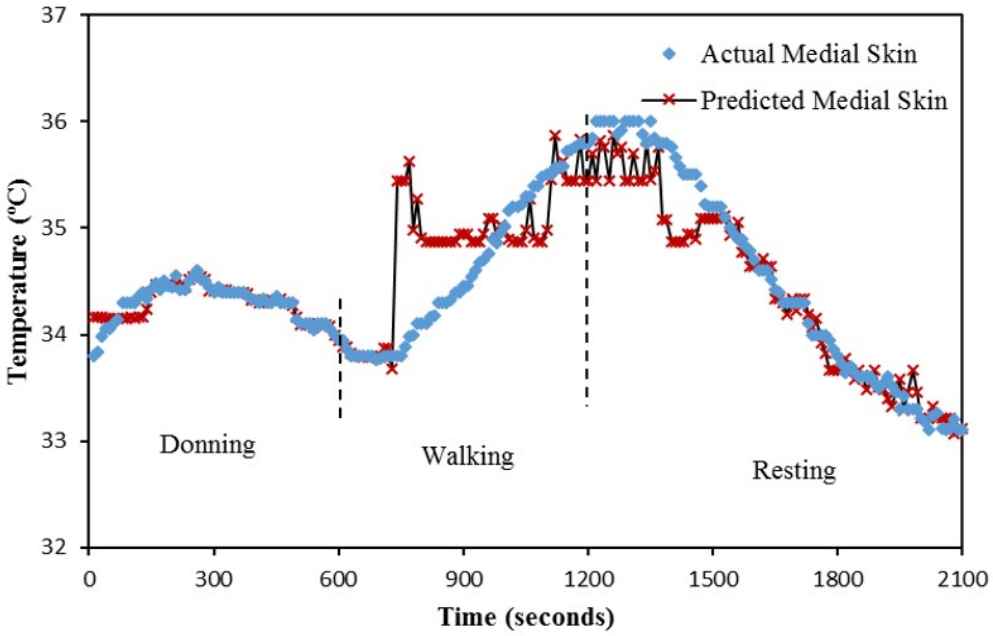

(b)

Figure 6.7: The predicted residual limb skin temperature from the ANFIS Model is shown along with the actual skin temperature at lateral and medial sides in (a) and (b) respectively at ambient temperature of 10°C.

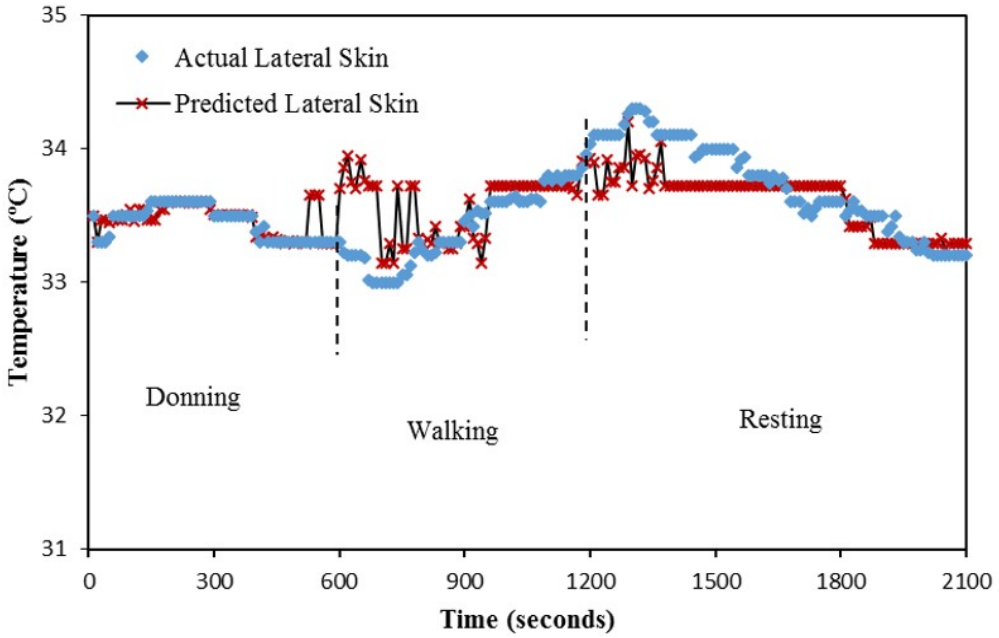

(a)

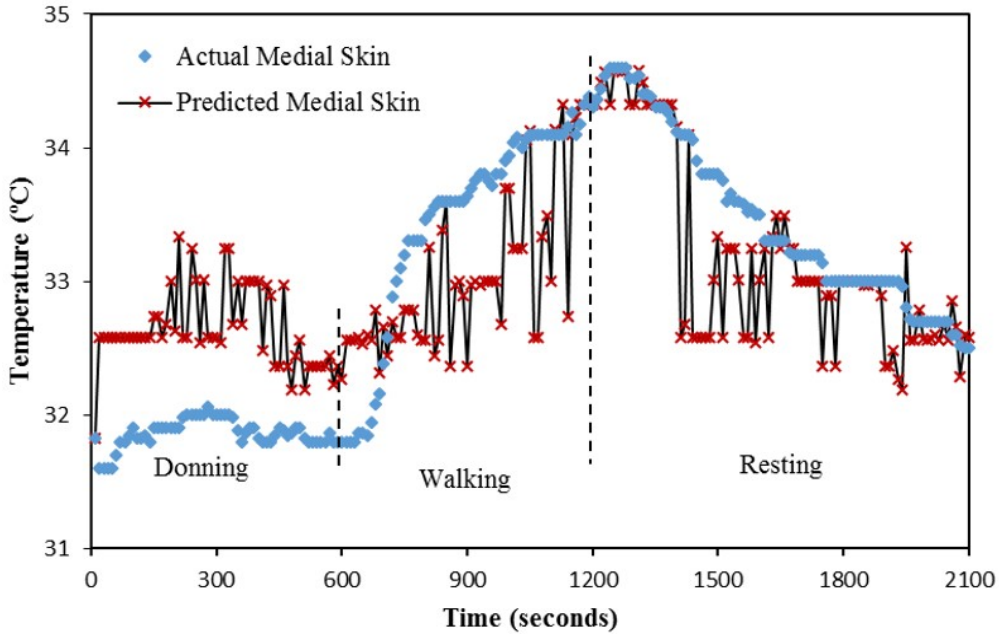

(b)

Figure 6.8: The predicted residual limb skin temperature from the ANFIS Model is shown along with the actual skin temperature at lateral and medial sides in (a) and (b) respectively at ambient temperature of 15°C.

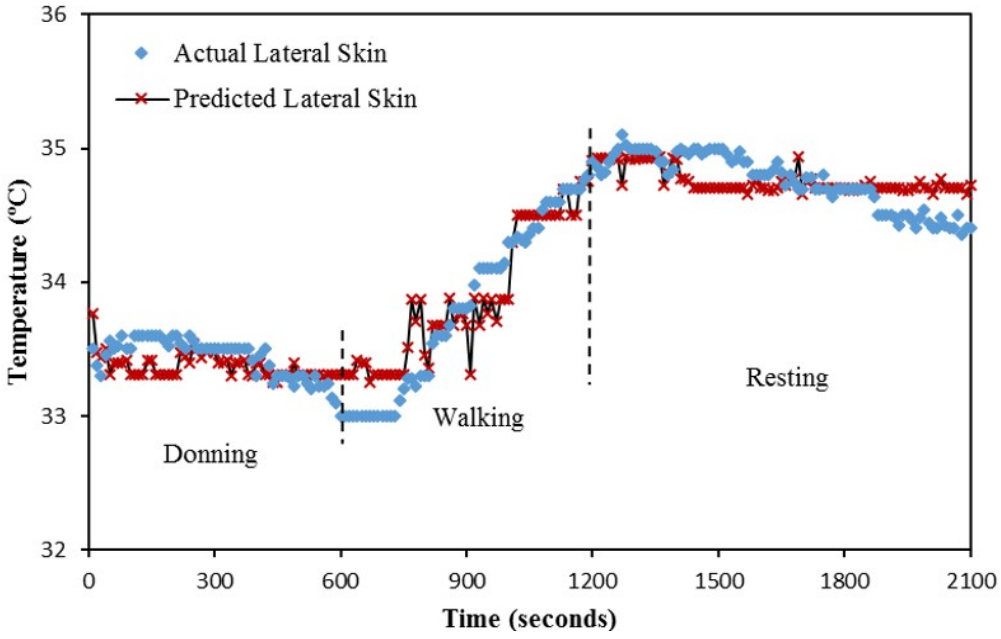

(a)

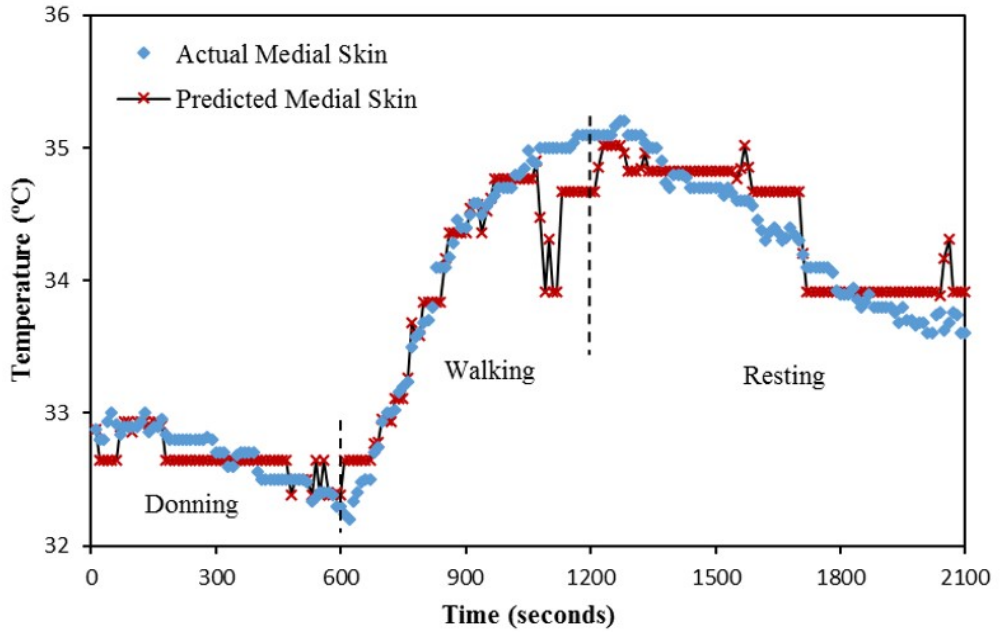

(b)

Figure 6.9: The predicted residual limb skin temperature from the ANFIS Model is shown along with the actual skin temperature at lateral and medial sides in (a) and (b) respectively at ambient temperature of 20°C.

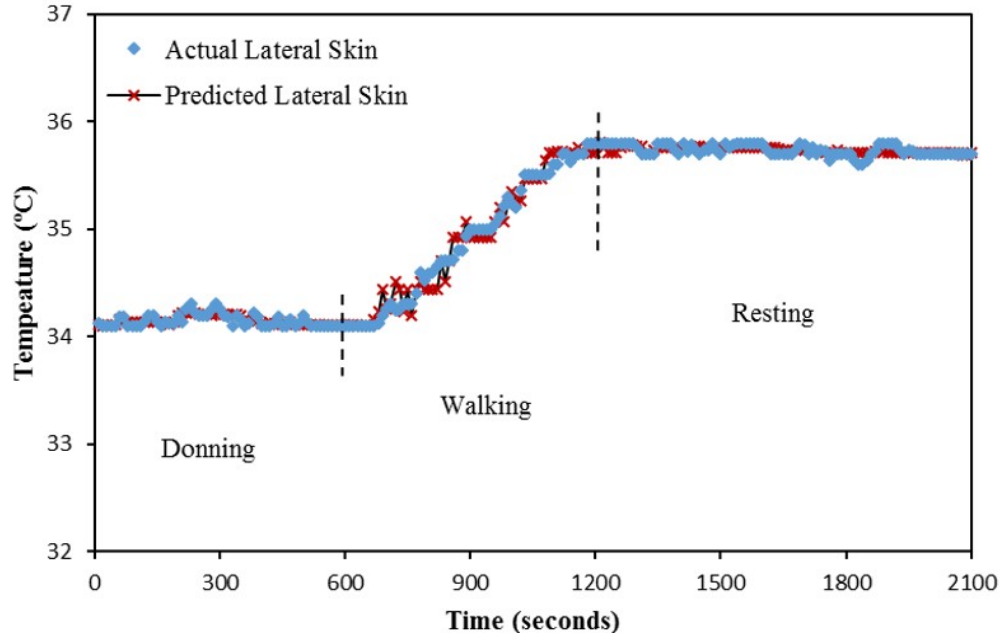

(a)

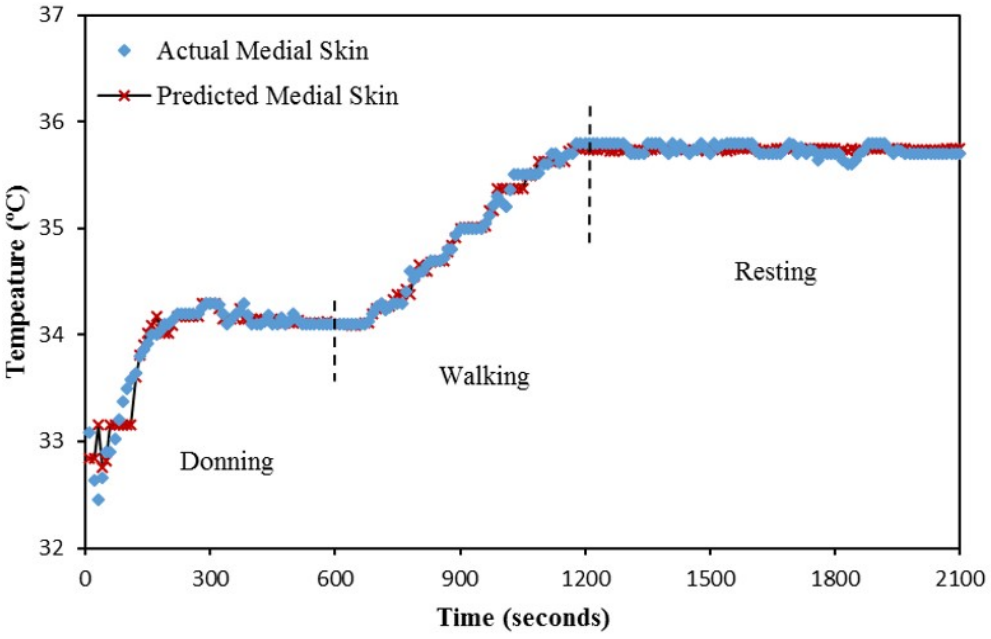

(b)

Figure 6.10: The predicted residual limb skin temperature from the ANFIS Model is shown along with the actual skin temperature at lateral and medial sides in (a) and (b) respectively at ambient temperature of 25°C.

6.5 Comparison Metrics of the ANFIS and GPML Model

It is seen that the residual limb temperature can be accurately predicted (albeit with fluctuations) by monitoring the temperature between the liner and the socket using ANFIS. In order deduce whether ANFIS or GPML (previously described in Chapter 5) have a better predictive ability they are compared by using some statistical tools like Mean Absolute Error (MAE), Root Mean Squared Error (RMSE), and R^2 criteria.

6.5.1 Mean Absolute Error (MAE)

The Mean Absolute Error (MAE) indicates how close the predictions are to the eventual outcomes which is given by

$$MAE = \frac{1}{n}\sum_{i=1}^{n}|f_i - y_i| = \frac{1}{n}\sum_{i=1}^{n}|e_i| \tag{6.12}$$

As seen in Equation 6.12, the mean absolute error can be defined as the average of absolute errors; the absolute error given by $|e_i| = |f_i - y_i|$, where f_i is the prediction and y_i the true value. It should be noted that in MAE, all the individual errors have equal weight in the average, making it a linear score.

6.5.2 Root Mean Squared Error (RMSE)

Calculation of Root Mean Squared Error (RMSE)involves squaring the difference between the predicted and corresponding observed values, averaging it over the

sample and then finally taking its square root. This can be written as

$$RMSE = \sqrt{\frac{1}{n}\sum_{i=1}^{n} e_i^2} \tag{6.13}$$

RMSE has a quadratic error rule, where the errors are squared before being averaged. As a result, a relatively high weight is given to large errors [127]. This could be useful when large errors are undesirable in a statistical model. From Tables 6.3 and 6.4 (for subjects 1 and 2 respectively), it can be deduced that for the Gaussian model the MAE and RMSE is slightly lower as compared to ANFIS. The large MAE and RMSE in some scenarios of ANFIS can be attributed to the number of epochs being 50 for each of the modelling scenarios which might not be sufficient if the training data differs significantly from the testing data. To reduce the errors, either the number of epochs can be increased or by introducing deep learning. In order to discriminate between the models for their predictive performance, the error metrics should be capable to differentiate amongst the model results. In this context, the MAE might be affected by large average error values by ignoring some large errors. The RMSE is generally better in reflecting the model performance differences [128] as it gives higher weight to the unfavourable conditions. The difference between the RMSE of the Gaussian model and ANFIS is not immense and hence both the models have comparable performance metrics. Therefore, in order to have a reliable statistical comparison between the mathematical models, both the MAE and RMSE can be used together to ascertain the variation in errors in a given set of predictions.

6.5.3 R^2 Criteria

Another measure of goodness-of-fit of the model is the R^2 criteria. Higher values are indicative that the predictive model fits the data in a better way. By definition, R^2 is the proportional measure of variance of one variable predicted from the other variable. Thus ideally the value of R^2 to approach one is always desirable. If a dataset has n values with y_i being the true value and f_i being the predicted, then the mean of the observed data $\overline{y}$ is given by

$$\overline{y} = \frac{1}{n}\sum_{i=1}^{n} y_i \tag{6.14}$$

Then, in order to measure the variability of the dataset, the residual sum of squares SS_{res} and the total sum of squares SS_{tot} as seen from Equations 6.14 and 6.15 are computed.

$$SS_{res} = \sum_{i}(y_i - f_i)^2 \tag{6.15}$$

$$SS_{tot} = \sum_{i}(y_i - \overline{y})^2 \tag{6.16}$$

In order to determine the R^2 criteria, SS_{res} is normalized w.r.t SS_{tot} which is given as

$$R^2 = 1 - \frac{SS_{res}}{SS_{tot}} \tag{6.17}$$

However, a high R^2 tells you that the curve came very close to the points but in reality it does not always indicate the model quality [129]. From Table 6.5 it is seen that both Gaussian and ANFIS models have similar R^2 values which are indicators that in both the modeling techniques, the prediction capability is similar. Using the R^2 criteria in conjunction with the MAE and RMSE, it can be fairly deduced that the Gaussian and ANFIS models can be used for the

prediction of residual limb temperature but the predictive ability of GPML model is better as it follows the trend and gives output without much fluctuations.

Table 6.3: Performance comparison of the ANFIS and GPML models for Subject 1

Scenario	MAE		RMSE	
	ANFIS	GPML	ANFIS	GPML
Lateral side at 10°C	0.1054	0.0865	0.0781	0.1020
Medial side at 10°C	0.0676	0.0819	0.0738	0.1125
Lateral side at 15°C	0.2172	0.0831	0.6985	0.0966
Medial side at 15°C	0.0485	0.0529	0.0742	0.0835
Lateral side at 20°C	0.1351	0.1484	0.1265	0.2967
Medial side at 20°C	0.0558	0.0667	0.0443	0.0942
Lateral side at 25°C	0.0899	0.1005	0.0696	0.1459
Medial side at 25°C	0.0889	0.0828	0.1519	0.1090

Table 6.4: Performance comparison of the ANFIS and GPML models for Subject 2

Scenario	MAE		RMSE	
	ANFIS	GPML	ANFIS	GPML
Lateral side at 10°C	0.1042	0.2128	0.0515	0.2183
Medial side at 10°C	0.2146	0.1845	0.4333	0.2212
Lateral side at 15°C	0.1561	0.1353	0.2634	0.1464
Medial side at 15°C	0.5265	0.2436	0.8139	0.2647
Lateral side at 20°C	0.1607	0.2098	0.2372	0.2170
Medial side at 20°C	0.1687	0.1217	0.1499	0.1468
Lateral side at 25°C	0.0463	0.0517	0.0801	0.0714
Medial side at 25°C	0.0527	0.0577	0.1171	0.0916

Table 6.5: R^2 criteria comparison of the ANFIS and GPML models both amputee subjects

Scenario	Subject 1		Subject 2	
	ANFIS	GPML	ANFIS	GPML
Lateral side at 10°C	0.9802	0.97	0.982	0.985
Medial side at 10°C	0.981	0.98	0.964	0.98
Lateral side at 15°C	0.953	0.98	0.977	0.986
Medial side at 15°C	0.988	0.989	0.945	0.979
Lateral side at 20°C	0.964	0.966	0.978	0.982
Medial side at 20°C	0.98	0.984	0.97	0.985
Lateral side at 25°C	0.979	0.978	0.987	0.989
Medial side at 25°C	0.98	0.9831	0.99	0.99

6.6 Summary

This chapter addresses the challenges of non-invasively measuring the in-socket residual limb temperature by comparing two different modeling techniques, namely ANFIS and Gaussian Processes. The temperature profile of the residual limb skin is dependent on the ambient temperature and the activity level of the subject. The performance metrics of both the models indicate that they are very similar in

their predictive ability with an accuracy of $\pm 0.5^{\circ}$C. However, this approach has certain limitations as well. The residual limb temperature profile will differ for every amputee as there are variations in physiological responses (such as differences in capillary dilatation) and variations in properties of the skin parameters (such as thickness/composition of the skin layers). Because of the varying residual limb temperature profile in individuals, these machine learning algorithms have to be personalised by training them with individual datasets for each of the amputee subjects. This study which was conducted on two amputee subjects a number of times, verified the success of the proposed approach. Therefore, this work could be used to figure out the envelope in estimating the statistical power i.e. how many people are needed to make the model clinically significant and it will be useful in extending it on a greater population in order to define a generic behaviour. Since the temperature profile of the residual limb is dependent on the ambient temperature, it puts a constraint on drawing up a generalised model for all ambient temperatures. This could potentially be resolved by using interpolation techniques in the model at a given ambient temperature to predict the residual limb temperature profile at another ambient temperature provided that the activity state of the subject is known.

Chapter 7

Towards Wearable Platform for e-Health

7.1 Introduction

In many areas of the world accessing professional physicians 'when needed/as needed' might not be always possible for a variety of reasons. Therefore, in such cases a targeted e-Health solution to safeguard patient long-term health could be a meaningful approach. Today's modern healthcare technologies, often built around electronic and computer-based equipment, require an access to a reliable electricity supply. Many healthcare technologies and products also presume access to the high speed internet is available, making them unsuitable for use in areas where there is no fixed-line internet connectivity, access is slow, unreliable and expensive, yet where the most benefit to patients may be gained.

In this chapter, the details of a mobile sensor platform is presented, based around readily-purchased consumer components, to facilitate a low cost and efficient means of monitoring the health of patients with prosthetic lower limbs. This platform is designed such that it can also be operated in a standalone mode i.e. in

the absence of internet connectivity, thereby making it suitable to the developing world. The platform works with an Android mobile device, in order to allow for the capture of data from a wireless sensor unit, and to give the clinician access to the results from the sensors. The results from the analysis, are demonstrated to be of use for remote monitoring. This is specifically targeted for monitoring the tissue health of lower limb amputees. The monitoring of residual limb temperature and gait can be a useful indicator of tissue viability in lower limb amputees particularly for those suffering from diabetes. The route wherein contactless monitoring of tissue health is achievable using the Gaussian process technique, ANFIS and complementary filter which is described in previous chapters is implemented in the platform. This knowledge will be useful in establishing biomarkers related to a possible deterioration in a patient's health or for assessing the impact of clinical interventions. Thus, this chapter discusses the design and development of a wearable sensor platform for lower limb amputees that is capable of gathering data from the sensors (placed on the elastomer), and store and transmit to a central health database, for the purpose of analysing it.

7.2 Wearable Mobile Sensor Module Design

7.2.1 System Overview

The design of the wearable sensor platform has to be such that it can unobtrusively gather data from a wearable sensor and transfer this information periodically to a database server, via a wireless transfer protocol. It would therefore be beneficial for lower limb diabetics, to be able to detect either the early signs of actual tissue injury before the development of serious complications; and/or monitor the conditions at the prosthetic socket/residual limb interface to give a warning of a significant increase in the risk of injury before it develops. If platforms like this were to be deployed to communities for use on an ongoing

basis, it can be useful in alerting a health professional of warning signs, improve patient quality of life and perhaps allow a significant reduction in the frequency of outpatient check-up appointments. In addition, the information gathered by a monitoring system on areas prone to damage could contribute towards improving prosthesis design. This design is architected in order to make as low-power a solution as possible, using as much off-the-shelf equipment as practical, such that kits maybe assembled out of commonly available items. Minimal equipment is used, in order to reduce the complexity of the system, and to reduce the cost of each unit as possible.

The building blocks of the wearable sensor platform system are the server and the data logger. The server can be placed remotely and need not be in the close proximity of the data logger. The server is Raspberry Pi Zero on which the data processing and storage is done. It also acts as a Wi-Fi access point, through a Universal Serial Bus (USB)-connected wireless adapter, eliminating the need for a dedicated wireless access point. The Raspberry Pi Zero hosts an Hypertext Transfer Protocol (HTTP)-based Application Programming Interface (API), and acts as a Dynamic Host Configuration Protocol (DHCP) server on the Wi-Fi network, allowing for the rest of the platform to be connected. The data logger device comprises of two components the prosthesis-mounted platform with sensors, and an Android smartphone. The wearable platform is mounted on the shank of the prosthetic user and consists of an Arduino board interfaced with thermistors (NTC type, 100k) and an IMU to monitor the liner-socket interface temperature and the gait of the user. Bluetooth is used to transmit the data from the Arduino to the smartphone. The Android smartphone acts as a gateway between the Arduino and the server by transmitting it to the server using Wi-Fi. In the absence of Wi-Fi connection, the Android stores the data locally in a database. The Android platform was selected on account of its widespread penetration within emerging markets, and the relatively low cost of entry-level

handsets, reducing the overall cost of the proposed solution. By connecting an Android device to the Wi-Fi hotspot created by the Raspberry Pi Zero, the application software may be downloaded directly from the Raspberry Pi Zero, where no internet access is available.

At the server end the gait and liner-socket interface temperature data are fed into MATLAB for processing, using the mathematical algorithms Complementary filter and GPML respectively (the techniques of which are discussed in Chapters 3 and 5). Hence, the residual limb skin temperature and the gait of an amputee user can be monitored in a contactless way. The server can be accessed by authorised medical personnel for access to the patient data. If a threshold level is reached for residual limb skin temperature or abnormal gait pattern, the clinician can trigger a warning signal from the server to the smartphone for alerting the prosthetic user. Interpolation technique is also introduced at the server end for the temperature data to reduce the need for calibrating the GPML model for all the ambient temperatures. The architecture of the wearable platform is illustrated in Figure 7.1.

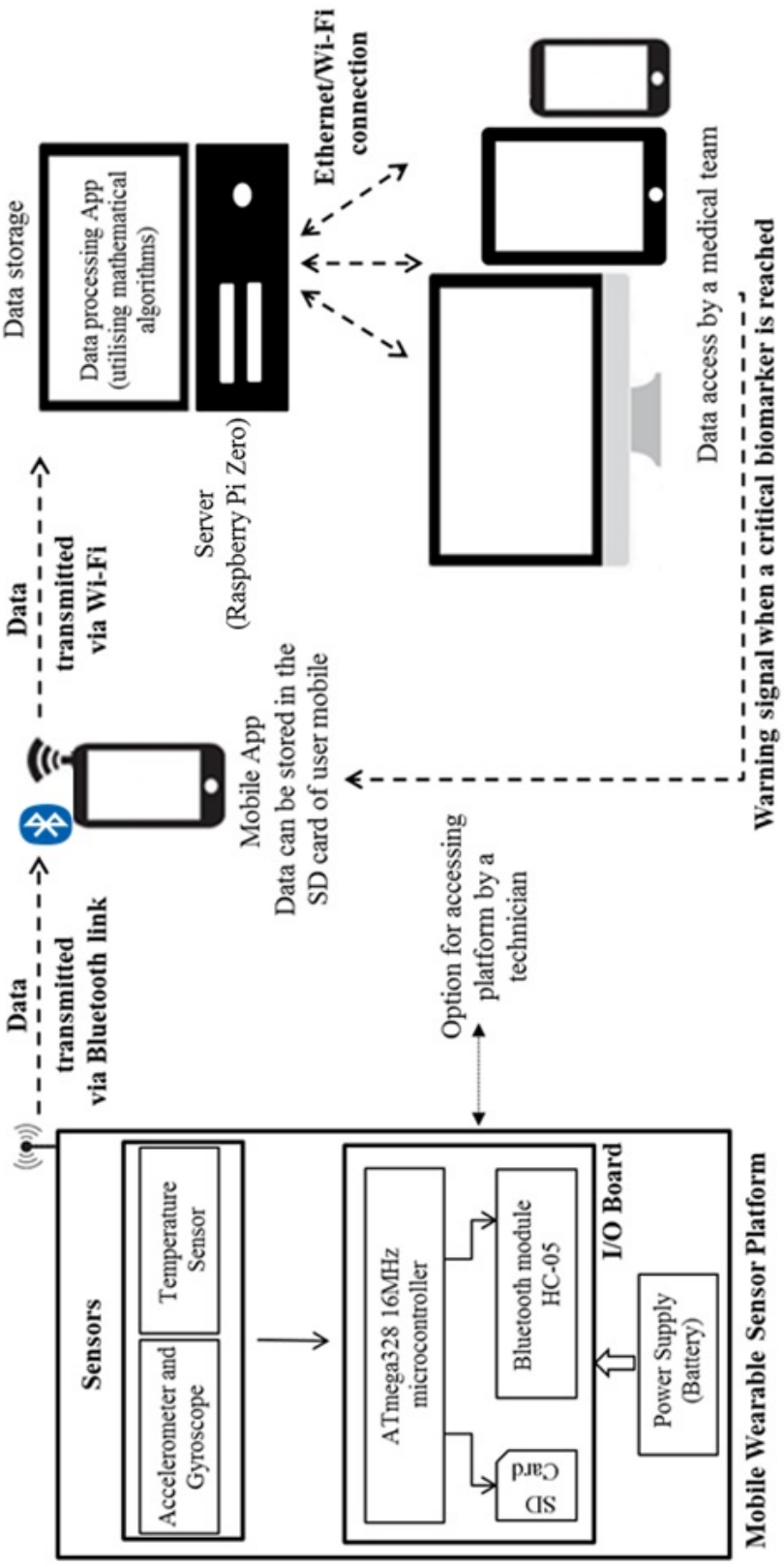

Figure 7.1: Architecture of the data flow in the multi-sensor wearable platform.

7.2.2 Hardware Overview

The sensing platform is composed of a number of discrete components. The center of the platform is an Arduino (ATmega328 16 MHz) microcontroller. The wearable platform can be interfaced with a number of sensors but in the design for the prosthetic users, temperature and gait measurement sensors are introduced. The temperature and gait of the residual limb of an amputee subject can be monitored by a medical team at pre-defined sampling rate. The Arduino platform is capable of communicating via Bluetooth, Wi-Fi or cellular networks.

The Bluetooth module HC-05 is an easy to use module, designed for transparent wireless serial connection setup. It has the footprint as small as 12.7 mm x 27 mm. Its low power operation at 1.8 V makes it even more compatible for use in this design.

The Wi-Fi shield for the Arduino connects to the internet wirelessly using the 802.11 wireless specifications. The Wi-Fi shield connects to an Arduino board using long wire-wrap headers which extend through the shield [130]. The current draw of the Arduino is roughly 25-50 mA whereas that of the Wi-Fi shield will be 60-500 mA depending upon how much network traffic is sending/receiving. Thus, the power consumption of this shield is huge and can drain out the battery fairly quickly.

The Arduino GSM shield connects the Arduino to the internet using the GPRS wireless network. The shield uses a radio modem M10 by Quectel. The M10 is a Quad-band GSM/GPRS modem that works at frequencies GSM 850 MHz, GSM 900 MHz, DCS 1800 Hz and PCS 1900 MHz. It supports TCP/UDP and HTTP protocols through a GPRS connection. GPRS data downlink and uplink transfer speed maximum is 85.6 kbps [131]. However, the modem can pull up to 2 A of current at peak usage, which can occur during data transmission and requires 700-1000 mA of current draw at other times [**132**]. This is of concern, as in the

realisation of the above requirements are the power consumption of the device and the longevity of the battery between charges. The power consumption of the Arduino when interfaced with the above mentioned communication modules is compared in Figure 7.2. It can be seen that the power consumption of the GSM shield is about 20 times more than the Bluetooth module. The Wi-Fi shield's power consumption is about 1763 mW as compared to 403.5 mW of the Bluetooth module. Since the Bluetooth module is small in size, with low power consumption due to reduced range and bandwidth, it was selected for data communication between the sensor and mobile phone. Further studies on the battery life w.r.t. the platform are discussed in Section 7.3 which also reiterates that Bluetooth communication is most power effective of all in wearable sensor design solution.

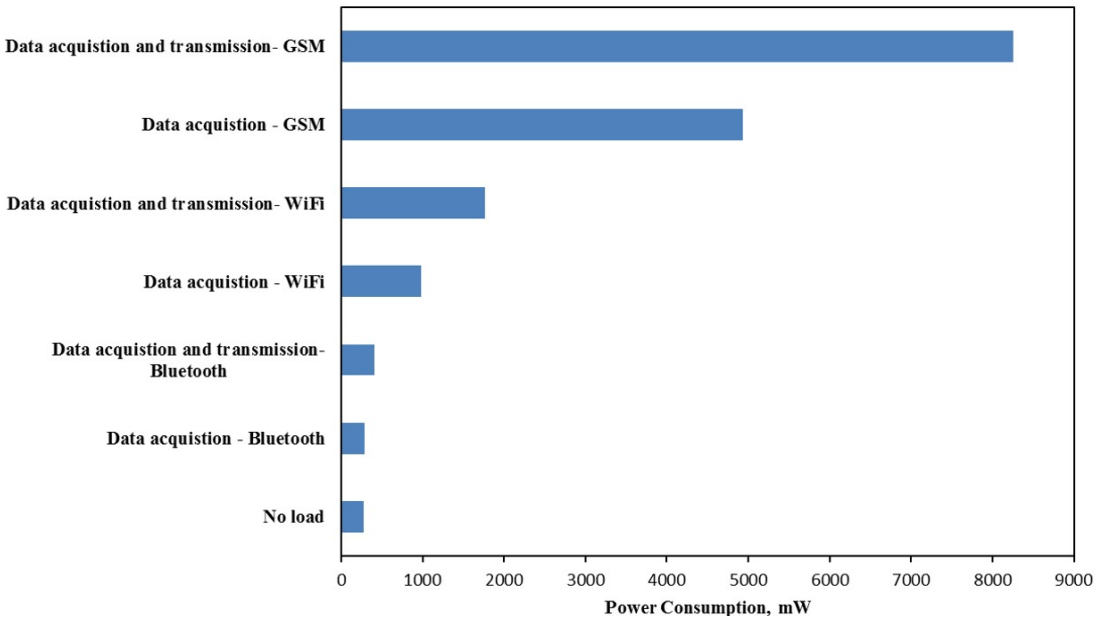

Figure 7.2: Comparison of wearable sensor platform power consumption with different modes of data communication (Data transfer rate = 1200 bytes/second).

The prosthesis-mounted equipment requires an Arduino microcontroller, an HC-05 serial Bluetooth module, two temperature sensors, and a MPU6050 6-axis

accelerometer and gyroscope module. The temperature, accelerometer and gyroscope data is transmitted from the Arduino microcontroller, over the Bluetooth link, to the Android smartphone running the data gathering software. The smartphone application maintains a local copy of the data on its Secure Digital (SD) card as backup, and transmits batched data over Wi-Fi to the Raspberry Pi Zero. The Android smartphone provides an interface to control the data logging, adjusting parameters as required to ensure that the patient information is kept separately, and ensuring that it is correctly associated with the patient the data was gathered from [2]. The microcontroller was connected to an HC-05 Bluetooth module, which communicated over Serial Port Profile (SPP). An Android smartphone was paired with this module and connected over Bluetooth such that the data collected by the Arduino board is transferred onto the software (customised mobile app) running on the smartphone. The data is simultaneously backed up on the SD card in the wearable sensor platform and also on the smartphone [50]. The schematic of the wearable sensor platform along with the Arduino code is provided in Appendix D.

After the data is received by the smartphone, it is then transmitted over Wi-Fi to the Raspberry Pi Zero, acting as the data collection server, where it is stored in a Postgres database after being received by the web API. This allows for the retrieval and processing of the sensor data using mathematical learning algorithms like Gaussian Processes modelling technique on a data processing app. This clinically relevant information can be then accessed by medical personnel, using the secure Wi-Fi link from their own device, or from the smartphone used for data collection. Where the system is deployed offline there may be scenarios where there is only one mobile device available, both for data gathering and retrieval. In order to facilitate this, the reporting interface is designed such that it be accessed from both desktop and mobile browsers.

The clinician has access to data for each of their patients from within their interface. After selecting a patient identifier, all previous sessions recorded with the monitoring platform are visible, and can be accessed. It is possible therefore to compare the gait profile and predicted residual limb skin temperature between patients, or to monitor deterioration or variations over time for one patient. The clinician interface provides access to the patient information, allowing for feedback to be given to the patient in real-time (residual limb skin temperature and the shank angle).

7.2.3 Software Overview

The comma-separated data from the sensors interfaced on the Arduino platform are transmitted via the Bluetooth link between the HC-05 module and Android smartphone. Each of these samples was transmitted over a single line of text data. Within the mobile app in the Android smartphone, the incoming data over Bluetooth is stored after each sample is tagged as a part of the 'stream'. The concept of streams is introduced in order to differentiate between samples of different scenarios, such that it can be analysed later. This allows for comparisons to be carried out, either between patients or for one patient over time, making it possible to compare previous experiments, identifying trends or deterioration.

The platform is equipped to handle connection failure scenarios like loss of Bluetooth link between HC-05 module and Android smartphone; and a lack of Wi-Fi network for the Android smartphone to connect to the server. If the Bluetooth connection is lost, then the HC-05 module buffers the unsent data (if sufficient memory is available) and then tries to retransmit the unsent samples upon re-establishing the connection. In the event of no Wi-Fi/cellular network being available on the Android smartphone to connect to the server, Android application creates a local database and stores all samples and timestamps. When

connectivity is available it carries out a synchronisation routine with the server. The synchronisation process involves identification of the last received sample ID for a given stream and then recognising if any further samples with a larger sample ID exist for that stream. It should be noted that for this synchronisation logic to be work the sample ID should always monotonically increment over time, as implemented in the application. Considering the need for the system to be both usable when given to a patient for use away from the clinician, as well as used with a clinician monitoring the readings being reported to the Raspberry Pi Zero server for analysis, the application permits either use-case, transparently and without configuration, by carrying out the synchronisation process whenever connectivity to the server is possible [**133**].

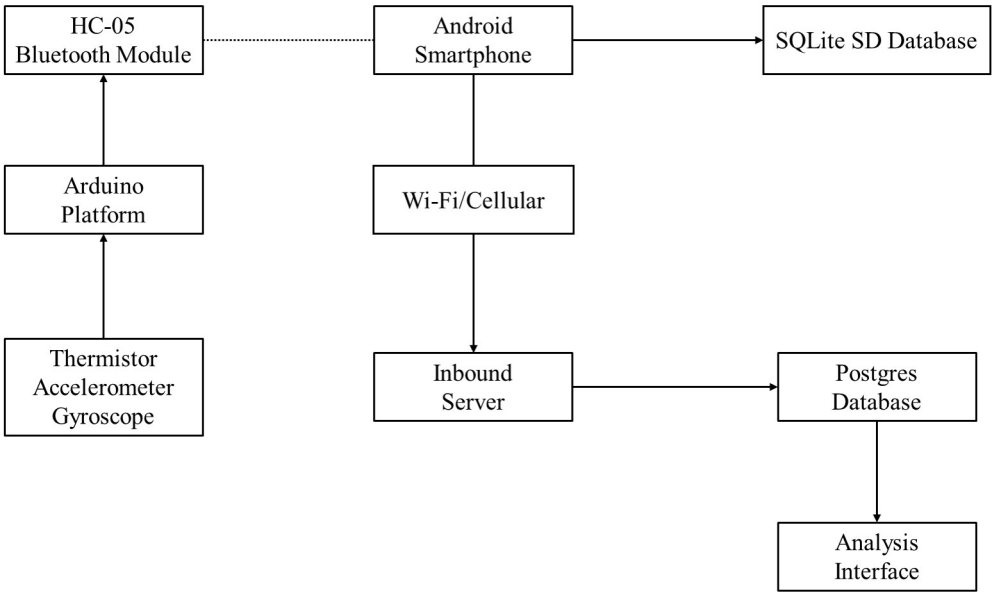

Figure 7.3: Data flow in the wearable sensor platform.

The data retrieval interface was implemented as a Flask-based web application, written in Python. A responsive Bootstrap interface was created, to allow the same management and data retrieval interface to be used from both fixed and mobile devices. The Flask application also presents an API for the synchroni-

sation of data to the server from the mobile application. The underlying data gathered from sensors is stored in a local Postgres database, held on the Raspberry Pi Zero. Figure 7.3 illustrates the route of the data communication from the sensors to the central database. The access to the health monitoring server is password protected with each clinician having a unique identifier to login as shown in Figure 7.4.

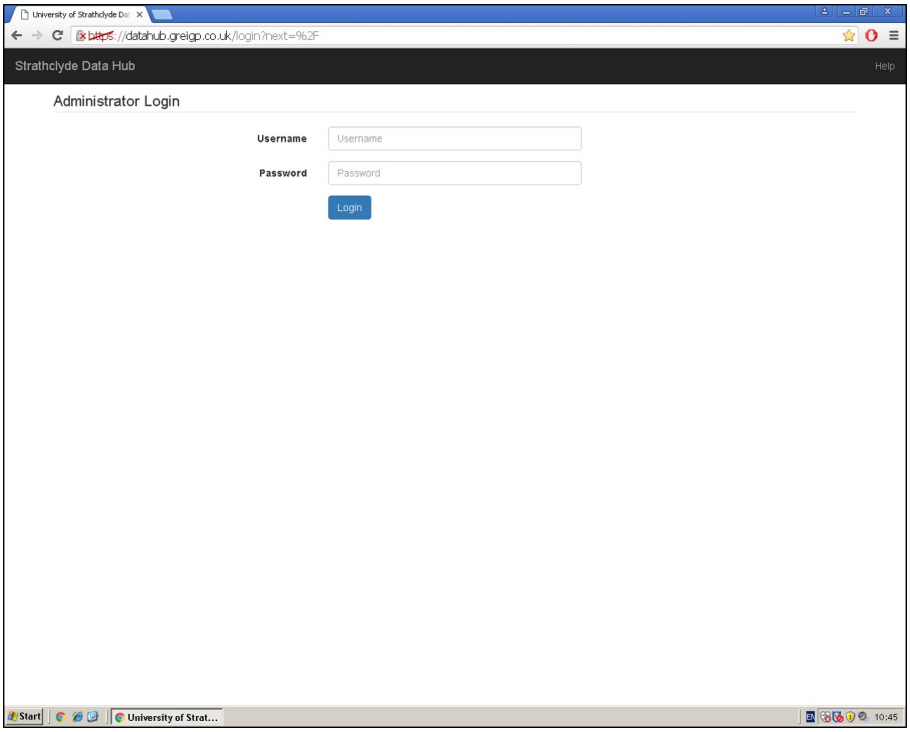

Figure 7.4: Login screen at the server interface.

In order to ensure that no personal or identifying information (even a patient identifier) is held on the smartphone (which may be shared between users, or also used by the clinician), a stream-based model for the upload of data is implemented. Within the stream-based model, the Android application requires only a single setting to be adjusted prior to issuing the device to a new patient for use. This is designed to facilitate use of the one platform, where all equipment must be self-contained and brought by the clinician, who may not be an expert

in configuring the platform. Rather than configuring accounts within the application, the clinician simply creates a new stream from the server configuration interface as seen in Figure 7.5. This displays a numerical stream ID, which is entered into the Android application. Having set the stream ID, the server is able to map this stream to a patient, but no information pertaining to the patient is exposed to the smartphone [50]. Once a successful connection is established between the Android smartphone and server, the data is uploaded to the server in the corresponding stream. This is illustrated in Figure 7.6.

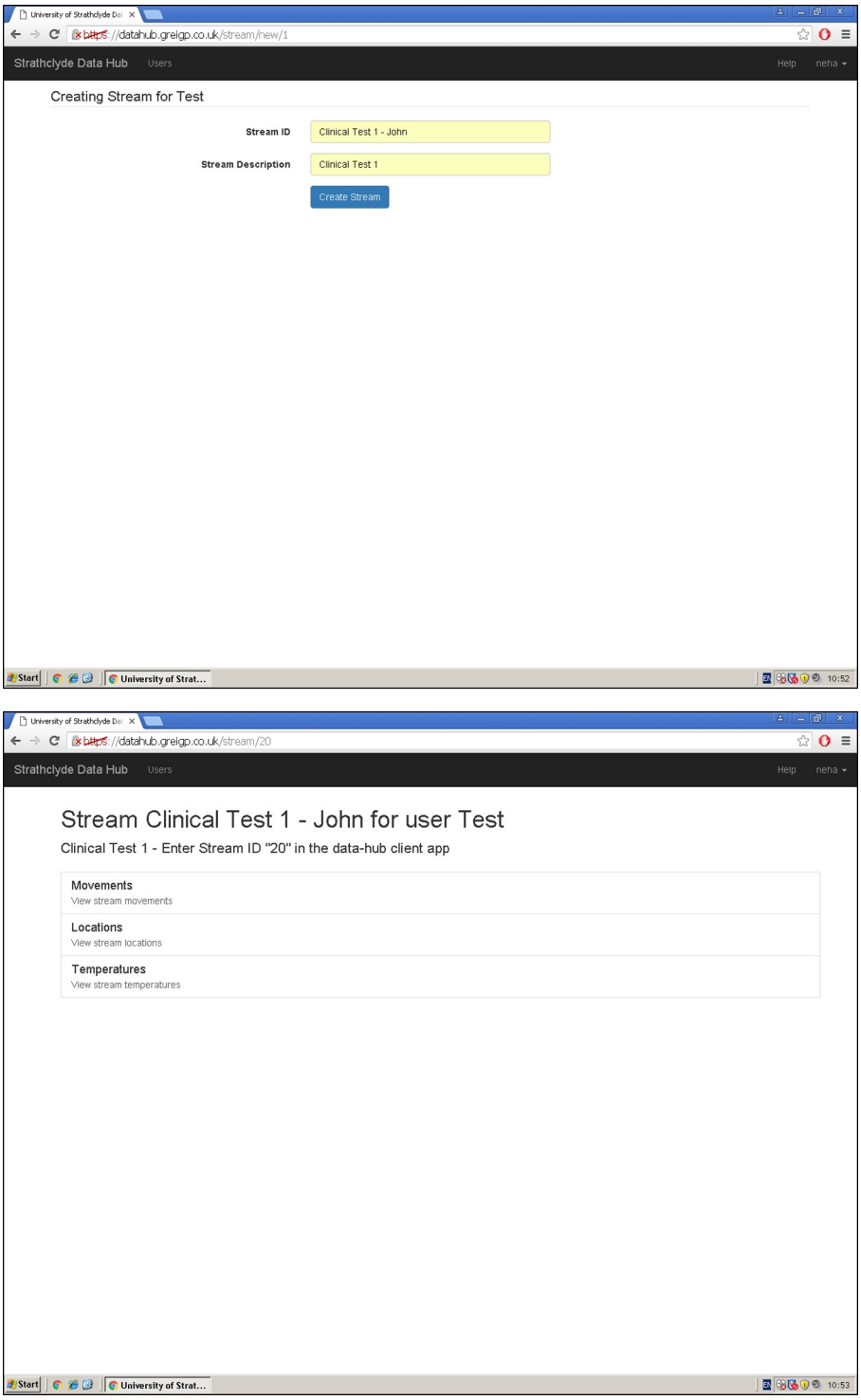

Figure 7.5: Creation of a new stream from the server configuration interface by the clinician.

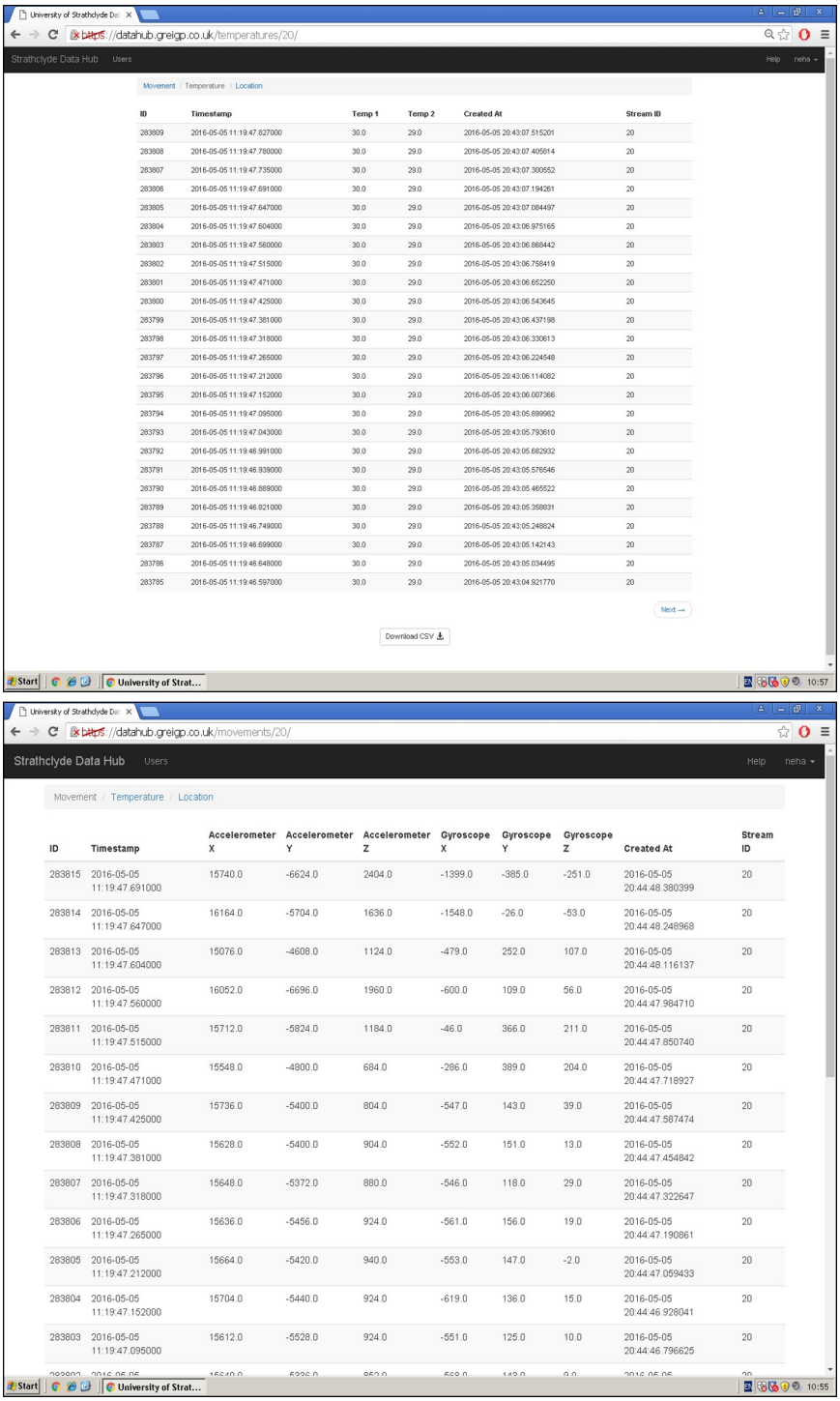

Figure 7.6: The temperature and gait data uploaded in the server at the corresponding stream.

7.2.4 Battery Monitoring

The wearable platform is entirely dependent on battery power for the realisation of monitoring the tissue viability in lower limb amputees. Continuous monitoring along with transmission of sensor data will deplete the battery powering the Arduino microcontroller over a period time, thereby leading to failures. In order to alleviate this situation, a battery monitoring unit is included in the design of the multi-sensor wearable platform. The design of the battery monitoring unit as seen in Figure 7.7, simply consists of a two resistor voltage divider circuit which converts the terminal voltage of the battery powering the board (typically 9-12 Volts) to a lower voltage in order to be read by the Arduino microcontroller. Utilising Ohm's law, the voltage drop V_{out} across resistor R_2 as seen in Equation 7.1, is fed to the analog input pin V_{in} of the microcontroller.

$$V_{out} = \frac{R_2}{R_1 + R_2} V_{Battery} \tag{7.1}$$

The reduced lower voltage seen by the microcontroller analog input pin is then converted to the actual battery voltage $V_{Battery}$ by multiplying it with the voltage conversion ratio. The system is designed such that when the battery monitoring circuit detects that $V_{Battery} \leq 5$ V, which is the minimum for arduino board to operate, a message saying 'Battery Level Low' is sent to the user's smartphone. This alerts the user with both a visual and audible indication, using the platform's notifications API. This enables the user to detect low battery levels of the platform and charge it, in order to minimise the risk of failing to capture data due to power failures [**3, 132**].

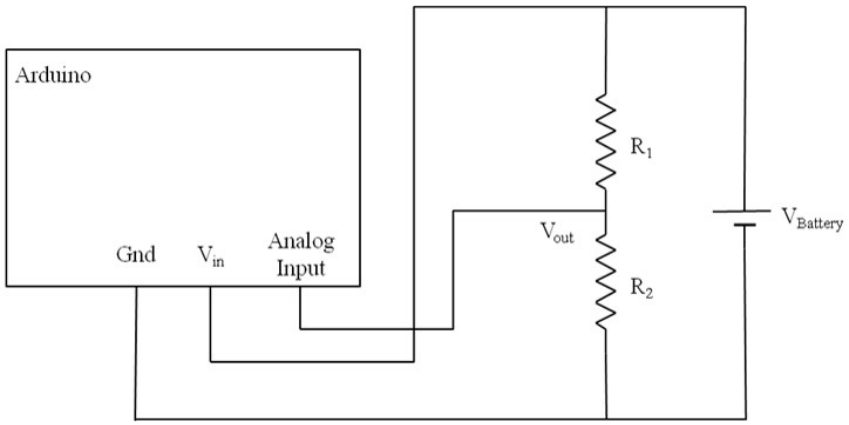

Figure 7.7: Battery monitoring circuit of the wearable sensor platform.

7.2.5 Overall Power Consumption

As discussed previously, the overall power consumption of the platform was designed to be minimised, in order to facilitate use in areas without reliable grid-based electricity. The monitoring platform's power consumption can be split into two main components the usage of the Raspberry Pi Zero-based server, and the wireless sensor unit (including mobile phone, if necessary). Note that the power consumption of the Android mobile phone is not considered within these measurements, since different devices have significantly different power profiles, and it is likely that an existing Android device would be used in order to reduce the overall cost of this system. The peak current consumption of the Raspberry Pi Zero (including all connected peripherals including Wi-Fi interface) was measured during initial power-up to be 357 mA. This settled in under a minute to a steady-state idle consumption of 190 mA. During active data logging, the current consumption rose to 218 mA. These current draws were measured at 5V DC, using a PortaPow Premium USB power monitor, and are accurate to ±0.2%. Therefore, with a 20 Ah 5 V USB power bank used as the power supply, a run-time of in excess of 3 days for the Raspberry Pi Zero-based server is achievable

from a full charge of the power bank. The wireless sensor unit draws 80.7 mA during the data acquisition and transfer of the sensor data via Bluetooth to the Android device [**133**]. In order to keep the mobile sensor unit light in weight for mounting on the patient's limb, it is connected with its own 9-12 V battery supply.

Using a 20 W USB output solar charger, capable of supplying 2.4 A to a single USB output, the 20 Ah power pack could be recharged in around 12 hours, assuming sufficient sunlight was available for the solar panel to operate without available light being a constraint.

7.3 Battery studies on the platform

As seen from the design of the wearable sensor platform in the previous section, it basically consists of a MCU for control and pre-processing of the sensors data; and a transmitter and a smartphone for data processing and data transfer via internet to a server. But for continuous monitoring, which could provide a more realistic view of the amputee's lower limb status which would otherwise go unrecorded, a reliable source of power i.e. the battery needs to be identified.

The mobile sensor platform was first interfaced with the Bluetooth module and temperature and gait data was sent over to the server at a sampling rate of 1 Hz constantly. The battery depletion rate was continuously monitored and logged using a custom built interface in LabView as seen in Appendix E. This test was run until the battery level was exhausted to the minimum threshold voltage of 5 V which is the minimum for the Arduino board to operate. The batteries involved in this study were the NiMH rechargeable battery (9 V),Zinc Chloride (9 V), Zinc Carbon (9 V), Alkaline (9 V), Li-ion rechargeable battery (3.7 V 1750 mAh each; used two in series) and LiPo rechargeable battery (7.4 V 3600

mAh). A comparison of the size of the batteries is seen in Figure 7.8. The rate of depletion was observed for all the batteries listed above. The above protocol was repeated for the other communication methods namely via the Wi-Fi and GSM shields. To study the effect of sampling rate on the battery life, the above routine was repeated for sampling rates of 0.2 Hz and 25 Hz. The data flow was similar to that described in Section 7.2.2. The results from all the cases were then compared in Table 7.1 to infer the best possible battery technology which could enable providing consistent data for a long period of time.

Figure 7.8: Various batteries used for the study.

It was observed that the NiMH battery is not able to support the high current draw demanded by the sensor platform and it can operate for a maximum of three hours when data is transmitted by Bluetooth at 0.2 Hz. Hence, it is not deemed suitable for medical sensor platform applications as with high drain-rate usage (1-4C), the change in shape in the voltage curve with the more rounded "knee"

to the curve means that an arbitrary 0.9 V/battery cut-off may be premature, leaving a significant fraction of the battery capacity untapped. The Li-ion on the other hand is a high density energy battery with the discharge curve being almost flat [17]. This simplifies the design of the application in which the battery is used since the supply voltage stays reasonably constant throughout the discharge cycle. When the sampling rate is decreased from 25 Hz to 0.2 Hz, the battery life is significantly increased in each mode of communication. However, when the data is transferred via Wi-Fi or GSM shield the battery life, none of the two batteries could last for more than 6 hours, making it the system short lived. Reducing the data sampling rate maybe a solution for reducing the battery consumption but when used to monitor critical amputee data, this may prove to be a detriment in identifying the biomarkers in tissue health.

Table 7.1: Battery life for various sampling rates and transmission scenarios

Battery	Capacity (mAh)	Bluetooth			Wi-Fi			GSM		
		0.2 Hz	1 Hz	25 Hz	0.2 Hz	1 Hz	25 Hz	0.2 Hz	1 Hz	25 Hz
NiMH	170	3 hours 5 minutes	2 hours 40 minutes	31 minutes	-	-	-	-	-	-
Zinc Carbon	224	2 hours 15 minutes	1 hour 15 minutes	22 minutes	-	-	-	-	-	-
Zinc Chloride	400	3 hours	2 hours 15 minutes	56 minutes	1 hour 27 minutes	50 minutes	7 minutes	-	-	-
Alkaline	550	8 hours 45 minutes	5 hours 45 minutes	3 hours 12 minutes	2 hours 15 minutes	1 hour 55 minutes	19 minutes	-	-	-
Li-ion	1750	21 hours	19 hours 40 minutes	7 hours 10 minutes	6 hours 35 minutes	4 hours 20 minutes	1 hour 20 minutes	2 hours 10 minutes	1 hour	<5 minutes
LiPo	3600	44 hours 4 minutes	40 hours 12 minutes	31 hours 36 minutes	20 hours	14 hours 14 minutes	11 hours 41 minutes	3 hours 42 minutes	2 hours	18 minutes

7.4 Challenges in the Wearable Platform Design

The design of the wearable sensor platform pose a number of challenges on design including reduction in power consumption, connectivity performance and calibration of the mathematical models for generalisation. To address these challenges,

each of them have been separately addressed in the following sections.

7.4.1 Power Consumption Reduction Strategies

Strategies for reducing power consumption take advantage of opportunities in many areas of system design, for example at the CMOS transistor level or by powering down the Arduino (putting in sleep mode) while idling, reducing the data sampling rate, reducing the MCU processor clock speed; and reducing the amount of data transmitted between MCU and smartphone and smartphone and server.

The use of power cycling provides an opening for reducing average power consumption in applications where energy use must be tightly managed. An important energy management technique, power cycling is the process for the MCU that allows it to use less power in exchange of disabling some of its functions. The period when the data is not sampled and transmitted is the idling time for the MCU. During this period the Arduino can be powered down and put in the sleep mode by the system's watchdog timer. The watchdog timer is a countdown timer that is driven by its own oscillator on the microcontroller. It is designed to run even when all the circuitry on the MCU is powered down, implying that the microcontroller is drawing as little power as possible without actually being turned off completely. When the specified sleep timer ticks are counted, the watchdog timer 'bites' and resumes the normal operation of the MCU. This enables a reduction in average power consumption P_{av}, as quantified by Equation 7.2.

$$P_{av} = P_{On} + P_{Off} \tag{7.2}$$

P_{On} is the system's power consumption in its normal operating state and P_{Off} is the system's power consumption in its Off state. This technique was investigated to compare the difference in power consumption when the sleep mode is

implemented for every 0.04 seconds (the sampling frequency being 25 Hz). It is seen from Figure 7.9 that there is a 26% reduction (for all the data transmission scenarios) in power consumption when the sleep routine is implemented.

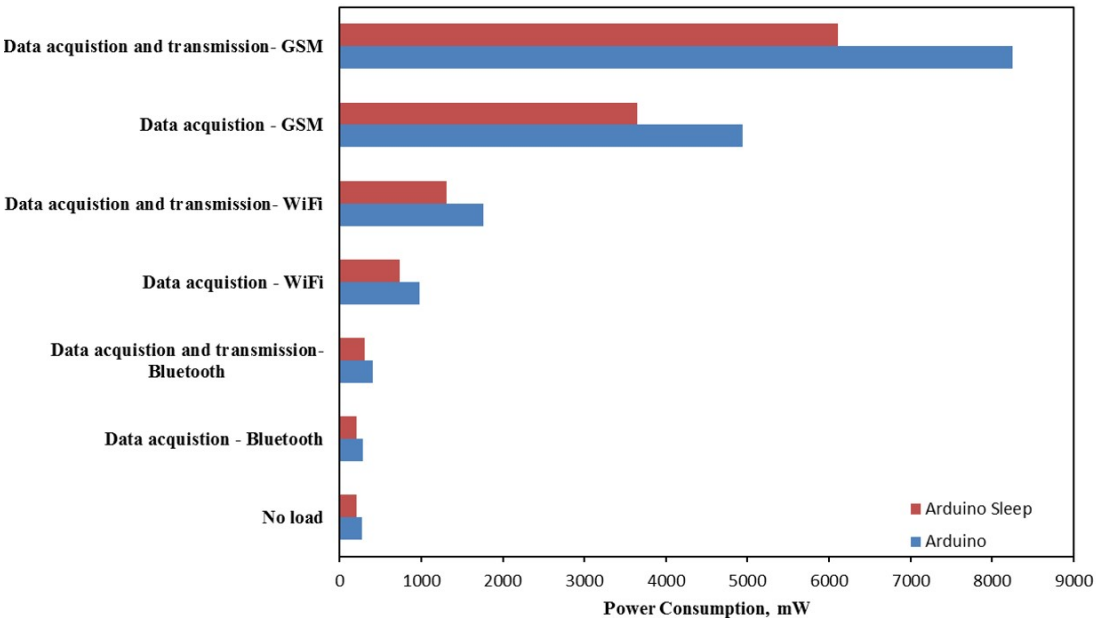

Figure 7.9: Comparison of wearable sensor platform power consumption with different modes of data communication and sleep cycle enabled (Data transfer rate = 1200 bytes/second).

At the transistor level, the dynamic power consumption of a Complimentary Metal-Oxide Semiconductor (CMOS) device is proportional to the clock frequency and the square of the supply voltage. The well-known relationship: $P = CV_{dd}^2 f$ illustrates this relationship where P is the transistor dynamic switching power consumption; C is the CMOS switch lumped capacitance which is the sum of the junction capacitances and gate capacitances; V_{dd} is the supply voltage; and f is the clock frequency. Maintaining V_{dd} constant while halving the clock frequency will reduce power consumption by half, however the total energy consumed will be unaffected. This is because the energy consumed is the time integral of power and therefore the energy consumed by an operation will not be reduced since the same number of clock cycles is required to do the same work. However, reducing

the clock frequency, f allows V_{dd} to be reduced leading to reduced power consumption. The reduction in V_{dd} increases the CMOS delay. However, this is of no consequence if the reduced clock speed is sufficient, that is where all operations required are completed in sufficient time before the next sample. Thus, reducing power consumption and voltage can significantly reduce power and energy consumption. Where this technique is used in conjunction with power cycling, careful consideration must be taken of the likely increase in data- acquisition time and start-up time which will have the consequence of reducing the P_{Off} time, offsetting the power saving achieved by reducing f.

Power consumption is also dependent on the sampling rate. The fewer the samples, the shorter can be the duty cycle. In addition fewer samples mean a further power saving through lower data transmission rates. However, when measuring health data careful consideration must be made between the relative importance of balancing the conflicting requirements of, on the one hand providing sufficient battery power supply life; and on the other, providing a sufficient level of information to ensure reliable diagnosis and decision making.

7.4.2 Calibration of the Mathematical Algorithm

It is seen in Chapter 3 that the residual limb temperature behaviour is a function of ambient temperature). Since the temperature profile of the residual limb and the ambient temperature are closely correlated, individual mathematical models were defined using the obtained data from experimentation (as discussed in Chapters 5 and 6) for temperatures of 10°C, 15°C, 20°C and 25°C. Both the GPML and ANFIS models were individually trained for each of the ambient temperatures on which the tests were done.

The predictive model developed led to results which are in 95% confidence interval and translate to an accuracy of ±0.5°C. However, with the residual limb tem-

perature profile varying with changes in environmental temperatures, the models have to be trained with individual datasets which correspond to changes in ambient temperature. The clinical trials required to calibrate the model are quite intensive as well as expensive. Hence, the introduction of estimation techniques, namely interpolation, can be utilised for prediction of residual limb temperature (at a given environmental temperature) from the mathematical model calibrated for a different ambient temperature. In the current design of the wearable sensor platform, the interpolation technique is implemented at the server (Raspberry Pi Zero) end. The liner-socket interface temperature data once received at the server is used to predict the residual limb skin temperature using GPML or ANFIS by using the interpolated model.

7.4.2.1 Introduction to Interpolation Techniques

Consider that there are a set of N data points $x_1, x_2, \ldots, x_N$ with function value *f(x)*. The determination of *f(x)* for any arbitrary $\mathbf{x}$ in between the smallest and largest x_i's is known as interpolation; if x lies outside the given range then it is known as extrapolation. With interpolation there is a greater likelihood of obtaining a valid estimate. When extrapolation is used, an assumption is made that the observed trend would continue for all values of x outside the range that was used to form the model. This might not be true and may lead to erroneous results. Hence, for this study only interpolation is considered for calibration of GPML and ANFIS model.

For the interpolation process, there are two-stages involved - fit an underlying function for the given data points and then evaluate that function for the target point x. However, this two stage method is computationally less efficient and more prone to round off errors. Interpolation done locally using the nearest neighbour approach is better than the previous but the interpolated values *f(x)* might not have a continuous first order or higher derivative. This is because the interpo-

lated function might become discontinuous because of the switching of the local points [134]. In numerical analysis, there are many techniques for interpolation like Linear, Lagrange's polynomial, Newton's form, Spline, and Cubic Splines etc. Cubic Spline interpolation has advantage over the techniques in the calculation of higher order derivatives. In Newton's form, with the increase in node, the order of the polynomial goes up. Similarly, with Lagrange's polynomial, each time the node changes, it needs to be recalculated. Therefore, in this thesis, the Cubic Spline technique is used for interpolation.

7.4.2.2 Cubic Spline Technique

In the predictive modeling using GPML and ANFIS, continuity of the derivatives is a concern and hence cubic spline interpolation technique is used. The basic principle of cubic spline is that on each interval between the data points the interpolation formula is represented by a cubic function. For N data points, the spline function *S(x)* can be represented as

$$S(x) = \begin{cases} C_1(x), & x_1 \leq x \leq x_2 \\ C_i(x), & x_{i-1} \leq x \leq x_i \\ C_N(x), & x_{N-1} \leq x \leq x_N \end{cases} \tag{7.3}$$

where each C_i is a cubic function. A general cubic function has the form

$$C_i(x) = a_i + b_i x + c_i x^2 + d_i x^3 \tag{7.4}$$

To define the spline function, the coefficients a_i, b_i, c_i and d_i are to be determined for each i by utilising the boundary conditions. Since there are $4N$ coefficients to be determined by $4N$ conditions, the known values can be plugged into the $4N$ conditions to solve the system of equations. First it is required that the spline be exact at the data (for every data point) which can be given by the following

equation

$$C_i(x_{i-1}) = y_{i-1} \quad \text{and} \quad C_i(x_i) = y_i \tag{7.5}$$

This can be written as

$$a_i + b_i x_{i-1} + c_i x_{i-1}^2 + d_i x_{i-1}^3 = y_{i-1} \quad \text{and} \quad a_i + b_i x_i + c_i x_i^2 + d_i x_i^3 = y_i \tag{7.6}$$

Since we get two conditions for each interval via Equation 7.6, $2N$ of these conditions are defined. Because the coefficients of the function are determined non-locally, the cubic spline function needs to be continuous through the second derivative. For all the points $x_1, x_2, x_3, \ldots, x_{N-1}$ this can be interpreted mathematically as

$$\begin{aligned} &C_i^{'}(x_i) = C_{i+1}^{'}(x_i) \quad \text{and} \\ &C_i^{''}(x_i) = C_{i+1}^{''}(x_i) \end{aligned} \tag{7.7}$$

Further, this can be written as

$$\begin{aligned} &b_i + 2c_i x_i + 3d_i x_i^2 = b_{i+1} + 2c_{i+1} x_i + 3d_{i+1} x_i^2 \quad \text{and} \\ &2c_i + 6d_i x_i = 2c_{i+1} + 6d_{i+1} x_i \end{aligned} \tag{7.8}$$

Equation 7.8 gives 2(N-1) of these conditions. So far we have $4N$-2 equations and in order to completely determine all the coefficients, additional 2 equations are required. Those 2 equations can determined by choosing either one of the boundary conditions as seen in Equations 7.9 and 7.10.

$$\textit{Natural} \quad \text{or} \quad \textit{Simple} \quad \text{boundary conditions:} \quad C_1^{''}(x_0) = C_n^{''}(x_n) = 0 \tag{7.9}$$

$$Clamped \quad \text{boundary conditions:} \quad C_1^{'}(x_0) = C_n^{'}(x_n) = 0 \tag{7.10}$$

With the $4N$ coefficients and $4N$ linear conditions, the equations defining them can be easily determined. Cubic splines tend to be more stable than polynomial function by reducing wild oscillations between the data points [135].

7.4.2.3 Results

In order to calibrate the model, first the performance of the cubic spline technique in interpolating the model needs to be investigated. The following scenarios were used to generate the interpolated model (for residual limb skin temperature) at a given ambient temperature and were compared for their accuracy with the predicted model at the same ambient temperature. For example in scenario 1, the data generated from the model at ambient temperatures of 10°C, 20°C and 25°C was used to interpolate the skin temperature at 15°C. This interpolated skin temperature was then compared with the values predicted by the model at 15°C. The interpolation exercise was carried out for the GPML and ANFIS models for both the amputee subjects.

1. Interpolated Skin Temperature at 15°C from 10°C, 20°C, 25°C
2. Interpolated Skin Temperature at 15°C from 10°C, 20°C
3. Interpolated Skin Temperature at 15°C from 10°C, 25°C
4. Interpolated Skin Temperature at 20°C from 10°C, 15°C, 25°C
5. Interpolated Skin Temperature at 20°C from 10°C, 25°C
6. Interpolated Skin Temperature at 20°C from 15°C, 25°C

Table 7.2 compares the interpolated model with the actual generated model (GPML and ANFIS) for both the subjects at various scenarios. The RMSE

is calculated which indicates the degree of closeness of interpolated values with the actual predicted values. The results indicate that the RMSE is substantially higher for the ANFIS model as compared to GPML. This can be easily explained as the predictions from ANFIS model are more prone to fluctuations because of the underlying fuzzy rules (as seen in Chapter 6). In the process of estimating a variable from such a model where the prediction range is not smooth, interpolation is subject to greater uncertainty. In spite of this, this estimation technique is able to identify the trend of the predictive model to a great extent. It can be easily further improved by reducing the 5°C temperature interval for which the interpolation is been done.

Table 7.2: RMSE for different scenarios of interpolation

Scenario	Subject 1		Subject 2	
	ANFIS	GPML	ANFIS	GPML
Interpolated Lateral Skin Temperature at 15°C from 10°C, 20°C, 25°C	1.1767	0.6659	1.1771	0.5445
Interpolated Medial Skin Temperature at 15°C from 10°C, 20°C, 25°C	0.6159	0.3001	3.4286	0.8281
Interpolated Lateral Skin Temperature at 15°C from 10°C, 20°C	0.7731	0.9646	0.7829	0.4893
Interpolated Medial Skin Temperature at 15°C from 10°C, 20°C	0.4506	0.5028	2.0067	0.8818
Interpolated Lateral Skin Temperature at 15°C from 10°C, 25°C	0.5257	1.0027	0.7274	0.8093
Interpolated Medial Skin Temperature at 15°C from 10°C, 25°C	0.4073	0.7446	1.2667	0.9661
Interpolated Lateral Skin Temperature at 20°C from 10°C, 15°C, 25°C	0.8554	1.0998	1.2561	0.7588
Interpolated Medial Skin Temperature at 20°C from 10°C, 15°C, 25°C	1.1339	0.3121	1.0556	1.3922
Interpolated Lateral Skin Temperature at 20°C from 10°C, 25°C	0.6056	0.3272	0.3025	0.3515
Interpolated Medial Skin Temperature at 20°C from 10°C, 25°C	0.4593	0.7829	0.9528	0.5249
Interpolated Lateral Skin Temperature at 20°C from 15°C, 25°C	0.6552	0.6309	5.5303	0.4341
Interpolated Medial Skin Temperature at 20°C from 15°C, 25°C	0.6858	0.5497	1.2391	0.7375

7.5 Overall Design Solution

The two design goals of the overall solution were to minimise the cost, while also keeping power consumption low. By using readily available, off-the-shelf components where possible, the cost of the solution was kept to a minimum, while also facilitating the sourcing of replacement parts for field repairs. Where possible, components are designed to be modular, using standard USB cables for interconnection and power.

Minimisation of power consumption was also a consideration, in order to allow for use of the system in areas with unreliable power supplies. In particular, the overall solution is designed to operate from a rechargeable USB power pack, therefore permitting use at night. Combining this with a USB solar panel would allow the power pack to be re-charged during daylight hours.

The main components used by the presented solution, along with their approximate retail costs for individual quantities, are as follows. A Raspberry Pi Zero (£4), micro SD card (£3) and USB Wi-Fi adapter (£6) are used as a server. The wireless sensor unit utilises an Arduino Uno (£6), a HC-05 Bluetooth module (£4), with a MPU-6050 movement sensor (£5), two thermistors (£1) and a 9 V 650 mAh rechargeable battery (£5). A 20,000 mAh power bank (£20) is used as the power supply for use off-grid, along with a USB output solar panel (£36). Finally, a LiPo charge controller (£1) is used to control the charging of the Raspberry Pi Zero's Lithium Polymer battery (£2), and various USB and micro USB cables are used to supply power to the various components. The only additional requirement is an Android smartphone, to be connected to the sensor platform. The above described design of the wearable sensor platform is then implemented. In Figure 7.10, an amputee subject is seen wearing the platform on the prosthesis for clinical trials.

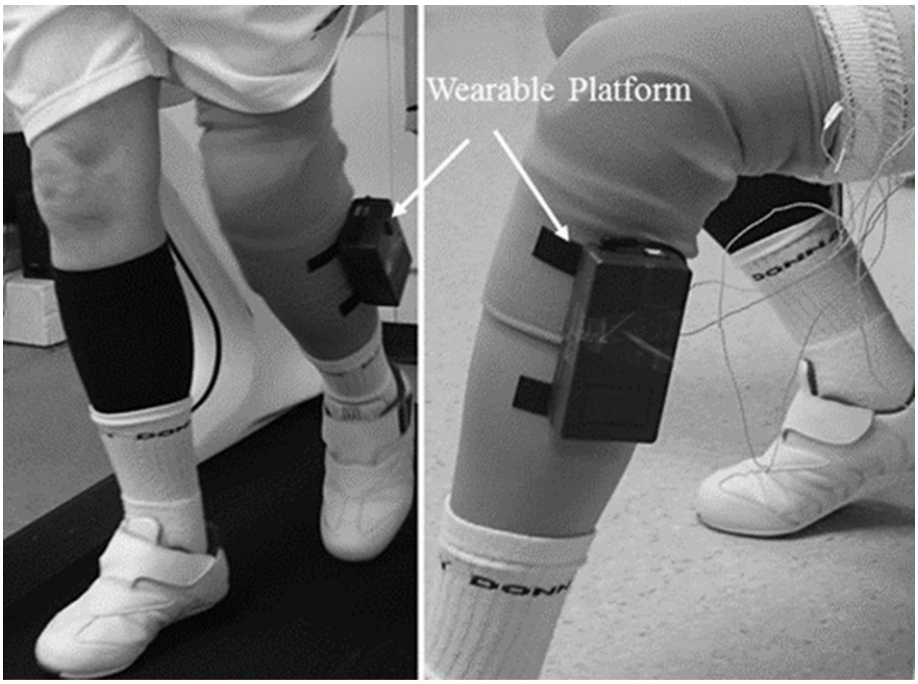

Figure 7.10: The wearable sensor platform positioned on the prosthesis of the amputee subject during various activity levels as (a) walking on treadmill at a self-selected speed (b) sitting/resting.

7.6 Summary

The feasibility of a multi-sensor wearable platform has been demonstrated for use in monitoring tissue viability in trans-tibial amputees. Both temperature and gait sensors can be used to predict the health of the residual limb in lower limb amputees. In particular, in order to bring about the benefits of being able to use this technology in areas of the developing world where there is no reliable network connectivity or electricity, the sensor platform has been designed to be counter various challenges like low power and low cost [**136**]. Therefore, the priorities of the design were to use readily available off-the-shelf hardware as possible, to facilitate ease of construction and maintenance of the sensor platform, while

also ensuring it had sufficiently low power consumption to make battery-operated operation feasible, with solar energy used to recharge the battery pack. Since the residual limb skin temperature is affected by the ambient temperature to a great extent, the wearable platform will also be interfaced with a temperature sensor to provide information about the ambient temperature in real-time in future. This will enable the presence of the estimation techniques as described previously in an accurate fashion for a non-clinical environment. With the inclusion of estimation techniques in the mathematical algorithms - GPML and ANFIS it has been possible to develop, demonstrate and validate a generalised model for contactless temperature prediction of the residual limb. This estimation technique is an added feature for the wearable sensor platform and is essential in reducing the cost of calibration for the model, thereby making it easier to roll out to a greater amputee population. Cubic spline interpolation was introduced in the model at a given ambient temperature to predict the residual limb temperature profile at another ambient temperature. It is also shown that if the RMSE are subtracted from the respective interpolated value then these estimates are as good as the predicted values which are in the 95% confidence interval. Sensor data has been reliably collected, transmitted and stored in a secure server application within a Raspberry Pi Zero, allowing for post processing in an offline environment where no internet connectivity is available. This permits a clinician to access and review user data to identify any possible deterioration in health. However, depending on the duration of the wearable platform usage, only a small time snippet of movement and skin temperature is recorded and processed, and this may not be necessarily representative. This remote monitoring platform would prove most useful aid for doctors and clinicians in the developing world, taking into account the unique challenges in such regions (lack of connectivity and reliable power supplies). But it should be noted that it does not do away with the need of having face to face appointments with them.

Chapter 8

Conclusions and Future Work

8.1 Conclusions

With developing technology, e-Health devices have become increasingly smaller, lighter and smarter, and hence more attractive for use in permanent and continuous monitoring of the patients. Of particular interest here is the use of the appropriate technologies in the monitoring of people with compromised circulation and/or who regularly wear prosthetic limbs. These people are particularly prone to the development of pressure sores due to ill-fitting prostheses, residual limb volume changes or poor footwear design. Continuous monitoring of the relevant metrics can provide a reliable indication of both skin and deep tissue perfusion. Additionally, the knowledge of the magnitude and distribution of direct and shear forces at the interface between the residual limb and the prosthetic socket will be useful in providing a reliable early warning of tissue damage.

Despite the fact that e-Health has become an increasingly popular concept, its application in the remote monitoring of the amputee's residual limb health has not been explored. This thesis focused upon the design of a wearable sensor platform, capable of monitoring, logging and transmitting the amputee's residual

limb temperature and gait data to a central health authority. The sensor platform was designed by identifying necessary constraints like low-cost, reliability, ease of use, sensor system size/weight and sensor/skin contact considerations. The central health database is designed such that it is password protected and can be accessed by only authorised people. The data received here is processed using machine learning algorithms to extract clinically relevant information. The capability of the wearable sensor platform is tested both at the amputee subject and at the clinician's end.

A review of the fundamental sensing techniques and state of the art in the field of e-Health that may be applied to develop and design the wearable sensor platform for lower limb amputees was presented in Chapter 2.

In Chapter 3 the effect of varying activity levels and ambient temperatures on the residual limb temperature and the gait profile has been investigated. This is particularly important as the gait profile can be calibrated and the various phases of gait pattern can be identified. This is done by placing the IMU on the shank of the amputee. The shank angle is derived by combining the accelerometer and gyroscope data using a complementary filter (refer to Appendix A for details). The results indicated that the normal gait pattern remains unaffected by the different ambient temperatures. On the other hand, the in-socket temperature results indicate that the residual limb temperature is a function of the activity level and the ambient temperature. Moreover, it is seen that the trace of the liner temperature follows that of the residual skin temperature, which is useful in developing the mathematical models for non-invasive measurement. The knowledge of the gait and the in-socket temperature would be important in identifying the health of the residual limb.

The contribution in Chapter 4 is the thermal characterisation of the prosthetic materials which is indicative of its temperature response. The thermal time con-

stant of the different prosthetic liner and socket materials (when used individually or in combination) was experimentally evaluated. It was deduced that when these materials are placed in combinations, the rate of heat transfer is slower suggesting that they can have a considerable impact on the residual limb skin temperature. This thermal study on prosthetic materials is utilised when designing the GPML model.

In Chapter 5 the development of a supervised mathematical algorithm GPML to predict the residual limb temperature of amputee is discussed. The motivation for this work arose from the fact that continuous monitoring at the skin level of amputees could induce possible discomfort and irritation, making the skin susceptible for breakdown. By implementing the Bayesian framework in this model along with the thermal time constant evaluated in Chapter 4, the accuracy of predicting the residual skin temperature from liner-socket interface temperature is found to be $\pm 0.5^{\circ}$C.

In Chapter 6, the development of another supervised learning algorithm ANFIS is discussed. This technique inherits both neural networks and fuzzy logic principles. The performance of the GPML and the ANFIS model is compared by using statistical tools like MAE, RMSE and R^2 criteria. Both the models have very similar performance metrics but the predictions by the GPML model are more smooth and devoid of random fluctuations as seen in the ANFIS model. This could be due to the fact that in ANFIS, the underlying fuzzy rule base has to be specifically defined for models at different ambient temperatures.

In Chapter 7, a wearable mobile sensor platform for remote monitoring of the residual limb health of the amputee is developed and validated. This wearable platform is designed such that the temperature and orientation of the residual limb of an amputee subject can be monitored by a medical team at a defined sampling rate. Therefore, by utilising the techniques - GPML, ANFIS and com-

plementary filtering, the data can be processed and transmitted to a smartphone (via Bluetooth) and from the smartphone to the server (via Wi-Fi). The challenges in the development of a low power, low cost platform such as reduction in power consumption, connectivity performance and interpolation technique for drawing a generalised model have been also addressed. The wearable platform has been tested on amputee subject and the results can be viewed by a clinician from a central database which is username and password protected.

8.2 Suggestions for Further Work

The developed wearable sensor platform measures the residual limb temperature and gait in a contactless way. Its ability to monitor, record and transmit the temperature and gait has been successfully verified on an amputee subject. The performance of the platform needs to studied for a greater amputee population for longer durations of time. This would enable in establishing the necessary biomarkers for practical use.

The sensor data is transmitted onto a server where it can be remotely monitored by a clinician for analysing the residual limb health. MATLAB environment is used to process the data after it has been received in the health server. Future work would be considering methods for integrating the MATLAB environment with the clinician GUI such the data is processed automatically as soon as it is received in the central health database.

For improving the results from the ANFIS modelling, the number of epochs used for training in the back propagation algorithm can be increased. This would be useful in reducing the training error. Other techniques for improving the learning ability of ANFIS could be - using the hybrid learning algorithm instead of back propagation and introducing deep learning in the model.

Additionally, interfacing more sensors in the wearable platform for monitoring the pressure and the moisture within the prosthetic socket could be considered. This would add another dimension in the analysis of the residual limb health.

Bibliography

[1] online, http://www.pewinternet.org/fact-sheets/health-fact-sheet/, November 2014.

[2] V. Chan, P. Ray, and N. Parameswaran, "Mobile e-health monitoring: an agent-based approach," *IET communications*, vol. 2, no. 2, pp. 223–230, 2008.

[3] A. Davidson, N. Mathur, I. Glesk, and A. Buis, "Power supply issues in e-health monitoring applications," in *Proc. ICREPQ 2015*, 2015, pp. 733–737.

[4] I. D. Federation, "International diabetes federation. idf diabetes, 7 ed. brussels, belgium:," online, http://www.diabetesatlas.org, 2015.

[5] H. Lewy, "Wearable technologies–future challenges for implementation in healthcare services," *Healthcare Technology Letters*, vol. 2, no. 1, pp. 2–5, 2015.

[6] P.-G. Svensson, "ehealth applications in health care management," *Ehealth international*, vol. 1, no. 1, p. 5, 2002.

[7] online, http://www.who.int/topics/ehealth/en/, October 2016.

[8] J. Ko, C. Lu, M. B. Srivastava, J. A. Stankovic, A. Terzis, and M. Welsh, "Wireless sensor networks for healthcare," *Proceedings of the IEEE*, vol. 98, no. 11, pp. 1947–1960, 2010.

[9] A. Samà, C. Pérez-López, D. Rodríguez-Martín, J. M. Moreno-Aróstegui, J. Rovira, C. Ahlrichs, R. Castro, J. Cevada, R. Graça, V. Guimarães *et al.*, "A double closed loop to enhance the quality of life of parkinson's disease patients: Rempark system," in *InMed Conference*. Piraeus, Greece: IOS Press, February 2014.

[10] K. Y. Au-Yeung, T. Robertson, H. Hafezi, G. Moon, L. DiCarlo, M. Zdeblick, and G. Savage, "A networked system for self-management of drug therapy and wellness," in *Wireless Health 2010*. San Diego, CA, USA: ACM, October 2010, pp. 1–9.

[11] Y.-L. Hsu, C.-C. Yang, T.-C. Tsai, C.-M. Cheng, and C.-H. Wu, "Development of a decentralized telehomecare monitoring system," *Telemedicine and e-Health*, vol. 13, no. 1, pp. 69–78, 2007.

[12] D. Wade and C. Collin, "The barthel adl index: a standard measure of physical disability?" *International disability studies*, vol. 10, no. 2, pp. 64–67, 1988.

[13] V. Ahanathapillai, J. Amor, M. Tadeusiak, and C. James, "Wrist-worn accelerometer to detect postural transitions and walking patterns," in *XIII Mediterranean Conference on Medical and Biological Engineering and Computing*, vol. 41. Springer, 2014, pp. 1515–1518.

[14] S. G. Mohiuddin, S. C. Brailsford, C. J. James, J. D. Amor, J. M. Blum, J. A. Crowe, E. H. Magill, and P. A. Prociow, "A multi-state model to improve the design of an automated system to monitor the activity patterns

of patients with bipolar disorder," *Journal of the Operational Research Society*, vol. 64, no. 3, pp. 372–383, 2013.

[15] . Office for National Statistics, "Statistical bulletin. national population projections, 2008 based," Office for National Statistics, Tech. Rep., 2009.

[16] H. H. Asada, P. Shaltis, A. Reisner, S. Rhee, and R. C. Hutchinson, "Mobile monitoring with wearable photoplethysmographic biosensors," *IEEE Engineering in Medicine and Biology Magazine*, vol. 22, no. 3, pp. 28–40, 2003.

[17] online, http://www.batteryuniversity.com, November 2014.

[18] K. Kim and V. D. Agrawal, "Ultra low energy cmos logic using below-threshold dual-voltage supply," *Journal of Low Power Electronics*, vol. 7, no. 4, pp. 460–470, 2011.

[19] X. Zhao, D.-Y. Fei, C. R. Doarn, B. Harnett, and R. Merrell, "A telemedicine system for wireless home healthcare based on bluetooth and the internet," *Telemedicine Journal & e-Health*, vol. 10, no. 2, pp. 110–116, 2004.

[20] online, http://www.bluetooth.com/Pages/what-is-bluetooth-technology.aspx/, November 2014.

[21] S. F. Donker and P. J. Beek, "Interlimb coordination in prosthetic walking: effects of asymmetry and walking velocity," *Acta Psychologica*, vol. 110, no. 2, pp. 265–288, 2002.

[22] A. L. Hof, R. M. van Bockel, T. Schoppen, and K. Postema, "Control of lateral balance in walking: experimental findings in normal subjects and above-knee amputees," *Gait and Posture*, vol. 25, no. 2, pp. 250–258, 2007.

[23] L. Nolan, A. Wit, K. Dudziñski, A. Lees, M. Lake, and M. Wychowañski, "Adjustments in gait symmetry with walking speed in trans-femoral and trans-tibial amputees," *Gait and Posture*, vol. 17, no. 2, pp. 142–151, 2003.

[24] L. E. Pezzin, T. R. Dillingham, and E. J. MacKenzie, "Rehabilitation and the long-term outcomes of persons with trauma-related amputations," *Archives of physical medicine and rehabilitation*, vol. 81, no. 3, pp. 292–300, 2000.

[25] H. E. Meulenbelt, J. H. Geertzen, M. F. Jonkman, and P. U. Dijkstra, "Determinants of skin problems of the stump in lower-limb amputees," *Archives of physical medicine and rehabilitation*, vol. 90, no. 1, pp. 74–81, 2009.

[26] N. L. Dudek, M. B. Marks, S. C. Marshall, and J. P. Chardon, "Dermatologic conditions associated with use of a lower-extremity prosthesis," *Archives of physical medicine and rehabilitation*, vol. 86, no. 4, pp. 659–663, 2005.

[27] J. M. Stepien, S. Cavenett, L. Taylor, and M. Crotty, "Activity levels among lower-limb amputees: self-report versus step activity monitor," *Archives of physical medicine and rehabilitation*, vol. 88, no. 7, pp. 896–900, 2007.

[28] J. M. Holden and G. R. Fernie, "Extent of artificial limb use following rehabilitation," *Journal of orthopaedic research*, vol. 5, no. 4, pp. 562–568, 1987.

[29] S. M. Jaegers, J. H. Arendzen, and H. J. de Jongh, "Prosthetic gait of unilateral transfemoral amputees: a kinematic study," *Archives of physical medicine and rehabilitation*, vol. 76, no. 8, pp. 736–743, 1995.

[30] B. J. Hafner and J. E. Sanders, "Considerations for development of sensing and monitoring tools to facilitate treatment and care of persons with lower limb loss," *Journal of rehabilitation research and development*, vol. 51, no. 1, p. 1, 2014.

[31] R. Gailey, M. S. Nash, T. Atchley, R. Zilmer, G. Moline-Little, N. Morris-Cresswell, and L. Siebert, "The effects of prosthesis mass on metabolic cost of ambulation in non-vascular trans-tibial amputees," *Prosthetics and Orthotics International*, vol. 21, no. 1, pp. 9–16, 1997.

[32] J. M. Czerniecki, A. Gitter, and K. Weaver, "Effect of alterations in prosthetic shank mass on the metabolic costs of ambulation in above-knee amputees." *American Journal of Physical Medicine & Rehabilitation*, vol. 73, no. 5, pp. 348–352, 1994.

[33] A. Gitter, J. Czerniecki, and M. Meinders, "Effect of prosthetic mass on swing phase work during above-knee amputee ambulation," *American journal of physical medicine & rehabilitation*, vol. 76, no. 2, pp. 114–121, 1997.

[34] C.-C. Yang and Y.-L. Hsu, "A review of accelerometry-based wearable motion detectors for physical activity monitoring," *Sensors*, vol. 10, no. 8, pp. 7772–7788, 2010.

[35] F. Foerster, M. Smeja, and J. Fahrenberg, "Detection of posture and motion by accelerometry: a validation study in ambulatory monitoring," *Computers in Human Behavior*, vol. 15, no. 5, pp. 571–583, 1999.

[36] H. B. Bussmann, P. J. Reuvekamp, P. H. Veltink, W. L. Martens, and H. J. Stam, "Validity and reliability of measurements obtained with an activity monitor in people with and without a transtibial amputation," *Physical therapy*, vol. 78, no. 9, pp. 989–998, 1998.

[37] H.-y. Lau, K.-y. Tong, and H. Zhu, "Support vector machine for classification of walking conditions of persons after stroke with dropped foot," *Human movement science*, vol. 28, no. 4, pp. 504–514, 2009.

[38] T. Zhang, J. Wang, L. Xu, and P. Liu, "Fall detection by wearable sensor and one-class svm algorithm," in *Intelligent computing in signal processing and pattern recognition*. Springer, 2006, pp. 858–863.

[39] F. R. Allen, E. Ambikairajah, N. H. Lovell, and B. G. Celler, "Classification of a known sequence of motions and postures from accelerometry data using adapted gaussian mixture models," *Physiological Measurement*, vol. 27, no. 10, p. 935, 2006.

[40] A. Mannini and A. M. Sabatini, "Machine learning methods for classifying human physical activity from on-body accelerometers," *Sensors*, vol. 10, no. 2, pp. 1154–1175, 2010.

[41] D. M. Pober, *Development of novel analytical techniques to classify physical activity mode using accelerometers*. University of Massachusetts Amherst, USA, 2007.

[42] G. Plasqui and K. R. Westerterp, "Physical activity assessment with accelerometers: an evaluation against doubly labeled water," *Obesity*, vol. 15, no. 10, pp. 2371–2379, 2007.

[43] S. E. Crouter, J. R. Churilla, and D. R. Bassett Jr, "Estimating energy expenditure using accelerometers," *European journal of applied physiology*, vol. 98, no. 6, pp. 601–612, 2006.

[44] H. B. Menz, S. R. Lord, and R. C. Fitzpatrick, "Age-related differences in walking stability," *Age and ageing*, vol. 32, no. 2, pp. 137–142, 2003.

[45] H. B. Menz, S. R. Lord, and R. C. Fitzpatrick, "Acceleration patterns of the head and pelvis when walking are associated with risk of falling in community-dwelling older people," *The Journals of Gerontology Series A: Biological Sciences and Medical Sciences*, vol. 58, no. 5, pp. 446–452, 2003.

[46] K. S. Tee, M. Awad, A. Dehghani, D. Moser, and S. Zahedi, "A portable gait monitoring system for lower limb prosthetic alignment," in *World Congress on Engineering*, vol. 3, 2011, pp. 2131–2134.

[47] E. Mueller and T. Hettinger, "Measuring pressure distribution in the socket of prostheses," *Orthopaedie-Technik*, vol. 9, pp. 222–225, 1954.

[48] M. B. Silver-Thorn, J. W. Steege, and D. S. Childress, "A review of prosthetic interface stress investigations," *Journal of rehabilitation research and development*, vol. 33, no. 3, p. 253, 1996.

[49] H. Seelen, S. Anemaat, H. Janssen, and J. Deckers, "Effects of prosthesis alignment on pressure distribution at the stump/socket interface in transtibial amputees during unsupported stance and gait," *Clinical rehabilitation*, vol. 17, no. 7, pp. 787–796, 2003.

[50] N. Mathur, I. Glesk, A. Davidson, G. Paul, J. Banford, J. Irvine, and A. Buis, "Wearable mobile sensor and communication platform for the in-situ monitoring of lower limb health in amputees," in *IEEE International Symposium on Circuits and Systems,Montreal,Canada*. IEEE, 2016.

[51] A. Shirinov and W. Schomburg, "Pressure sensor from a pvdf film," *Sensors and Actuators A: Physical*, vol. 142, no. 1, pp. 48–55, 2008.

[52] C. Sun, J. Shi, D. J. Bayerl, and X. Wang, "Pvdf microbelts for harvesting energy from respiration," *Energy & Environmental Science*, vol. 4, no. 11, pp. 4508–4512, 2011.

[53] X. Li, T. Reissman, F. Yu, and E. C. Kan, "A low-range drift-free biocompatible pressure sensor based on p (vdf-trfe) piezoelectric thin film," in *MRS Proceedings*, vol. 1222. Cambridge Univ Press, 2009, pp. 1222–DD05.

[54] R. S. Dahiya, P. Mittendorfer, M. Valle, G. Cheng, and V. J. Lumelsky, "Directions toward effective utilization of tactile skin: A review," *IEEE Sensors Journal*, vol. 13, no. 11, pp. 4121–4138, 2013.

[55] E. A. Huff, W. R. Ledoux, J. S. Berge, and G. K. Klute, "Measuring residual limb skin temperatures at the skin-prosthesis interface," *JPO: Journal of Prosthetics and Orthotics*, vol. 20, no. 4, pp. 170–173, 2008.

[56] J. T. Peery, W. R. Ledoux, and G. K. Klute, "Residual-limb skin temperature in transtibial sockets," *Journal of rehabilitation research and development*, vol. 42, no. 2, pp. 147–154, 2005.

[57] J. Klute, E. Huff, and W. Ledoux, "In-socket skin temperature and perception of comfort over a whole day," in *American Academy of Orthotists and Prosthetists Annual Meeting and Scientific Symposium. Chicago, IL: AAOP*, 2006.

[58] G. Klute, J. Berge, E. Huff, and W. Ledoux, "The effect of rest and exercise on residual limb skin temperatures," in *American Academy of Orthotists and Prosthetists Annual Meeting and Scientific Symposium. Chicago, IL: AAOP*, 2006.

[59] K. S. Maluf, R. E. Morley, E. J. Richter, J. W. Klaesner, and M. J. Mueller, "Monitoring in-shoe plantar pressures, temperature, and humidity: reliability and validity of measures from a portable device," *Archives of physical medicine and rehabilitation*, vol. 82, no. 8, pp. 1119–1127, 2001.

[60] A. Stekelenburg, D. Gawlitta, D. L. Bader, and C. W. Oomens, "Deep tissue injury: how deep is our understanding?" *Archives of physical medicine and rehabilitation*, vol. 89, no. 7, 2008.

[61] C. VanGilder, G. D. MacFarlane, P. Harrison, C. Lachenbruch, and S. Meyer, "The demographics of suspected deep tissue injury in the united states: an analysis of the international pressure ulcer prevalence survey 2006-2009," *Advances in skin & wound care*, vol. 23, no. 6, pp. 254–261, 2010.

[62] M. W. Whittle, *Gait analysis: an introduction*. Butterworth-Heinemann, 2014.

[63] W. Tao, T. Liu, R. Zheng, and H. Feng, "Gait analysis using wearable sensors," *Sensors*, vol. 12, no. 2, pp. 2255–2283, 2012.

[64] A. Esquenazi, "Gait analysis in lower-limb amputation and prosthetic rehabilitation," *Physical medicine and rehabilitation clinics of North America*, vol. 25, no. 1, pp. 153–167, 2014.

[65] T. Seel, J. Raisch, and T. Schauer, "Imu-based joint angle measurement for gait analysis," *Sensors*, vol. 14, no. 4, pp. 6891–6909, 2014.

[66] J. Perry and J. M. Burnfield, *Gait analysis: normal and pathological function*. Slack Thorofare, NJ, 1992.

[67] I. Karaulova, P. M. Hall, and A. D. Marshall, "Tracking people in three dimensions using a hierarchical model of dynamics," *Image and Vision Computing*, vol. 20, no. 9, pp. 691–700, 2002.

[68] Y. Inoue, T. Matsuda, K. Shibata, Y. Yamasaki, and Y. Kai, "Estimation of vertical reaction force and ankle joint moment by using plantar pressure sensor," in *JSME, Symposium on human dynamics*, 2003, pp. 57–62.

[69] M. Ye, C. Yang, V. Stankovic, L. Stankovic, and A. Kerr, "A depth camera motion analysis framework for tele-rehabilitation: Motion capture and person-centric kinematics analysis," *IEEE Journal of Selected Topics in Signal Processing*, vol. 10, no. 5, pp. 877–887, 2016.

[70] C. Yang, U. C. Ugbolue, A. Kerr, V. Stankovic, L. Stankovic, B. Carse, K. T. Kaliarntas, and P. J. Rowe, "Autonomous gait event detection with portable single-camera gait kinematics analysis system," *Journal of Sensors*, vol. 2016, 2016.

[71] W. Y. Wong, M. S. Wong, and K. H. Lo, "Clinical applications of sensors for human posture and movement analysis: a review," *Prosthetics and orthotics international*, vol. 31, no. 1, pp. 62–75, 2007.

[72] H. Zheng, N. D. Black, and N. D. Harris, "Position-sensing technologies for movement analysis in stroke rehabilitation," *Medical and biological engineering and computing*, vol. 43, no. 4, pp. 413–420, 2005.

[73] K. Turcot, R. Aissaoui, K. Boivin, M. Pelletier, N. Hagemeister, and J. A. de Guise, "New accelerometric method to discriminate between asymptomatic subjects and patients with medial knee osteoarthritis during 3-d gait," *IEEE Transactions on Biomedical Engineering*, vol. 55, no. 4, pp. 1415–1422, 2008.

[74] A. Zijlstra, J. H. Goosen, C. C. Verheyen, and W. Zijlstra, "A body-fixed-sensor based analysis of compensatory trunk movements during unconstrained walking," *Gait & posture*, vol. 27, no. 1, pp. 164–167, 2008.

[75] A. K. Bourke and G. M. Lyons, "A threshold-based fall-detection algorithm using a bi-axial gyroscope sensor," *Medical engineering & physics*, vol. 30, no. 1, pp. 84–90, 2008.

[76] J. Favre, F. Luthi, B. Jolles, O. Siegrist, B. Najafi, and K. Aminian, "A new ambulatory system for comparative evaluation of the three-dimensional knee kinematics, applied to anterior cruciate ligament injuries," *Knee Surgery, Sports Traumatology, Arthroscopy*, vol. 14, no. 7, pp. 592–604, 2006.

[77] K. Aminian and B. Najafi, "Capturing human motion using body-fixed sensors: outdoor measurement and clinical applications," *Computer animation and virtual worlds*, vol. 15, no. 2, pp. 79–94, 2004.

[78] J. J. Kavanagh and H. B. Menz, "Accelerometry: a technique for quantifying movement patterns during walking," *Gait and posture*, vol. 28, no. 1, pp. 1–15, 2008.

[79] B. Coley, B. Najafi, A. Paraschiv-Ionescu, and K. Aminian, "Stair climbing detection during daily physical activity using a miniature gyroscope," *Gait and posture*, vol. 22, no. 4, pp. 287–294, 2005.

[80] H.-Y. Lau, K.-Y. Tong, and H. Zhu, "Support vector machine for classification of walking conditions using miniature kinematic sensors," *Medical & biological engineering & computing*, vol. 46, no. 6, pp. 563–573, 2008.

[81] B. Najafi, K. Aminian, F. Loew, Y. Blanc, and P. A. Robert, "Measurement of stand-sit and sit-stand transitions using a miniature gyroscope and its application in fall risk evaluation in the elderly," *IEEE Transactions on biomedical Engineering*, vol. 49, no. 8, pp. 843–851, 2002.

[82] K. Aminian, P. Robert, E. Buchser, B. Rutschmann, D. Hayoz, and M. Depairon, "Physical activity monitoring based on accelerometry: validation and comparison with video observation," *Medical & biological engineering & computing*, vol. 37, no. 3, pp. 304–308, 1999.

[83] H. Lau and K. Tong, "The reliability of using accelerometer and gyroscope for gait event identification on persons with dropped foot," *Gait and posture*, vol. 27, no. 2, pp. 248–257, 2008.

[84] I. P. Pappas, T. Keller, S. Mangold, M. R. Popovic, V. Dietz, and M. Morari, "A reliable gyroscope-based gait-phase detection sensor embedded in a shoe insole," *IEEE Sensors Journal*, vol. 4, no. 2, pp. 268–274, 2004.

[85] I. P. Pappas, M. R. Popovic, T. Keller, V. Dietz, and M. Morari, "A reliable gait phase detection system," *IEEE Transactions on neural systems and rehabilitation engineering*, vol. 9, no. 2, pp. 113–125, 2001.

[86] J. M. Jasiewicz, J. H. Allum, J. W. Middleton, A. Barriskill, P. Condie, B. Purcell, and R. C. T. Li, "Gait event detection using linear accelerometers or angular velocity transducers in able-bodied and spinal-cord injured individuals," *Gait and Posture*, vol. 24, no. 4, pp. 502–509, 2006.

[87] T. Liu, Y. Inoue, and K. Shibata, "Development of a wearable sensor system for quantitative gait analysis," *Measurement*, vol. 42, no. 7, pp. 978–988, 2009.

[88] "Mpu-6050 six-axis (gyro + accelerometer) mems motiontracking devices," https://www.invensense.com/products/motion-tracking/6-axis/mpu-6050, September 2016.

[89] online, http://playground.arduino.cc/Main/MPU-6050, December 2014.

[90] online, https://www.invensense.com/products/motion-tracking/6-axis/mpu-6050/, December 2014.

[91] A. M. Sabatini, "Estimating three-dimensional orientation of human body parts by inertial/magnetic sensing," *Sensors*, vol. 11, no. 2, pp. 1489–1525, 2011.

[92] I. Lihinikaduarachchi, S. A. Rajapaksha, C. Saumya, V. Senevirathne, and P. Silva, "Inertial measurement units based wireless sensor network for real time gait analysis," in *TENCON 2015-2015 IEEE Region 10 Conference*. IEEE, 2015, pp. 1–6.

[93] K. Hagberg and R. Brånemark, "Consequences of non-vascular transfemoral amputation: a survey of quality of life, prosthetic use and problems," *Prosthetics and orthotics international*, vol. 25, no. 3, pp. 186–194, 2001.

[94] F. Hoaglund, H. Jergesen, L. Wilson, L. Lamoreux, and R. Roberts, "Evaluation of problems and needs of veteran lower-limb amputees in the san francisco bay area during the period 1977-1980." *Journal of rehabilitation R&D/Veterans Administration, Department of Medicine and Surgery, Rehabilitation R&D Service*, vol. 20, no. 1, pp. 57–71, 1983.

[95] S. Derler and L.-C. Gerhardt, "Tribology of skin: review and analysis of experimental results for the friction coefficient of human skin," *Tribology Letters*, vol. 45, no. 1, pp. 1–27, 2012.

[96] J. E. Sanders, B. S. Goldstein, and D. F. Leotta, "Skin response to mechanical stress: adaptation rather than breakdown–a review of the literature," *Journal of rehabilitation research and development*, vol. 32, no. 3, p. 214, 1995.

[97] A. F. Mak, M. Zhang, and D. A. Boone, "State-of-the-art research in lower-limb prosthetic biomechanics-socket interface: a review," *Journal of rehabilitation research and development*, vol. 38, no. 2, p. 161, 2001.

[98] S. W. Levy, M. Allende, and G. H. Barnes, "Skin problems of the leg amputee," *Archives of dermatology*, vol. 85, no. 1, pp. 65–81, 1962.

[99] R. B. Barnes, "Thermography," *Annals of the New York Academy of Sciences*, vol. 121, no. 1, pp. 34–48, 1964.

[100] G. Klute, G. Rowe, A. Mamishev, and W. Ledoux, "The thermal conductivity of prosthetic sockets and liners," *Prosthetics and orthotics international*, vol. 31, no. 3, pp. 292–299, 2007.

[101] R. C. Eberhart and A. Shitzer, *Heat Transfer in Medicine and Biology: Analysis and Applications*. Springer Science & Business Media, 2012, vol. 2.

[102] Y. Houdas and E. Ring, *Temperature distribution. Human body temperature its measurements and distribution*. New York, NY: Plenum Publishing, 1982.

[103] J. T. Peery, G. K. Klute, J. J. Blevins, and W. R. Ledoux, "A three-dimensional finite element model of the transibial residual limb and prosthetic socket to predict skin temperatures," *IEEE Transactions on neural systems and rehabilitation engineering*, vol. 14, no. 3, pp. 336–343, 2006.

[104] R. Clark and O. G. Edholm, *Man and his thermal environment*. Arnold London, 1985.

[105] E. Schönbaum, P. Lomax *et al.*, *International encyclopedia of pharmacology and therapeutics. Section 131. Thermoregulation, physiology and biochemistry*. Pergamon Press, 1990.

[106] R. Emrich and K. Slater, "Comparative analysis of below-knee prosthetic socket liner materials," *Journal of medical engineering & technology*, vol. 22, no. 2, pp. 94–98, 1998.

[107] M. J. Gerschutz, M. L. Haynes, D. Nixon, and J. M. Colvin, "Strength evaluation of prosthetic check sockets, copolymer sockets, and definitive laminated sockets," *Journal of rehabilitation research and development*, vol. 49, no. 3, pp. 405–426, 2012.

[108] M. L. Haynes, D. M. Nixon, and J. M. Colvin, "Tensile strength and impact resistance properties of materials used in prosthetic check sockets, copolymer sockets, and definitive laminated sockets," *Journal of rehabilitation research and development*, vol. 48, no. 8, pp. 987–1004, 2011.

[109] N. Mathur, I. Glesk, and A. Buis, "Thermal time constant: optimizing the skin temperature predictive modelling in lower limb prostheses using gaussian processes," *IET Healthcare Technology Letters*, vol. 3, no. 2, pp. 98–104, 2016.

[110] C. K. Williams and C. E. Rasmussen, "Gaussian processes for regression," *Neural Information Processing Systems*, vol. 8, pp. 514–520, 1996.

[111] C. E. Rasmussen and C. K. I. Williams, *Gaussian Processes for Machine Learning (Adaptive Computation and Machine Learning*, T. M. Press, Ed. The MIT Press, 2005.

[112] M. N. Gibbs, "Bayesian gaussian processes for regression and classification," Ph.D. dissertation, University of Cambridge, 1998.

[113] C. E. Rasmussen and C. K. I. Williams, "Gaussian processes for machine learning software," Online, http://www.gaussianprocess.org/gpml/code/matlab/doc/.

[114] N. Mathur, I. Glesk, and A. Buis, "Skin temperature prediction in lower limb prostheses," *IEEE Journal of Biomedical and Health informatics*, vol. 20, no. 1, pp. 158–165, 2016.

[115] S. W. Smith, *The scientist and engineer's guide to digital signal processing.* California Technical Pub. San Diego, 1997.

[116] N. Mathur, I. Glesk, and A. Buis, "Thermal time constant: Improving the accuracy of skin temperature predictive modelling in lower limb prosthetic users," in *ISPO World Congress 2015*, vol. 39, no. 1, International Society of Prosthetics and Orthotics. Lyon, France: SAGE Publications, June 2015, pp. 72–73.

[117] N. Mathur, I. Glesk, and A. Buis, "Comparison of adaptive neuro-fuzzy inference system (anfis) and gaussian processes for machine learning (gpml) algorithms for the prediction of skin temperature in lower limb prostheses," *Medical Engineering and Physics*, vol. 38, no. 10, pp. 1083–1089, 2016.

[118] A. Kusagur, S. Kodad, and D. B. V. S. Ram, "Modeling, design & simulation of an adaptive neuro-fuzzy inference system (anfis) for speed control of induction motor," *International Journal of Computer Applications (0975–8887) Volume*, 2010.

[119] J.-S. Jang, "Anfis: adaptive-network-based fuzzy inference system," *IEEE transactions on systems, man, and cybernetics*, vol. 23, no. 3, pp. 665–685, 1993.

[120] N. Nedjah and L. de Macedo Mourelle, *Fuzzy systems engineering: theory and practice.* Springer Science & Business Media, 2005, vol. 181.

[121] M. Sugeno and G. Kang, "Structure identification of fuzzy model," *Fuzzy sets and systems*, vol. 28, no. 1, pp. 15–33, 1988.

[122] M. Sugeno and K. Tanaka, "Successive identification of a fuzzy model and its applications to prediction of a complex system," *Fuzzy sets and systems*, vol. 42, no. 3, pp. 315–334, 1991.

[123] T. Takagi and M. Sugeno, "Fuzzy identification of systems and its applications to modeling and control," *IEEE transactions on systems, man, and cybernetics*, no. 1, pp. 116–132, 1985.

[124] A. Celikyilmaz and I. B. Turksen, *Modeling Uncertainty with Fuzzy Logic*. Springer, 2009.

[125] O. Castillo and P. Melin, "Modelling, simulation and behavior identification of non-linear dynamical systems with a new fuzzy-fractal genetic approach," *Edited Book in the Series of Advances in Fuzzy Systems edited by B. Bouchon, R. Yager, & LA Zadeh, World Scientific*, pp. 95–106, 2000.

[126] Matlab, "Neuro-adaptive learning and anfis," Online, https://uk.mathworks.com/help/fuzzy/neuro-adaptive-learning-and-anfis.html.

[127] T. Chai and R. R. Draxler, "Root mean square error (rmse) or mean absolute error (mae)?–arguments against avoiding rmse in the literature," *Geoscientific Model Development*, vol. 7, no. 3, pp. 1247–1250, 2014.

[128] J. S. Armstrong and F. Collopy, "Error measures for generalizing about forecasting methods: Empirical comparisons," *International journal of forecasting*, vol. 8, no. 1, pp. 69–80, 1992.

[129] G. S. Maddala and K. Lahiri, *Introduction to econometrics*. Wiley, 2009.

[130] online, https://www.arduino.cc/en/Main/ArduinoWiFiShield, December 2014.

[131] online, https://www.arduino.cc/en/Main/ArduinoGSMShield, December 2014.

[132] N. Mathur, I. Glesk, and A. Buis, "Issues in wearable mobile sensor platform for lower limb prosthetic users," in *2015 17th International Conference on Transparent Optical Networks (ICTON)*. IEEE, 2015, pp. 1–4.

[133] N. Mathur, G. Paul, J. Irvine, M. Abuhelala, A. Buis, and I. Glesk, "A practical design and implementation of a low cost platform for remote monitoring of lower limb health of amputees in the developing world," *IEEE Access*, vol. 4, pp. 7440–7451, 2016.

[134] W. H. Press, S. A. Teukolsky, W. T. Vetterling, and B. P. Flannery, *Numerical recipes in FORTRAN: the art of scientific computing*. Cambridge University Press Cambridge, 1992, vol. 2.

[135] T. Young and M. J. Mohlenkamp, "Introduction to numerical methods and matlab programming for engineers," *Free Software Foundation, youngt@ ohio. edu*, 2014.

[136] N. Mathur, A. Davidson, A. Buis, and I. Glesk, "Tissue viability monitoring - a multi-sensor wearable platform approach," in *20th Slovak-Czech-Polish on Wave and Quantum Aspects of Contemporary Optics SCPOC*, vol. 1014205, International Society for Optics and Photonics. SPIE, September 2016.

Appendix A

Complementary Filter Code

This code was developed on MATLAB 8.4 (Release name: R2014b).

```
% loading the raw accelerometer and gyroscope values
load('gait_data.mat');
% Sampling step size
dt = 0.04;
t = 1:dt:2100;
% Filter coefficient
alpha = 0.98;
% Scaling factors for acceleration and angular velocity
acc_sensitivity = 1/16384;
gyro_sensitivity = 1/131;
% Converting the raw data into acceleration or angular
    velocity values by scaling
ax = gait_data(:,1).*acc_sensitivity;
ay = gait_data(:,2).*acc_sensitivity;
az = gait_data(:,3).*acc_sensitivity;
gx = gait_data(:,4).*gyro_sensitivity;
gy = gait_data(:,5).*gyro_sensitivity;
```

```
gz = gait_data(:,6).*gyro_sensitivity;
% Estimating the shank angle using the complimentary
    filter
m = size(gy)
shank_ang_y(1) = gy(1,1);
for i=2:m(:,1)
shank_ang_y(i) = alpha.*(shank_ang_y(i-1) + gy(i).*dt)+
    (1-alpha).*ay(i);
end
% Plotting the shank angle in the y direction
plot(t,shank_ang_y)
xlabel('Time(seconds)');
ylabel('Shank Angle( ^\circ)');
```

Appendix B

GPML Code

This code was developed on MATLAB 8.4 (Release name: R2014b) using the GPML toolbox.

Copyright for GPML toolbox

```
GAUSSIAN PROCESS REGRESSION AND CLASSIFICATION Toolbox version 4.0
for GNU Octave 3.2.x and Matlab 7.x
The code is released under the FreeBSD License.
Copyright (c) 2005-2016 Carl Edward Rasmussen & Hannes Nickisch.
All rights reserved.
Redistribution and use in source and binary forms, with or without
modification, are permitted provided that the following conditions
are met:
1. Redistributions of source code must retain the above copyright
notice, this list of conditions and the following disclaimer.
2. Redistributions in binary form must reproduce the above
copyright notice, this list of conditions and the following
disclaimer in the documentation and/or other materials provided
with the distribution.
THIS SOFTWARE IS PROVIDED BY CARL EDWARD RASMUSSEN & HANNES NICKISCH
''AS IS'' AND ANY EXPRESS OR IMPLIED WARRANTIES, INCLUDING, BUT NOT
```

LIMITED TO, THE IMPLIED WARRANTIES OF MERCHANTABILITY AND FITNESS
FOR A PARTICULAR PURPOSE ARE DISCLAIMED. IN NO EVENT SHALL CARL
EDWARD RASMUSSEN & HANNES NICKISCH OR CONTRIBUTORS BE LIABLE FOR ANY
DIRECT, INDIRECT, INCIDENTAL, SPECIAL, EXEMPLARY, OR CONSEQUENTIAL
DAMAGES(INCLUDING, BUT NOT LIMITED TO, PROCUREMENT OF SUBSTITUTE
GOODS OR SERVICES; LOSS OF USE, DATA, OR PROFITS; OR BUSINESS
INTERRUPTION) HOWEVER CAUSED AND ON ANY THEORY OF LIABILITY, WHETHER
IN CONTRACT, STRICT LIABILITY, OR TORT (INCLUDING NEGLIGENCE OR
OTHERWISE) ARISING IN ANY WAY OUT OF THE USE OF THIS SOFTWARE, EVEN
IF ADVISED OF THE POSSIBILITY OF SUCH DAMAGE.
The code and associated documentation is available from
http://gaussianprocess.org/gpml/code.

```
% loading the training and testing data
load('Training_Data.mat');
load('Testing_Data.mat');
% define the number of data points
n = 1050;
% defining the training input-output data pairs
x1 = Training_Data(:,1);
y1 = Training_Data(:,2);
% defining the testing input-output data pairs
x2 = Testing_Data(:,1);
y2 = Testing_Data(:,2);
% defining the mean function
meanfunc = {@meanSum, {@meanLinear, @meanConst}}; hyp.mean
    = [0.5; 1];
% defining the squared exponential covariance function
```

```
covfunc = @covSEiso; hyp2.cov = [0; 0]; hyp2.lik = log
    (0.1);
% defining the likelihood function as Gaussian
likfunc = @likGauss; sn = 0.1; hyp.lik = log(sn);
% specifying the corresponding hyperparameters
K = feval(covfunc{:}, hyp2.cov, x1);
mu = feval(meanfunc{:}, hyp.mean, x1);
% plotting the training data
figure(1)
plot(x1, y1, '+')
grid on
xlabel('Liner Temperature')
ylabel('Skin Temperature')
% optimising the hyperparameters by minimising the
    negative log marginal likelihood w.r.t. the
    hyperparameters.
hyp2 = minimize(hyp2, @gp, -100, @infExact, [], covfunc,
    likfunc, x1, y1);
exp(hyp2.lik)
% calculate the negative log marginal likelihood
nlml2 = gp(hyp2, @infExact, [], covfunc, likfunc, x1, y1)
[m s2] = gp(hyp2, @infExact, [], covfunc, likfunc, x1, y1,
    x1');
% test the predictive ability of the model on the training
    data points
figure(2)
f = [m+2*sqrt(s2); flipdim(m-2*sqrt(s2),1)];
x = [1:length(m)];
```

```
fill([x; flipdim(x,1)], f, [7 7 7]/8)
hold on; plot(m, 'LineWidth', 2); plot(x1, y1, '+')
grid on
% computing the training root mean squred error
rmse_train = sqrt(mse(y1' - m));

% Testing scenario
% plotting the testing data
figure(3)
plot(x2, y2, '+')
grid on
xlabel('Liner Temperature')
ylabel('Skin Temperature')
% calculate the negative log marginal likelihood
[m s2] = gp(hyp, @infExact, [], covfunc, likfunc, x1, y1,
    x2');
% test the predictive ability of the generated model on
    the testing data points
figure(4)
f = [m+2*sqrt(s2); flipdim(m-2*sqrt(s2),1)];
x = [1:length(m)];
fill([x; flipdim(x,1)], f, [7 7 7]/8);
hold on; plot(m, 'LineWidth', 2); plot(x2, y2, '+')
xlabel('Liner Temperature')
ylabel('Skin Temperature')
legend('95% confidence interval', 'Prediction', '
    Observations')
% move legend to upper left
```

```
legend('Location','NorthWest')
% plotting the actual output and predicted output
figure(5)
y2r(:,n) = m;
plot(n, y2, n, y2r)
xlabel('Time (seconds)')
ylabel('Temperature (^\circC)')
legend('Actual Skin Temperature', 'Predicted Skin
    Temperature')
% computing the testing root mean squred error
rmse_test = sqrt(mse(y2' - m));
end
```

Appendix C

ANFIS Code

This code was developed on MATLAB 8.4 (Release name: R2014b).

```
% loading the training and the checking data
load('TrainingData.mat');
trndata = TrainingData;
load('CheckingData.mat');
chkdata = CheckingData;
% number of iterations required to train the model
numepochs = 50;
x = 1:10:2100;
% number of input membership functions
nummfs = 3;
% gaussian input membership function
mftype = 'gaussmf';
% Generates an initial Sugeno-type FIS for ANFIS training
    using a grid partition
fismat = genfis1(trndata,nummfs,mftype);
% tunes the FIS parameters using the input/output training
     data stored in trndata.
```

```
[fismat1,trnerr,ss,fismat2,chkerr] = anfis(trndata,fismat,
    numepochs,NaN,chkdata);
% plotting all of the membership functions in the FIS
    associated with a given variable
figure(1)
plotmf(fismat1,'input',1)
% simulates the Fuzzy Inference System FIS for the input
    data and returns the output data
out = evalfis(chkdata(:,1),fismat1);
% plotting the output generated from the FIS for checking
    data
figure(2)
plot(chkdata(:,1),out,'*');
% plotting the actual output and the predicted output
figure(3)
plot(x,chkdata(:,2),'r*',x,out,'-*')
xlabel('Time(seconds)')
ylabel('Temperature( ^\circC)')
legend('Actual Skin', 'Predicted Skin')
% move legend to upper left
legend('Location','NorthWest')
```

Appendix D

Arduino Schematic and Code

This code was developed on Arduino 1.8.0 environment.

```
#include<Wire.h>
#include <SD.h>
#include <SPI.h>
#include <math.h>

int CS_pin = 10;

// analog pin 0 for thermistor 1
int thermistorPin = A0;

// analog pin 1 for thermistor 2
int thermistorPin1 = A1;

// I2C address of the MPU-6050
const int MPU=0x68;
int16_t AcX,AcY,AcZ,Tmp,GyX,GyY,GyZ;
```

```
// input pin for the voltage divider circuit
int batMonPin = 2;

// variable for the A/D value
int val2 = 0;

// variable to hold the calculated voltage
float pinVoltage = 0;
float batteryVoltage = 0;

// ratio of voltages measured from the circuit
float ratio = 2.00;
const int threshold = 5;

// For storing the id # of the reading
long id = 1;
void setup() {
    Wire.begin();
    Wire.beginTransmission(MPU);

// PWR_MGMT_1 register
    Wire.write(0x6B);

// set to zero (wakes up the MPU-6050)
    Wire.write(0);
    Wire.endTransmission(true);
    Serial.begin(9600);
```

```
    Serial.println("Initializing Card");

// Initialize Card
  if (!SD.begin(CS_pin))
  {
      Serial.println("Card Failure");
      return;
  }
      Serial.println("Card Ready");

// Write Log File Header
  File logFile = SD.open("LOG.csv", FILE_WRITE);
  if (logFile)
  {
// Just a leading blank line, incase there was previous
   data
    logFile.println(",,,,,,,,,,");
    String header = "ID, AcX, AcY, AcZ, GyX, GyY, GyZ,
       temp, temp1, batteryVoltage";
    logFile.println(header);
    logFile.close();
    Serial.println(header);
  }
  else
  {
    Serial.println("Could not open log file");
  }
}
```

```
// Function to perform the maths of Steinhart-Hart
   equation
double Thermister(int RawADC) {
    double Temp;
    Temp = log(((10240000/RawADC) - 10000));
    Temp = 1 / (0.001129148 + (0.000234125 +
        (0.0000000876741 * Temp * Temp ))* Temp );

// Convert Kelvin to Celsius
    Temp = Temp - 273.15;
    return Temp;
}
void loop() {
    Wire.beginTransmission(MPU);
// starting with register 0x3B (ACCEL_XOUT_H)
    Wire.write(0x3B);
    Wire.endTransmission(false);

// request a total of 14 registers
    Wire.requestFrom(MPU,14,true);

// 0x3B (ACCEL_XOUT_H) and 0x3C (ACCEL_XOUT_L)
    AcX=Wire.read()<<8|Wire.read();

// 0x3D (ACCEL_YOUT_H) and 0x3E (ACCEL_YOUT_L)
    AcY=Wire.read()<<8|Wire.read();
```

```
// 0x3F (ACCEL_ZOUT_H) and 0x40 (ACCEL_ZOUT_L)
    AcZ=Wire.read()<<8|Wire.read();

// 0x41 (TEMP_OUT_H) and 0x42 (TEMP_OUT_L)
    Tmp=Wire.read()<<8|Wire.read();

// 0x43 (GYRO_XOUT_H) and 0x44 (GYRO_XOUT_L)
    GyX=Wire.read()<<8|Wire.read();

// 0x45 (GYRO_YOUT_H) and 0x46 (GYRO_YOUT_L)
    GyY=Wire.read()<<8|Wire.read();

// 0x47 (GYRO_ZOUT_H) and 0x48 (GYRO_ZOUT_L)
    GyZ=Wire.read()<<8|Wire.read();

// Create an integer variable
    int val;

// Variable to hold a temperature value
    double temp;

// Read the analog port 0 and store the value
    val=analogRead(thermistorPin);

// Runs the math on the raw analog value
    temp=Thermister(val);

// Create an integer variable
```

```
    int val1;

// Variable to hold a temperature value
    double temp1;

// Read the analog port 1 and store the value
    val1=analogRead(thermistorPin1);

// Runs the math on the raw analog value
    temp1=Thermister(val1);

// Read the voltage on the divider
    val2 = analogRead(batMonPin);

// Calculate the voltage on the A/D pin. A reading of 1
   for the A/D = 0.0048mV.
// If the A/D reading is multiplied by 0.00488 then the
   voltage on the pin can be obtained
    pinVoltage = val * 0.00488;

// Use the ratio to calculate the battery voltage
    batteryVoltage = pinVoltage * ratio;

// Create Data string for storing to SD card using the CSV
    Format
    String dataString = String(id) + "
        , " + String(AcX) + " , " + String(AcY) + "
        , " + String(AcZ) + " , " + String(GyX) + "
```

```
        , " + String(GyY) + " , " + String(GyZ) + "
        , " + String(temp) + " , " + String(temp1) + "
        , " + String(batteryVoltage)+ " , ";

// Open a file to write to. Only one file can be open at a
    time
    File logFile = SD.open("LOG.csv", FILE_WRITE);
    if (logFile)
    {
     logFile.println(dataString);
     logFile.close();
     Serial.println(dataString);
    }
    else
    {
     Serial.println("Could not open log file");
    }
    //Increment ID number
    id++;
    delay(40);
    }
```

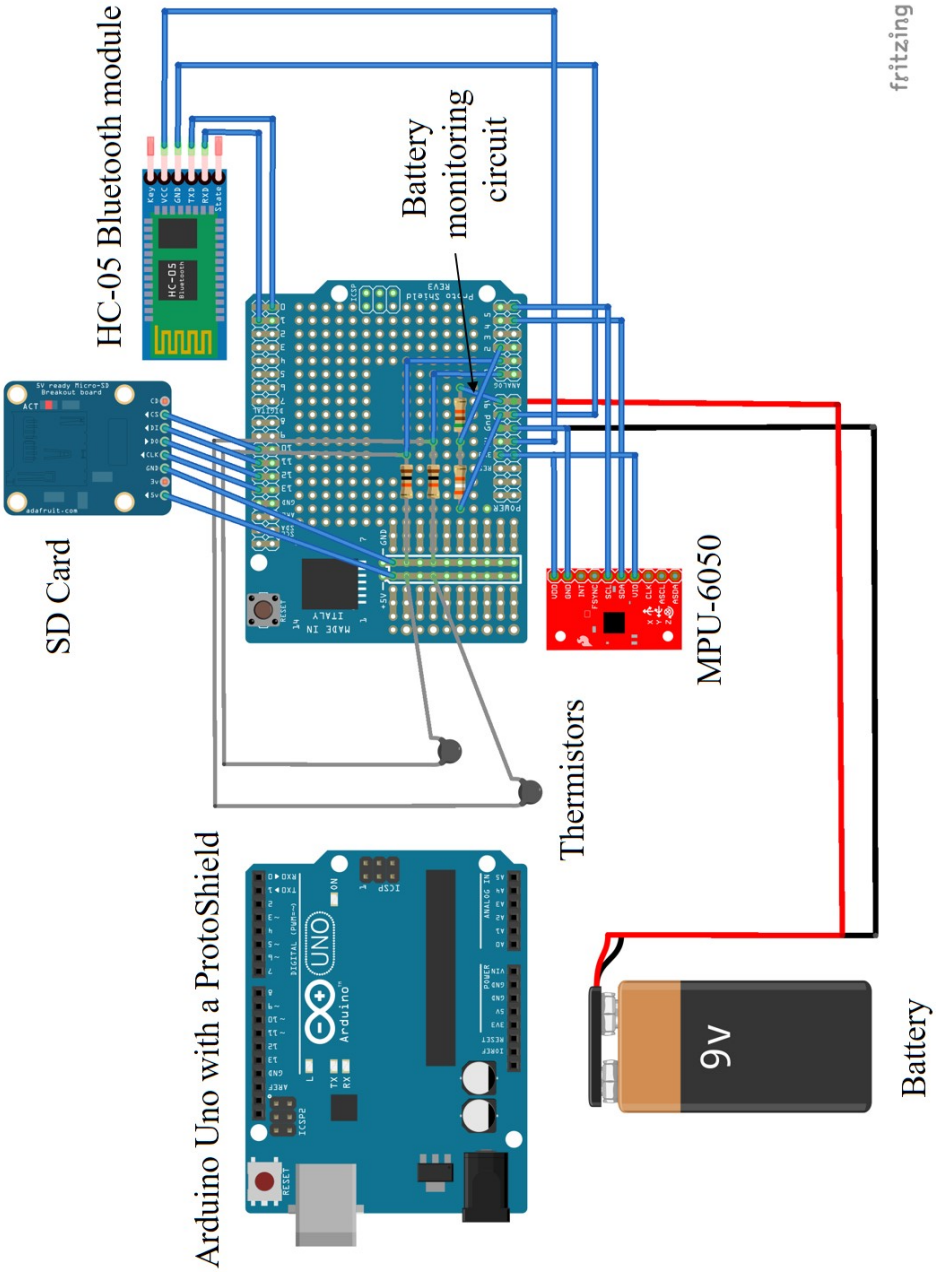

Figure D.1: Schematic of the multi-sensor wearable platform. This schematic of the wearable sensor platform is designed in Fritzing software package.

Appendix E

LabView Schematic

This interface is developed in LabView. The block diagram and the front panel window are shown in the following figures.

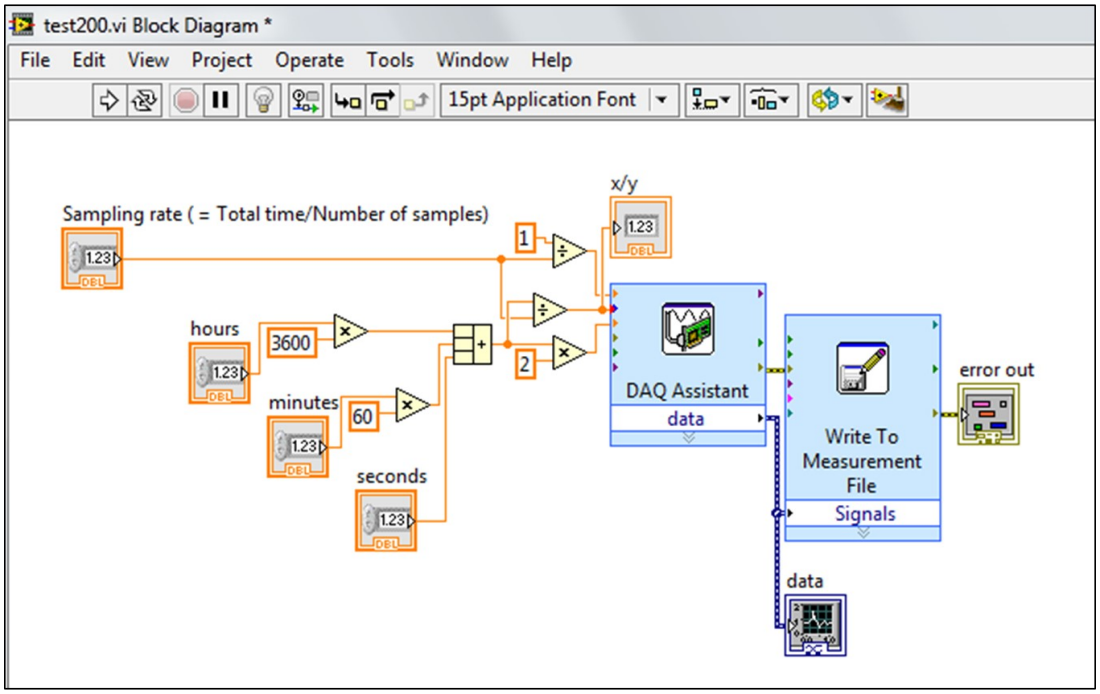

Figure E.1: Block diagram for monitoring the battery depletion rate.

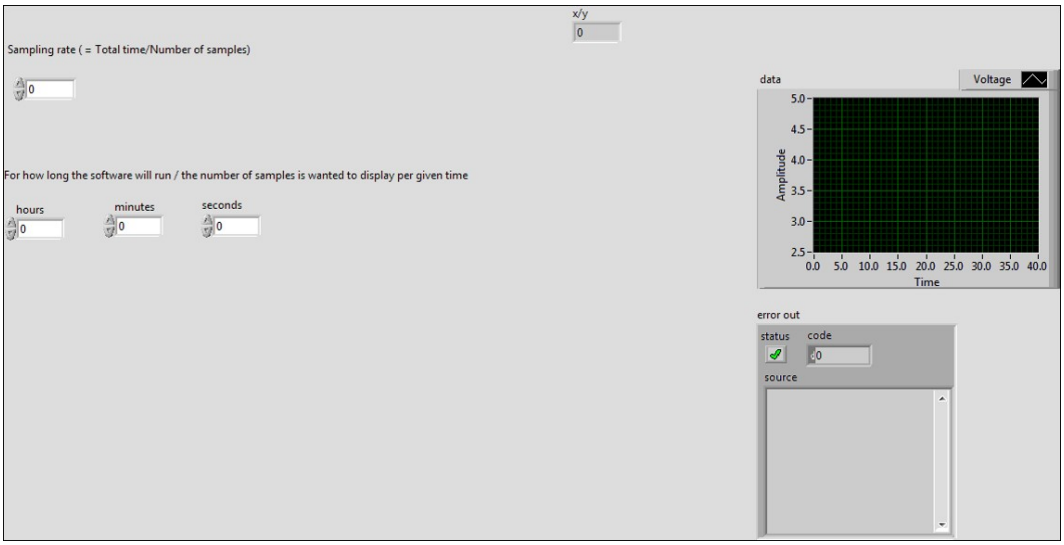

Figure E.2: Front panel for monitoring the battery depletion rate.